50 Jahre 1956 - 2006

GKSS FORSCHUNGSZENTRUM in der HELMHOLTZ-GEMEINSCHAFT

Sensitivity of the Large-to Meso-Scale Atmospheric Relationship to Orbital Forcing: A Model Based Study

(Vom Fachbereich Geowissenschaften der Universität Hamburg als Dissertation angenommene Arbeit)

Author:
N. Groll

wissen schafft nutzen

ISSN 0344-9629

HELMHOLTZ | GEMEINSCHAFT

GKSS 2007/4

GKSS 2007/4

Sensitivity of the Large-to Meso-Scale Atmospheric Relationship to Orbital Forcing: A Model Based Study

(Vom Fachbereich Geowissenschaften der Universität Hamburg als Dissertation angenommene Arbeit)

Author

N. Groll

(Institute for Coastal Research)

GKSS-Forschungszentrum Geesthacht GmbH • Geesthacht • 2007

Die Berichte der GKSS werden kostenlos abgegeben.
The delivery of the GKSS reports is free of charge.

Anforderungen/Requests:

GKSS-Forschungszentrum Geesthacht GmbH
Bibliothek/Library
Postfach 11 60
D-21494 Geesthacht
Germany
Fax.: (49) 04152/871717

Als Manuskript vervielfältigt.

ISSN 0344-9629

GKSS-Forschungszentrum Geesthacht GmbH · Telefon (04152)87-0
Max-Planck-Straße 1 · D-21502 Geesthacht / Postfach 11 60 · D-21494 Geesthacht

GKSS 2007/4

Sensitivity of the Large-to Meso-Scale Atmospheric Relationship to Orbital Forcing: A Model Based Study

(Vom Fachbereich Geowissenschaften der Universität Hamburg als Dissertation angenommene Arbeit)

Nikolaus Groll

105 pages with 28 figures and 4 tables

Abstract

To infer past large-scale climate from regional climate information, such as observations or proxy data, often statistical methods are used. To apply the statistical relationship between the large -and the regional -or local-scale, in periods different to the fitting period, the stability of these scale relationships is important. It is assumed that these relationships are stable, but for periods with substantially different climate conditions, such as glacials and interglacials this assumptions may be problematic.

Here the sensitivity of these scale relationships to orbital forcing is investigated. Three periods are compared: 125 kyr BP- the early Eemain (last interglacial); 115 kyr BP- the last glacial inception and the preindustrial period (1800 AD). Due to the lack of proxy data with high temporal resolution during the first two periods, quasi-equilibrium simulations with the AOGCM ECHO-G are used as a surrogate for the real climate.

In all simulations the mean climate response to insolation changes is as expected. The changed mean atmospheric circulation modifies the atmospheric flow characteristics at high and low phases of the Northern Annular Mode (NAM) over certain regions (e.g., Europe). These differences in the flow character reduce or increase the strength of the relationship between NAM and regional temperatures. The NAM-temperature signal is weaker over Europe and stronger over Siberia during the early Eemain than in the other periods. These differences of the NAM-temperature signal strongly effect the relationship between temperature variability in different regions, also called temperature teleconnections. For regions where the NAM-temperature signal is moderate to strong the temperature teleconnections are dominated by the NAM and where the NAM-temperature signal is weak the temperature teleconnection are influenced by different mechanisms to the NAM.

These results should be taken into account when the large-scale climate is inferred from regional climate information (e.g., proxy data) and when highly temporally resolved temperature estimates from proxy data from different regions are compared and merged. Similar results can be expected for periods with similar orbitally-induced insolation changes, such as the mid-Holocene.

Sensitivität von atmosphärischen Beziehungen zwischen der grossräumigen und der Mesoskala in Abhängigkeit des orbitalen Antriebs: Eine Modellstudie

Zusammenfassung

Um das vergangene großräumige Klima mit Hilfe von regionalen Klimainformationen, wie Beobachtungen oder Proxy Daten, zu untersuchen, werden oft statistische Methoden verwendet. Um den statistischen Zusammenhang zwischen der großräumigen- und der regionalen Skala in anderen Zeiträumen, als jene in der der statistische Zusammenhang aufgestellt wurde, anwenden zu können wird diesr Skalenzusammenhang als stabil angenommen. Aber für Perioden mit deutlich anderen klimatischen Bedingungen als jene in der der Zusammenhang aufgestellt wurde, wie Eiszeiten oder vergangene Warmzeiten, kann diese Stabilitätsannahme problematisch sein.

In dieser Arbeit wird der statistische Skalenzusammenhang in Abhängigkeit des orbitalen Antriebs untersucht. Es werden drei Perioden miteinander verglichen: 125000 Jahre vor heute - der Beginn der letzten Warmzeit (das Eem); 115000 Jahre vor heute - der Übergang zur Eiszeit und die vorindustrielle Periode (1800 AD). Da für die ersten beiden Perioden keine Proxy Daten mit ausreichender zeitlicher Auflösung für diese Untersuchung existieren, wurden Quasi-Gleichgewichtssimulation mit dem gekoppelten Atmosphären-Ozean Modell ECHO-G, als Erzatz für reale Klimainformationen verwendet.

In allen Simulationen reagiert das mittlere Klima auf die geänderten Einstrahlungsbedingungen wie erwartet. Die Änderung der mittleren atmosphärischen Zirkulation führt zu einer Änderung der Strömungseigenschaften in Phasen positiven und negativen Northern Annular Mode (NAM) in verschiedenen Regionen (z.B. in Europa). Diese Unterschiede der Strömungseigenschaften führen zu einer Abschwächung oder Verstärkung des Zusammenhangs zwischen NAM und der regionalen Temperatur. Die NAM erklärt weniger der europäischen und mehr der sibirischen Temperaturvariabilität im EEM als in den beiden anderen Perioden. Die Änderungen im NAM-Temperatur Signal beinflussen den Zusammenhang von Temperaturvariabilität in verschiedenen Regionen untereinander (Temperatur Telekonnetionen). In Regionen in denen das NAM-Temperatur Signal stark ausgeprägt ist werden die Temperatur Telekonnektionen stark von der NAM beeinflusst, in Regionen in denen das NAM-Temperatur Signal schwach ist werden Temperatur Telekonnektionen durch andere Prozesse beeinflußt.

Die vorgestellten Ergebnisse sollten in Betracht gezogen werden, wenn das grossräumige Klima mit Hilfe von regionaler Klimainformation untersucht wird und wenn zeitlich hochaufgelöste Temperaturzeitreihen von Proxydaten aus unterschiedlichen Regionen miteinander verglichen oder verknüpft werden. Ähnliche Änderungen des Skalenzusammenhangs sind auch bei ähnlichen Änderungen des orbitalen Antriebs zu erwarten, wie z.B. wÄhrend des mittleren Holozäns.

Manuscript received / Manuskripteingang in TDB: 14. January 2007

Contents

List of Papers

This thesis is based on the following pre-reviewed journal articles:

Groll, N., M. Widmann, J.M. Jones, F. Kaspar and S.J. Lorenz, 2005:
Simulated relationship between regional temperatures and large-scale circulation: 125kyr BP (Eemian) and the preindustrial period.
Journal of Climate, **18**(19), 4032-4045, doi:10.1175/JCLI3327.1

Groll, N. and M. Widmann, 2006:
Sensitivity of temperature teleconnections to orbital changes in AO-GCM simulations.
Geophysical Research Letters, **33**, L12705, doi:10.1029/2005GL025578

Chapter 1

Introduction and thesis outline

Climate change is one of today's most discussed subjects, not only in the scientific community but also in the public. Besides the question of how future climate may change and how it will affect our life, the influence of human activities on climate is heavily discussed. A prerequisite to quantify the amount of man-made climate change is to distinguish between natural and anthropogenically forced climate variability.

To estimate the magnitude of natural climate variability climate model simulations or long time series of climate variables are necessary. For the later, climate records before the industrial period (mid-19^{th} century) are essential to asses the climate variability before human activities influenced climate on the global scale. Whereas observations can only provide climate information since approximately the 17^{th} century, natural climate records, so-called proxy data (e.g., ice cores, tree rings), can provide climate information over long time periods before meteorological measurements are available. But both types of climate records provide only climate information on the regional- or local-scale, whereas climate information on the hemispheric or global scale is often required. Thus, to investigate the large-scale climate variability from regional climate data one needs a dense spatial coverage of regional climate informations. For periods before such an spatial coverage of climate information exists, one need a method to infer the large-scale climate from only few regional- or local-scale information.

These methods are based on the statistical relationship between the large-and the meso-scale climate and are also called upscaling models. Statistical upscaling has not only been used for periods before the instrumental period, but also for periods and regions where only few observations exist (e.g., the Southern Hemisphere). Usually, these models are fitted and validated within the last 50 years (relatively good data coverage) and the statistical relationship is then used to reconstruct the large-scale climate from the regional climate information for a certain period of interest. Upscaling models are based on different statistical methods and have been used to estimate various aspects of the global or hemispheric temperatures (e.g.,

Mann et al. 1999; Briffa et al. 2001; Esper et al. 2002; Luterbacher et al. 2004; Moberg et al. 2005) and the large-scale atmospheric circulation (e.g., Luterbacher et al. 1999; Luterbacher et al. 2002; Cook et al. 2002; D'Arrigo et al. 2003; Jones and Widmann 2003; Jones and Widmann 2004). The reconstructions derived from upscaling models have been commonly used to investigate the climate variability over the last millennium.

When analyzing the large-scale climate variability using proxy data before the Late Holocene (3000-0 years before present (3-0 kyr BP)), additionally problems in the climatic interpretation of proxies occur. Dating uncertainties of the proxy data make it difficult to merge proxy data from different locations. Thus the large-scale climate can not be inferred from a network of different proxy data, which is the standard approach for the Late Holocene, particularly for the last millennium. Furthermore, it is difficult to fit the upscaling model with proxy data, because often the period that is covered by proxy data does not overlap with observations. However even if the aforementioned problems were solved (i.e., proxy data from different regions with high enough dating accuracy and long continuous time series till the instrumental period existed), one still has to handle another issue. The assumption of the stability of the relationship between the large- and the meso-scale climate. For all reconstructions based on regional climate information it is assumed that the relationship between the large- and the meso-scale is stable, as this is a basic for all reconstructions. For periods with substantially different climate conditions, such as glacials or interglacials, this assumption is possibly more problematic than for the last millennium. Because there are no proxy data that would allow to investigate this assumption, climate model simulations are used as a surrogate for the real climate. The use of climate simulations to investigate aspects of climate reconstructions is a common tool during the Late Holocene and is known as a pseudo-proxy approach. Long quasi-equilibrium simulations with a fully coupled atmosphere ocean general circulation model (AOGCM) for the three periods are used in this thesis. The main focus is to investigate the sensitivity of the relationship between the large-and the meso-scale atmospheric climate under orbital forcing conditions for the early Eemian - the last interglacial (125 kyr BP), the last glacial inception (115 kyr BP) and the preindustrial period (1800 AD).

This thesis is based on two publications (Groll et al. 2005; Groll and Widmann 2006). The first publication (Groll et al. 2005) considers the overall influence of orbital forcing variations to the mean climate, the extratropical Northern Hemisphere atmospheric circulation variability and the relationship between the large-scale circulation and the regional temperature on multidecadal timescales for the early Eemain (125 kyr BP) and the preindustrial period. Furthermore an explanation of the changed relationship is presented.

Results from the first publication led to the question whether the relationship between temperatures at different locations are also influenced by orbital forcing. The second publication (Groll and Widmann 2006) thus investigates the link between regional temperatures, so-called temperature teleconnections, on annual timescales under different orbital forcing

conditions. A simulation for the period of the glacial inception (115 kyr BP) is also considered in this analysis. It is shown that the change of the temperature teleconnections are associated with changes of the relationship between the large-scale circulation and regional temperatures.

The contents of the thesis is organized as follows: In chapter two a short overview of paleoclimatology, based on the books of Bradley (1999) and Saltzman (2002), is presented. Special focus is put on types of external forcing that drove past climate variations and methods to investigate those changes. Chapter three contains an extended summary[1] of the two publications (Groll et al. 2005; Groll and Widmann 2006), including some material from Widmann et al. (2007a). Compared to the first publication, the content of chapter three is extended to use all three simulations and to consider annual timescales, for most analysis. Finally, in chapter four a conclusion of the presented results is given, as well as an outlook of possible future analyses. Finally, the two publications, are attached in the appendix, as published in the peer-reviewed journals.

[1]Note, that in this thesis the term Northern Annular Mode is used instead of Arctic Oscillation, which is used in the publications. Both terms describe the same phenomenon, but in recent studies often Northern Annular Mode is used, because the term Oscillation implies an oscillation of the circulation, which is not the case.

Chapter 2

Short overview on paleoclimatology

This chapter is primarily based on the books of Bradley (1999) and Saltzman (2002) and gives a brief overview on paleoclimatology. First a motivation is presented why the study of past climates is important, than types of internal and external forcings are discussed. Furthermore a short overview of types of proxy data and climate models used in paleoclimatology is presented and finally approaches to compare and combine proxy data with model simulations is given.

2.1 Motivation

Climate has always varied on all spatial and temporal scales. The knowledge of the causes of former climate changes helps for a better understanding of the entire climate system, the climate subsystems and the feedback mechanisms between these systems.

Paleoclimatology is the study of past climate and can be used to investigate the sensitivity of climate variability to altered climate forcing. Paleoclimatology also helps to identify non-linear processes in the climate system, for instance abrupt temperature changes during glacial times. Studies of the past climate also help to identify the response of the ocean circulation to freshwater input (e.g., Stouffer et al. 2006). An improved understanding of the mechanisms of former climate changes can help to estimate future climate variations (Bradley and Eddy 1991).

Various types of climate models that are used for simulating future climate scenarios can be tested under paleoclimate conditions (e.g., different external forcings and different boundary conditions) and compared, whenever possible, with natural climate archives. The gained knowledge from these paleoclimate simulations can give more confidence in future climate scenarios derived from such models. Furthermore, an improved understanding of processes within the climate system helps to improve these climate models, but also show their limitations.

The forcings and boundary conditions of past climate are different to today's or to those of the future and due to the nonlinear mechanisms past climate changes should not be used as direct analogs for possible future changes. However, the study of past climate helps to asses the natural climate variability and relate it to the range of anthropogenically forced climate variability.

2.2 Climate variations

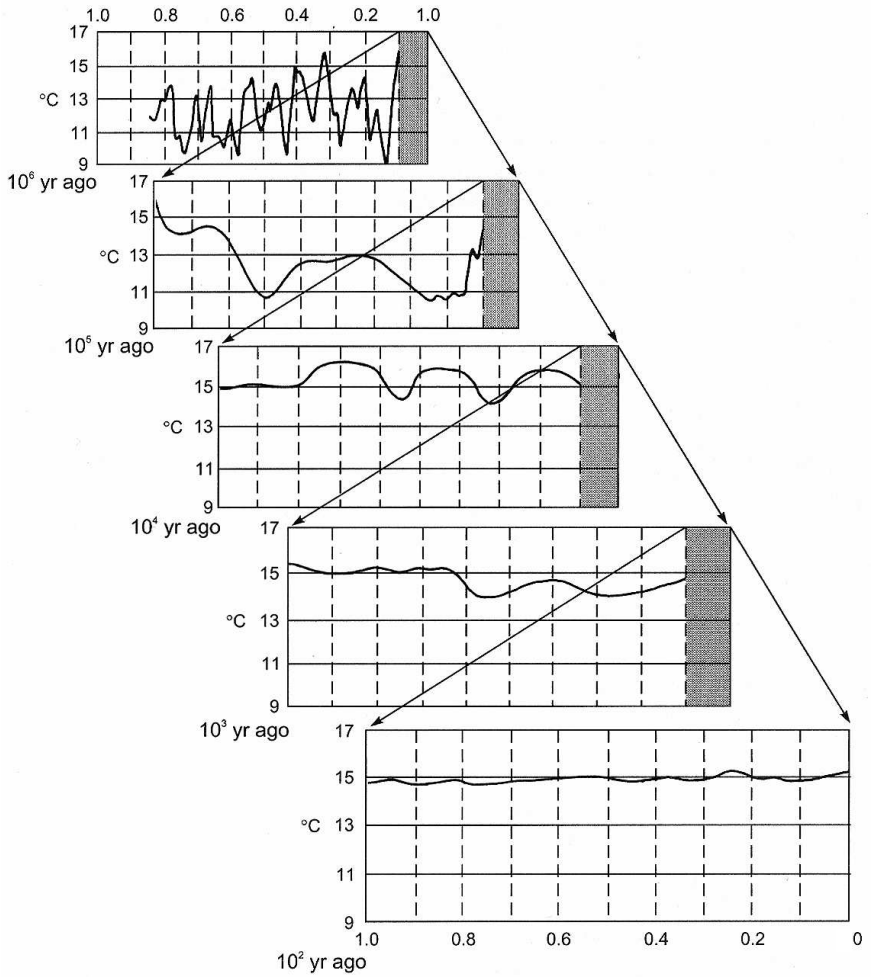

Figure 2.1: Schematic diagram of known climate fluctuations, in terms of global mean annual temperature (y-axis), on various timescales over the last 1 million years (Myr). Timescales range from 1 Myr to 100 yr with an expansion by a factor of ten of the last interval of the row above. Note that the temperature scale is the same on all panels. Diagram from Bradley (1999).

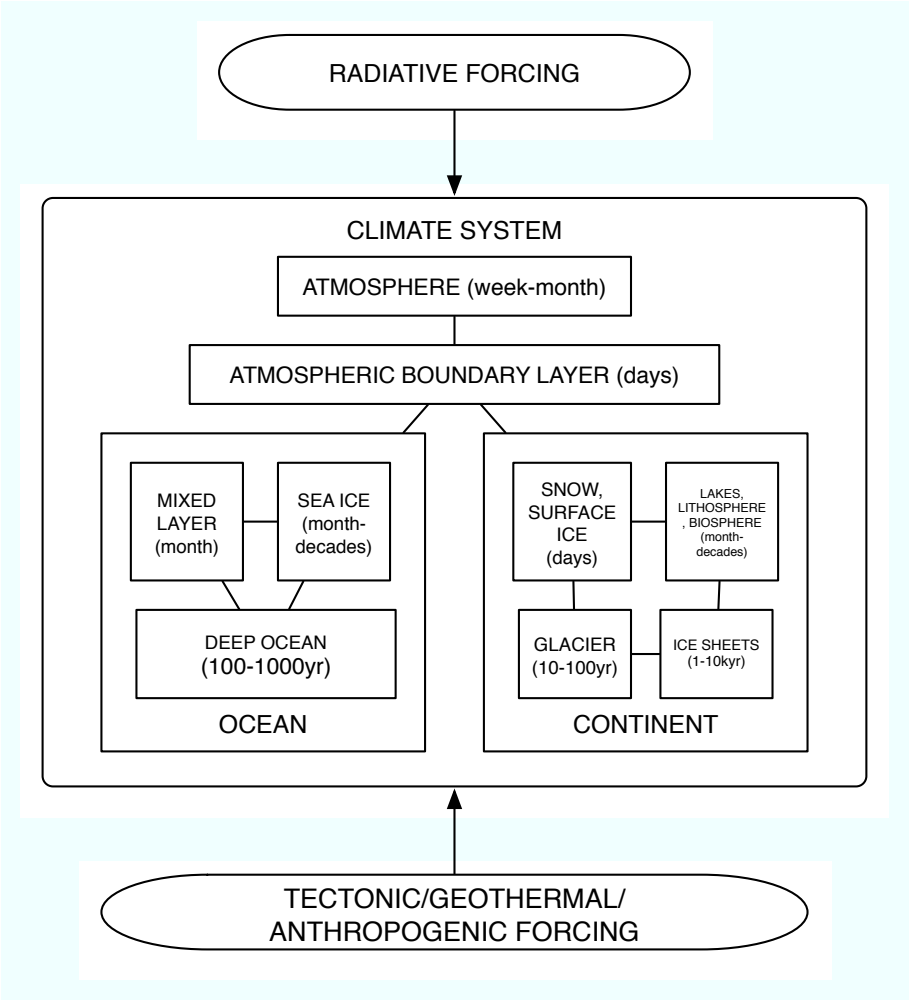

Figure 2.2: Schematic box plot of the climate system, it subsystems, their typical response times and external forcing factors, adapted from Saltzmann (2002).

Throughout the Earth's history climate has always been changing, with warmer and colder climate states compared to present day. Climate fluctuates on various timescales and with different magnitudes. A schematic diagram (Fig. 2.1) illustrates the main fluctuations over the last million years on different timescales. Temperature variations show larger amplitudes on longer timescales, than over the last 100 years. Depending on the time scale, different mechanisms are responsible for climate fluctuations. On short timescales, diurnal to annual, climate variations mainly depend on internally generated variability of the climate system, e.g., the autovariation of the atmosphere or the ocean. On decadal to millennium or longer timescales, external factors influence the climate, e.g. variations of the Earth's orbital parameter or of the solar output. Of course, both internal and external mechanisms may affect the

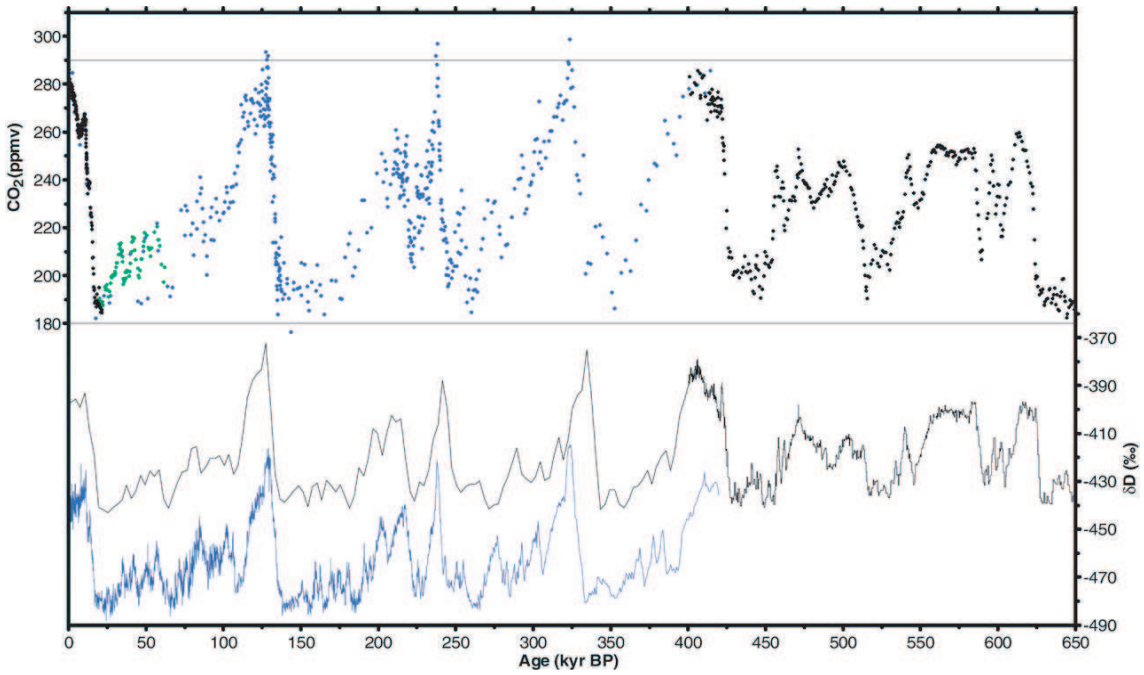

Figure 2.3: A composite CO_2 record over six and a half ice age cycles, back to 650 kyr BP The record results from the combination of CO_2 data from three Antarctic ice cores: Dome C (black), 0 to 22 kyr BP and 390 to 650 kyr BP, Vostok (blue), 0 to 420 kyr BP and Taylor Dome (light green), 20 to 62 yr BP. Black line indicates δD from Dome C, 0 to 400 kyr BP and 400 to 650 kyr BP. The blue line indicates δD from Vostok, 0 to 420 kyr BP, figure and caption from Siegenthaler et al. (2005).

climate and the climate response to those may vary at different times of the past.

2.2.1 Internal forcing

Climate variations that are forced by processes within the climate system (Fig. 2.2) are called internally generated variability or variability due to internal forcing. Such processes are stochastic processes of the atmosphere and the ocean, or variations of the dominant modes of the atmosphere, like the Northern Annular Mode[1] (NAM) or the Southern Annular Mode[2] (SAM). Climate variations according to ocean circulation changes like the El-Niño/ Southern Oscillation (ENSO) phenomena are also internally generated as well as variations caused by changes of the biosphere. Another important type of internal forcing are natural variations of the composition of greenhouse gases and aerosols of the atmosphere, that lead to a changed

[1]The Northern Annular Mode is also called the Arctic Oscillation (AO) and their North Atlantic/ European sector is comparable to the North Atlantic Oscillation (NAO)

[2]The Southern Annular Mode is equivalent with the Antarctic Oscillation (AAO)

radiative forcing. Greenhouse gas concentrations have varied throughout the Earth's history within a broad range. Atmospheric CO_2 concentrations, for instance, have ranged between 180 ppm and 290 ppm (Fig. 2.3) over the last one million years (Myr). These changes are driven by various natural sinks and sources of greenhouse gases (e.g., biological pump in the ocean (Broecker 1982a; Broecker 1982b)) and lead to variations of the strength of the natural greenhouse effect.

Internal climate variability is not only related to one sort of internal forcing at one time but depends on the combinations and feedback mechanisms of several internal factors acting on several timescales (Hasselmann 1976).

2.2.2 External forcing

All forcings that influence the climate from outside the climate system are called external forcings. These forcings usually lead to climate fluctuations on longer timescales, from a couple to even billions of years. Well-known examples of external forcing are the variations of the orbital parameters of the Earth and of the solar activity. Whereas the effect of variations of the orbital parameters is well known and accepted, the amplitude of climate variations due to variations of solar activity is still under debate (Bengtsson et al. 2006).

Besides the internal variations of the greenhouse gases, the atmospheric composition of greenhouse gases is altered by volcanic activity and anthropogenic emissions, which belong to the group of external forcings. On timescales of billions of years, tectonics trigger climate variations, like the uplift of the Himalaya which is important for the Indian monsoon (Molnar et al. 1993) or changes in the land-sea distribution (e.g., the formation of the Isthmus of Panama) which lead to changes in ocean circulation (Mikolajewicz et al. 1993; Murdock et al. 1997).

2.2.2.1 Orbital forcing

One of the best known external forcings of the climate system are variations of the Earth's position and orientation relative to the Sun. Familiar variations are daily and annual changes according to the Earth's rotation and it's revolution around the Sun. On longer timescales perturbations of the position and orientation of the Earth relative to the Sun are the major source for variations of external forcings that initiate important changes of the climate system.

In the mid/late 19^{th} century Adhémar (1842) and Croll (1875) suggested that changes of the Earth's orbital parameters are the major cause of former glaciations in Earth's history. Milankovitch (1941) described this relation in a quantitative way. He stated that changes of the orbital parameters lead to a different distribution of the available solar energy at the top of the atmosphere and that these variations are responsible for glacial and interglacial periods. This relation is often referred to as the Milankovitch theory. The orientation and position of the Earth relative to the Sun is prescribed by three orbital parameters:

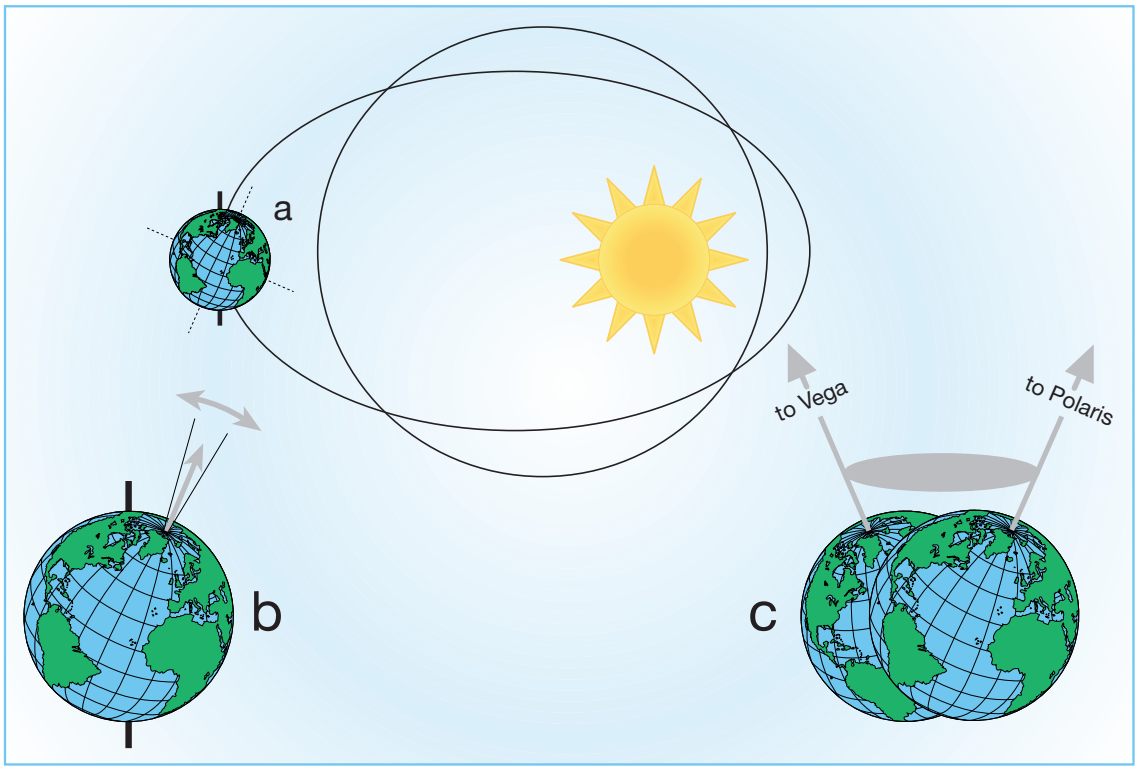

Figure 2.4: Schematic picture of eccentricity variations (a), the obliquity or axis tilt of the Earth's rotation axis (b) and of precession of the Earth's axis (c). Note that in reality the shape of the orbit (a) is almost circular and that the Northern Hemisphere is tilted towards the sun at aphelion[4] when the Earth axis points to Polaris (c) and that the Southern Hemisphere is tilted towards the sun at aphelion when the Earth axis points to Vega. In the picture the position on the orbit of the Earth is at aphelion (a).

1. Eccentricity

   The eccentricity (Fig. 2.4a) describes the shape of the Earth's orbit around the Sun. The annual revolution of the Earth around the Sun varies between an almost circular and a more elliptical orbit. The orbital eccentricity has major periods of around 100 kyr and 400 kyr. The effect of the variations of the eccentricity on the net annual incoming solar radiation is small. Assuming today's solar constant of 1370 Wm^{-2} the difference between a minimum (near circular) and a maximum eccentricity is about 2 Wm^{-2}, comparable to solar variations. Changes of the eccentricity also affect the difference of the amount of solar energy received by the Earth between aphelion[3] and perihelion[4] - reasoning almost no difference exists when the orbit is near circular. This leads to a

[3]Aphelion is the point at the orbit, where the Earth is farthest from the Sun
[4]Perihelion is the point at the orbit, where the Earth is closest to the Sun

change in the relative intensities of the seasons, with opposite effect in each hemisphere. Changes of the eccentricity further modulate the precession cycle (see point 3 below).

2. Obliquity
   Obliquity (Fig. 2.4b) refers to the axis tilt relative to the plane of the ecliptic[5]. The Earth's axis tilt varies between 21.8° and 24.4° with a period of 41 kyr. The effect of changes of the axis tilt is hemispherically symmetric and increases (decreases) summer (winter) radiation at high (low) latitudes at high values of tilt. Thus, changes in obliquity amplify or suppress the seasonality.

3. Precession
   Precession (Fig. 2.4c) is a slight wobble of the Earth's axis of rotation. The precession, with major periods of 19 kyr and 23 kyr, modulates the timing of the equinoxes[6] and solstices[7] relative to a fixed point at the Earth's orbit (often the perihelion is used). The timing of the equinoxes and solstices leads to a different length of the seasons (e.g. longer boreal winter around 125 kyr BP), with an opposite effect on the hemispheres. Additionally the eccentricity cycle modulates the effect of the precession cycle. During periods when the Earth's orbit is nearly circular the effect of the timing of the equinoxes and solstices is only small and larger when the orbit is more elliptical.

So, obliquity mainly influences high latitudes and is hemispherically symmetric, whereas the combined effect of eccentricity and precession generally influence low latitudes and is asymmetric between both hemispheres. All orbital parameters together lead to an almost unchanged annual mean level of incoming solar radiation, but to a seasonal redistribution of the available solar energy, in a way that a high winter (boreal or austral) radiation sum is compensated by a low summer total and vice versa. Changes in orbital parameters result in an always varying complex pattern of insolation at the top of the atmosphere (Fig. 2.5).

2.2.2.2 Solar forcing

The Sun is the energy source of the Earth and changes in the solar radiation influence the climate. Solar variability effects the climate on shorter timescales (e.g., decadal to centennial) than orbital variations. Well known variations of the solar radiation are the Schwabe cycle having a mean period of 10.8 years, which is related to the sunspot activity[8] and are imprinted in temperature observations (Mende and Stellenmacher 2001). Perturbations of solar activity are suggested to have strongly contributed to climate variations over the last millennia, like the Little Ice Age in Europe (e.g., Lean and Rind 1999; Shindell et al. 2001a). Over the last

[5]Imaginary plane in which the Earth rotates around the Sun.
[6]Vernal and autumn equinox refer to the point of the Earth's orbit where day and night are equal.
[7]Summer and winter solstices refer to the point of the Earth's orbit where day or night are longest.
[8]Periods of high sunspot activity are related to high solar radiation and vice versa

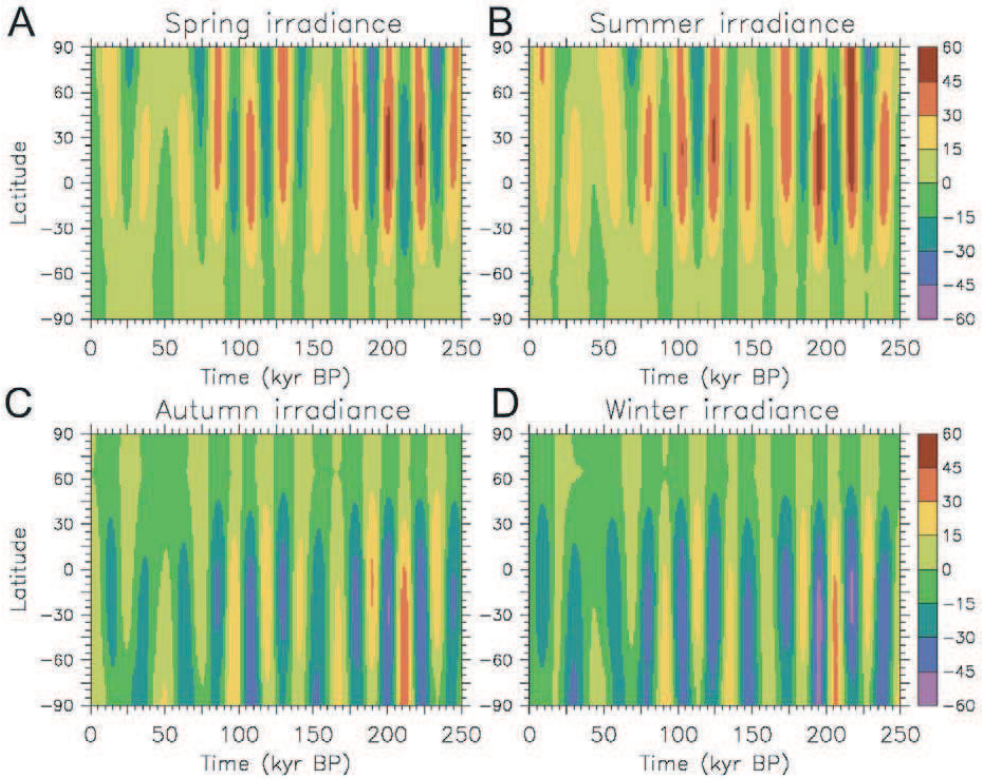

Figure 2.5: Deviation of the seasonal averaged insolation (i.e., total seasonal insolation divided by the length of the season) over the last 250 kyr with respect to the present day value. (A) boreal Spring; (B) boreal Summer; (C) boreal Autumn; (D) boreal Winter. Units are Wm^{-2}, figure and caption from Loutre et al. (2004).

500 years the solar constant may have varied by up to 6 Wm^{-2} (Crowley 2000). Note that reconstructions of the solar constant differ in absolute value and variability (see Fig.2.6). Recent studies suggest even smaller amplitudes of the solar constant (Wang et al. 2005). Besides variations of the total amount of solar radiation, changes in the solar spectrum are found to be also important (Beer et al. 2000), e.g., via their influence on ozone chemistry (Shindell et al. 2001a; Shindell et al. 2001b).

2.2.2.3 Volcanic and anthropogenic forcing

Whereas natural variations of atmospheric greenhouse gas concentrations are normally referred to as internal forcing, changes through volcanic activity or greenhouse gas emissions caused by human activities are referred to as external forcings. Large volcanic eruptions are thought to be responsible for a net global cooling over some years (e.g., Robock 2000), but regional winter warming can also occur (e.g., Kirchner et al. 1999). The usage of carbon fuel

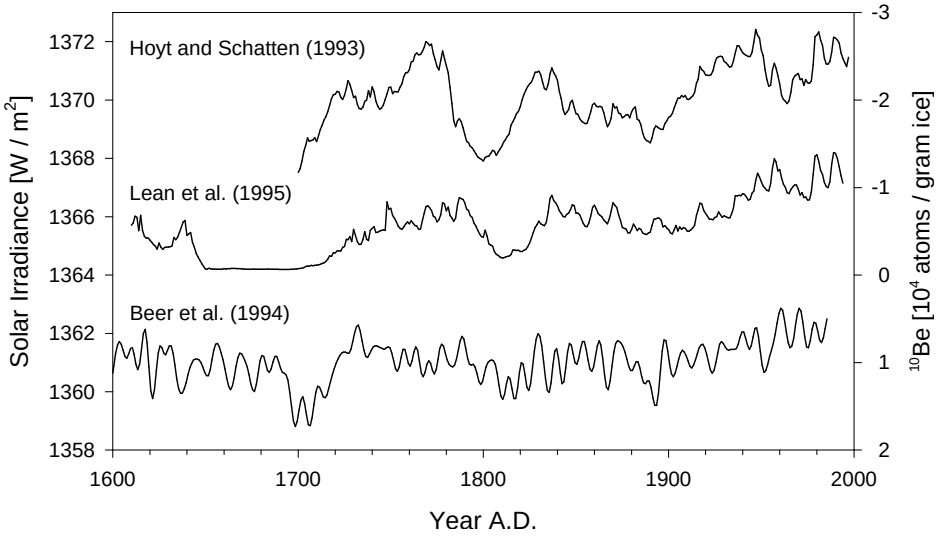

Figure 2.6: Comparison of different solar reconstructions, by Hoyt and Schatten (1993), Lean et. al (1995) and Beer et al. (1994) - all reconstructions are based on ^{10}Be. Note the difference in absolute value and variability, figure from Oh et al. (2003).

since the mid 19^{th} century and the extension of farming has led to a rapid increase of greenhouse gas concentrations during the last century, known as the anthropogenic greenhouse gas effect, which is though to be responsible for the global warming in the last decades (Mitchell et al. 2001).

2.2.2.4 Externally forced climate change

The external forcings mentioned above and their variations lead to changes in the Earth's radiative budget. Variations of the solar and greenhouse gas forcings result in a global change of the radiative budget, but can lead to a different regional effects, according to differences in the albedo, biosphere and land-ocean distribution. Not only temperature is triggered by the radiative budget, but also feedback processes like changes in water vapor, clouds, ice/snow cover, atmospheric and ocean transport and resulting circulation changes (Shindell et al. 2001b).

Additionally, changes in the Earth's orbital parameters lead to a latitudinal and seasonal redistribution of insolation. For instance a latitudinal redistribution of insolation leads to changes in the global energy exchange between low and high latitudes, which result in a modified general circulation of the atmosphere (e.g., Hall et al. 2005). An often discussed orbitally controlled phenomenon is the strength of the African and Asian monsoons. In times of a higher summer insolation the land/sea temperature contrast is increased. This leads to a stronger ocean to land circulation and results in a stronger summer monsoon. The

same mechanism leads to a stronger winter monsoon in times of weaker winter radiation. This relationship between orbitally controlled radiation variations and monsoon activity is found in many proxy data (e.g., Emeis et al. 1995; Kutzbach et al. 1996; de Noblet et al. 1996; Rohling et al. 2002; Liu et al. 2004) and model studies (e.g., Prell and Kutzbach 1987; Montoya et al. 2000; Harrison et al. 2003).

2.3 Proxy data

Only at a few stations are meteorological measurements available back to about 1650. But a dense observation network is a prerequisite to study the climate variability on large spatial scales. This required station density was reached in some areas not before the mid 19^{th} century in the Northern Hemisphere. To investigate climate before this period one is restricted to use indirect measurements. These indirect measurements are called proxy data. One can distinguish between documentary and natural proxy data.

2.3.1 Documentary proxy data

Documentary proxy data are usually descriptions of the climate or weather in ship logs or chronicles. For instance droughts and flood events recorded by monks or harvest recording of crop and grapes can be interpreted as special states of climate (e.g., Ogilvie 1992; Brazdil et al. 2005). Documentary proxy data are difficult to interpret because their are often subjective and are discontinuous in space and time.

2.3.2 Natural proxy data

Natural proxy data are indirect measurements of climate variables and are frequently used in climate science. Various variables, like the width of tree rings, pollen or isotope concentrations, that are all influenced by the climate can be related to climate variables by transfer functions. The temporal resolution and the length of the period that can be investigated depends on the proxy data. Generally, proxy data with high temporal resolution (e.g., annual) cover only a short period (10-1000 years) and proxy data with a coarse temporal resolution (e.g., centennial and greater) cover longer periods (from 1000 to even million years and beyond). Table 2.1 comprises a summary of natural proxy data and their typical characteristics.

Natural climate archives are the only way to investigate past climate variations based on real world data (not simulated) before the instrumental period. Proxy data can help to detect and understand past climate changes and abrupt events, e.g., glaciation/deglaciation, or

Table 2.1: Summary of paleoclimatic data sources, from Saltzmann (2002).

Proxy data source	Some of the variables measured	Possible climate interference	Potential study period	Typical sampling interval
ice cores	$\delta\ ^{18}O$, δD,	temperature,	40 kyr,	1-10 yr
	CO_2, CH_4, dust,	atmospheric circulation	100-500 kyr	10-100 yr
	ice chemistry			
tree rings	ring width	temperature		
	$\delta\ ^{18}O$, δD,	precipitation (drougth)	10 kyr	1 kyr
	$\delta\ ^{13}C$, $\Delta\ ^{14}C$	solar variability		
coral	$\delta^{18}O$	SST, precip-evap,	100-1000 yr	1 month,
	Sr/Ca	sea level		1 yr
pollen	percent,	temperature,	10-100 kyr	10-100 yr
	influx	precipitation		
soils	$\delta^{13}C$,	CO_2	1-10 Myr	snapshots
	loess	wind		
closed-basin lakes	lake levels	precip-evap	10-100 kyr	snapshots
lake sediments	$\delta^{18}O$,	temperature,	10-100 kyr	10-100 yr
	diatoms	salinity		
ice sheets	former extent,	area,thickness	1 Myr	snapshots
	glacial rebound	bedrock depression		
mountain glaciers	former extent	snowline	10 kyr	snapshots
marine	$\delta^{18}O$, $\delta^{13}C$	global ice mass,	10 Myr	1 kyr
sediments	foraminiferal	ocean circulation,	500 kyr	100 yr
	assemblages	SST	50 kyr	1-10 yr
raised shoreline	evaluation	sea level	1 Myr	snapshots
		bedrock depression		
laminated	reflectance,	precipitation,		
or varved sediments	magnetic properties	wind	10 kyr	1 yr

Heinrich[9] and Dansgaard/Oeschger[10] events. Furthermore, proxy data can reveal the driving mechanisms behind these changes and which region led or lagged another one. Besides the

[9]Heinrich events are abrupt climate changes during glacial times with large ice-bergs discharging most from the Laurentide ice-sheet. These large amount of freshwater input into the North Atlantic causes a deruption of the thermohaline circulation and lead to a global cooling.

[10]Dansgaard/Oeschger (D/O) are closely related to Heinrich events but with rapid warming (about 10years) followed by a cooling over a longer period (1000a), the causes of D/O events are yet not completely understood.

interpretation of measured variables to investigate past sea level or ice volume variations (e.g., $\delta^{18}O$ in ocean cores), proxy data are used to reconstruct the local- and the large-scale climate. To reconstruct global and hemispheric mean temperature often different types of proxy data are used together (e.g., Jones et al. 1998; Mann et al. 1999; Luterbacher et al. 2004; Moberg et al. 2005), so called multi-proxy studies (Jones and Mann 2004). Recently, climate characteristics which can not be directly interpreted by proxy data were also reconstructed and investigated based on statistical methods, like circulation indices (NAM, SAM), by e.g., Cook et al. (2002) and Jones and Widmann (2003).

However, there are limitations and uncertainties in the usage of proxy data. Often the climatic interpretation of a proxy data is difficult, because generally more than one factor (climatic and non-climatic) influences the measured variable. The growth rate of tree rings for instance depends not only on temperature but also on factors such as the amount of available water and a sufficient supply of nutrients. Another uncertainty is related to the dating of proxy data. One can distinguish between four groups of dating methods: (i) radioisotopic; (ii) paleomagnetic; (iii) chemical and (iv) biological methods. Radioisotopic methods make use of the radioactive decay of unstable isotopes (e.g., ^{14}C). Paleomagnetic methods are based on past reversals of the Earth's magnetic field. Chemical methods rely on time-dependent chemical changes or characteristics in organic or inorganic samples. Biological methods are based on growth rates of layers (e.g., tree rings). Accurate dating is important to investigate if a certain climate event occurred at the same time in different regions, if two timeseries are synchronous, or if one region led or lagged another one. Accurate dating is also essential to access how fast past climate or environmental changes take place to compare proxy data with climate simulations.

2.4 Climate models used in paleoclimate research

In the last 25 years model simulations have become an important tool in paleoclimate research. Early studies have been carried out with simple models by Kutzbach (1980) or using general circulation models (GCMs) of the atmosphere (e.g., Kutzbach and Otto-Bliesner 1982; Royer et al. 1983; Prell and Kutzbach 1987). Until now a large family of models have been used to investigate past climate, from simple energy balance models to complex state-of-the-art coupled atmosphere-ocean GCMs (AOGCMs). Simulations under different boundary conditions for different periods have been investigated. So far focus has been on periods like the last millennium, the mid-Holocene and the last glacial maximum, but also on previous interglacials and glacial cycles. Model simulations are used to investigate the influence of external forcings on climate dynamics and to identify which forcing or mechanism is potentially responsible for certain changes within the climate system. For many questions in paleoclimate research it is necessary to know on which spatial scale a climate change happened or how a certain

regional climate change is related to a process in another region.

Which type of climate model one should use depends on the spatial resolution needed to answer a certain question and on the available computational resources. In the next section a short overview of different types of climate models that are commonly used in paleoclimatology is presented.

2.4.1 Types of climate models

- Energy balance models (EBMs) are the simplest physical atmosphere models. They are based on the thermodynamic balance between net in- and outgoing radiative fluxes. They range from a simple zero-dimensional approach, which predicts the global equilibrium temperature, to one- and two-dimensional models. The latter for instance include the vertical structure of the atmosphere and the horizontal heat transport in a parametrized way. EBMs are of low computational costs and are primarily used to investigate the sensitivity of temperature to changes of the incoming radiation or greenhouse gas concentrations (e.g., Crowley and Kim 1995; Crowley 2000; Hegerl et al. 2006).

- Earth system models of intermediate complexity (EMICs) are based on simplified equations of the atmosphere and ocean dynamics but also contain other parts of the climate system (e.g., vegetation or ice sheets). Climate processes, feedback mechanisms and interaction between different parts of the climate system are often parametrized. These simplifications make it possible to run such models for long periods of time and allow for many simulations under different boundary conditions (so called ensemble studies). EMICs are often used in paleoclimate studies, for instance to test the sensitivity of the climate system to different forcings and the interaction between different parts of the climate system (e.g., Kubatzki et al. 2000; Weber 2001; Crucifix and Loutre 2002; Wasson and Claussen 2002). However, due to the simplifications and the normally coarse spatial resolution, it is often difficult to compare EMIC results with proxy data or to investigate processes that are parametrized in an EMIC. Nevertheless, results from EMICs often focus on a certain region or process that is important for key mechanisms of climate variations. An overview of EMICs and their role in climate science is given by Claussen et al. (2002).

- GCMs are complex climate models. They are based on physical equations taking into account the exchange of energy, mass and momentum and dynamical processes in all three dimensions at all gridpoints. Depending on the horizontal and vertical resolution some processes still need to be parametrized e.g., convective cells in the ocean and the atmosphere. These calculations require a lot of computer power limit the length and number of the simulations (e.g., sensitivity tests and ensemble simulations) that can be obtained in an adequate time. With increased computer power simulations could

be carried out for longer periods and/or with higher resolution. Especially in paleoclimate research long simulation periods or large numbers of runs for sensitivity studies are required to understand climatic variations. To reduce the computational effort, often atmosphere (e.g., Hall and Valdes 1997) or ocean-only GCMs (AGCM or OGCM respectively) are used. A step towards a more complete coupled system between atmosphere and ocean are AGCMs with a slab or mixed layer ocean (e.g., Vettoretti and Peltier 2004). In recent years more and more fully coupled AOGCMs have been used in paleoclimate research (e.g., Cubasch et al. 1997; Montoya et al. 2000; Collins et al. 2002; Zorita et al. 2004).

- Earth System Models are the most recent type of climate models. They consist of classical AOGCMs that are interactively coupled to models for other parts of the climate system, like the biosphere, carbon cycle, atmospheric chemistry, continental ice sheet or the stratosphere. Such models are computationally expensive and until now only few paleoclimate simulations exists (e.g., Gallimore et al. 2005; Schrugers et al. 2006).

2.4.2 Comparing proxy data and climate model simulations

For a comprehensive understanding of past climate variations it is necessary to use both proxy data and model simulations. In recent years an increasing number of proxy-model data comparison studies have been undertaken. They have helped to validate model results and to increase the reliability of future climate scenarios by simulations. Furthermore, a comparison helps to understand which processes and climate variables are responsible for certain changes or variations in proxy data and to understand the dynamics behind these variations.

But as proxy data and model simulations provide climate information on different spatial scales, one has to bridge this scale difference to compare and combine proxy data with climate model output.

A straightforward approach is to compare the proxy-based climate information directly with the output of a climate model simulation. One either compares the temporal climate variability (e.g., Collins et al. 2002; Weber 2005) or a spatial pattern (e.g., Kaspar et al. 2005). But a prerequisite for such a comparison is a good spatial coverage of the proxy data. Another possible way to close the scale gap would be to use regional climate models, which are driven by large-scale climate simulated by GCMs under past forcing conditions. But until now only few regional climate model experiment exists for previous periods before the last century (e.g., Diffenbaugh and Sloan 2004) and they are computational expensive.

There are also other approaches to handle the scale discrepancy between proxy data and climate simulations. One is e.g., based on a standard statistical downscaling approach. This approach uses meteorological data of the large-scale (e.g., SLP) and the local-scale (e.g., precipitation) to setup a downscaling model. These model are then applied to the simulated

large scale field of a GCM to estimate the local parameters. This estimate could directly compared with a reconstructed timeseries based on one or a set of proxy data (e.g., Wagner et al. 2007). Another method uses a climate timeseries on the local-scale, based on statistical methods or non-statistical methods, to estimate a measured proxy data variable, such as tree ring width, ice core layers or mass balance of glaciers. This simulated proxy data variable is then compared with the measured variable of the real proxy data. This method of directly simulating the proxy data with local climate data, is also called forward modeling (e.g., Reichert et al. 2001; Weber and Oerlemans 2003; González-Rouco et al. 2006).

Another approach uses a reconstructed timeseries based on a proxy data as a predictor for an upscaling model to generate a large-scale climate pattern. This large scale pattern is then compared with the model output (e.g., Zorita et al. 2004). Recent studies aim to assimilate this large- scale patterns into climate simulations using different methods (e.g., von Storch et al. 2000; van der Schrier and Barkmeijer 2005; Widmann et al. 2007b), to provide model results that are closer to the real world climate and to better understand climate variations and relations between different climate variables.

Chapter 3

Sensitivity of atmospheric scale relationships to orbital forcing

3.1 Introduction

In this chapter an extended summary of the two publications (Groll et al. 2005; Groll and Widmann 2006) is presented. Additionally some material and images are taken or adapted from Widmann et al. (2007a). First a description of the used model and the experimental setup of the used simulations is given. The response of the mean climate and the extratropical Northern Hemispheric circulation variability to orbital forcing variations is discussed in section 3.4 and section 3.5 for all simulations, which is also discussed in Groll et al. (2005). The content of section 3.5 is mostly taken from Widmann et al. (2007a). The sensitivity of the relationship between the large-scale circulation and the regional temperature to orbital variations is presented in section 3.6, which is the main scope of Groll et al. (2005). Finally, section 3.7 discusses the sensitivity of the relationship between Northern Hemisphere regional temperatures in different regions to orbital variations, which is the main focus in Groll and Widmann (2006) and is also partly discussed in Widmann et al. (2007a) but for different regions. Compared to Groll et al. (2005) and Widmann et al. (2007a) in this summary all discussed results are on annual timescales instead of multi-year to multidecadal timescales. Note analysis of the mean climate and the dominate mode of circulation variability is investigated on annual timescales in all publications. Additionally not shown results for the glacial inception simulation are included and a new explicit comparison between the early Eemian and glacial inception simulation for most analysis are presented in this chapter.

3.2 Model description

The climate model ECHO-G (Legutke and Voss 1999) used in this study, consists of the atmosphere model ECHAM4 (Roeckner et al. 1996) and the ocean model HOPE-G. The ocean model HOPE-G is an improved version of the ocean model HOPE (Wolff et al. 1997) which includes a thermodynamic-dynamic sea ice model. All models are developed at the Max Planck Institute for Meteorology in Hamburg.

ECHAM4 is the fourth generation of an atmosphere general circulation model which originates from a spectral weather prediction model of the European Center for Medium-Range Weather Forecast (ECMWF). In this study the ECHAM4 model is integrated with a spectral horizontal resolution of T30 (approximately 3.75° x 3.75°). It contains of 19 irregular vertical levels on a hybrid sigma-pressure coordinate system, with highest resolution in the atmospheric boundary layer and a vertical extension up to a pressure level of 10 hPa (approximately 30 km).

The ocean general circulation model HOPE-G is used with a horizontal resolution of about 2.8° x 2.8° with a meridional grid refinement in the tropical regions for the purpose of simulating a more realistic ENSO variability. The ocean model consists of 20 irregular vertical levels.

The models are combined by the coupling software OASIS (Terray et al. 1998) and a flux correction for heat and freshwater is applied to avoid a climate drift. Both fluxes are constant in time and zero when averaged globally over the ocean.

3.3 Experimental setup

1000 years of three existing quasi-equlibrium simulations with fixed external forcing are analyzed:

- A preindustrial simulation (hereafter PI) with present day insolation and greenhouse gas concentrations at 1800 AD (Lorenz and Lohmann 2004).
- A last interglacial simulation (hereafter EEM) with insolation at 125 kyr BP - the early Eemian - with respective greenhouse gas concentrations (Kaspar et al. 2005).
- A last glacial inception simulation (hereafter GI) with insolation at 115 kyr BP, with respective greenhouse gas concentrations (Cubasch et al. 2006).

Insolation for a given set of orbital parameters is calculated according to Berger (1978) and differences to present day insolation are shown in Fig. 3.1. For the period of the last interglacial insolation is higher during boreal summer, but lower during austral summer. For the period of the last glacial inception insolation is lower during boreal summer and higher during austral summer, but the magnitude of insolation differences is somewhat smaller compared to the

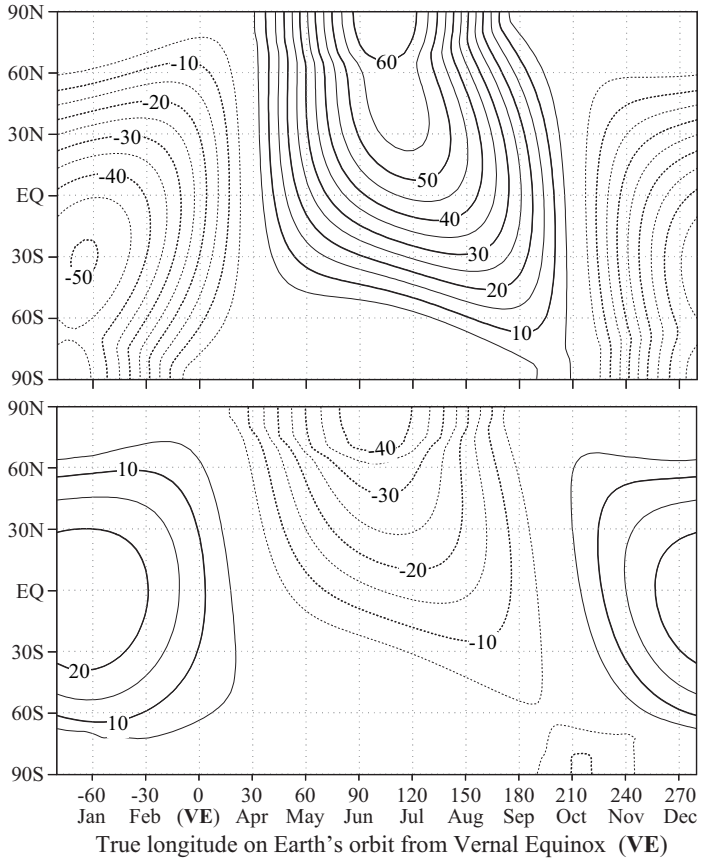

Figure 3.1: Zonally averaged insolation anomalies (relatively to today's insolation) between 125 kyr before present (upper) and 115 kyr before present (lower) as a function of true longitude on the earth's orbit from vernal equinox, units in Wm^{-2}, according to Berger (1978).

insolation differences at 125 kyr BP. Not only the absolute insolation values for a specific month and latitude change, but also the meridional gradient between the polar region and the Equator changes. Greenhouse gas concentrations (GHG conc.) are taken from the Vostok ice core (CO_2 and CH_4: Petit et al. 1999; N_2O: Sowers 2001).

In all simulations a small global temperature trend is evident (not shown). Additionally, the GI simulation shows an increase of Northern Hemisphere snow cover due to the lower insolation during boreal summer (Cubasch et al. 2006). The first 1000 years of the GI simulation are used, which show only a slight increase of snow cover. To compensate for the trend in snow cover and the global temperature trend in the simulations, all model output used in this study is detrended at each grid cell separately prior to the analysis. In particular, the trend in the GI simulation indicates that under constant orbital forcing conditions at 115 kyr BP no stable

Table 3.1: Greenhouse gas concentration (GHG conc.) and earth orbital parameters used in the three experiments (exp). PI: simulation with preindustrial GHG conc. and today's orbital parameters; EEM and GI: simulation with GHG conc. and orbital parameters of 125 kyr BP and 115 kyr BP respectively; vernal equinox (VE).

exp	CO_2 (ppm)	CH_4 (ppb)	N_2O (ppb)	Eccent. (%)	Obliquity axis tilt (°)	Perihelion (° from VE)
PI	280	700	310	1.67	23.44	282.7
EEM	270	630	260	4.00	23.79	127.3
GI	265	520	270	4.14	22.41	290.9

climate could establish. However, the first 1000 years of the GI simulation could be treated as a snapshot at the start of the glacial inception. Furthermore, insolation at 115 kyr BP is at the other end of the orbitally induced insolation variations compared to 125 kyr BP. The range of this insolation differences helps to identify the sensitivity of large- to regional-scale relationships to orbital variations.

Vegetation is fixed to its modern state in all simulations and therefore possible feedbacks of a changed vegetation to the climate system (Claussen et al. 2003) are not included in this analysis. But, short test simulations with a changed vegetation but the same orbital parameters show only minor differences in the large-scale climate (Frank Kaspar pers. com.). Besides changes in the insolation, variations of the orbital parameters also lead to a different length of the seasons (Joussaume and Braconnot 1997). The effect of an expansion or reduction of seasons on the discussed results was tested by adding or omitting one month to the standard definition of the season. Results (not shown) show smaller differences than differences between the simulations. Therefore the standard definition[1] of the seasons is used in all discussed results. After a model spin up of 1300 years for PI and 1000 years for EEM and GI, a 1000 yr long simulation period is analyzed. Orbital parameters and GHG conc. of the three simulations are shown in Table 3.1.

3.4 Mean climate

For a basic understanding of the effect of a different distribution of the solar energy at the top of the atmosphere to the climate system, the large-scale mean climate in terms of seasonal means of 2m-temperature and sea level pressure (SLP) of the three simulations is illustrated in Fig. 3.2 (JJA[1]) and Fig. 3.3 (DJF[1]).

The higher boreal summer insolation during the early Eemian leads to higher temperatures

[1][December-February](DJF); [March-May](MAM); [June-August](JJA); [September-November](SON)

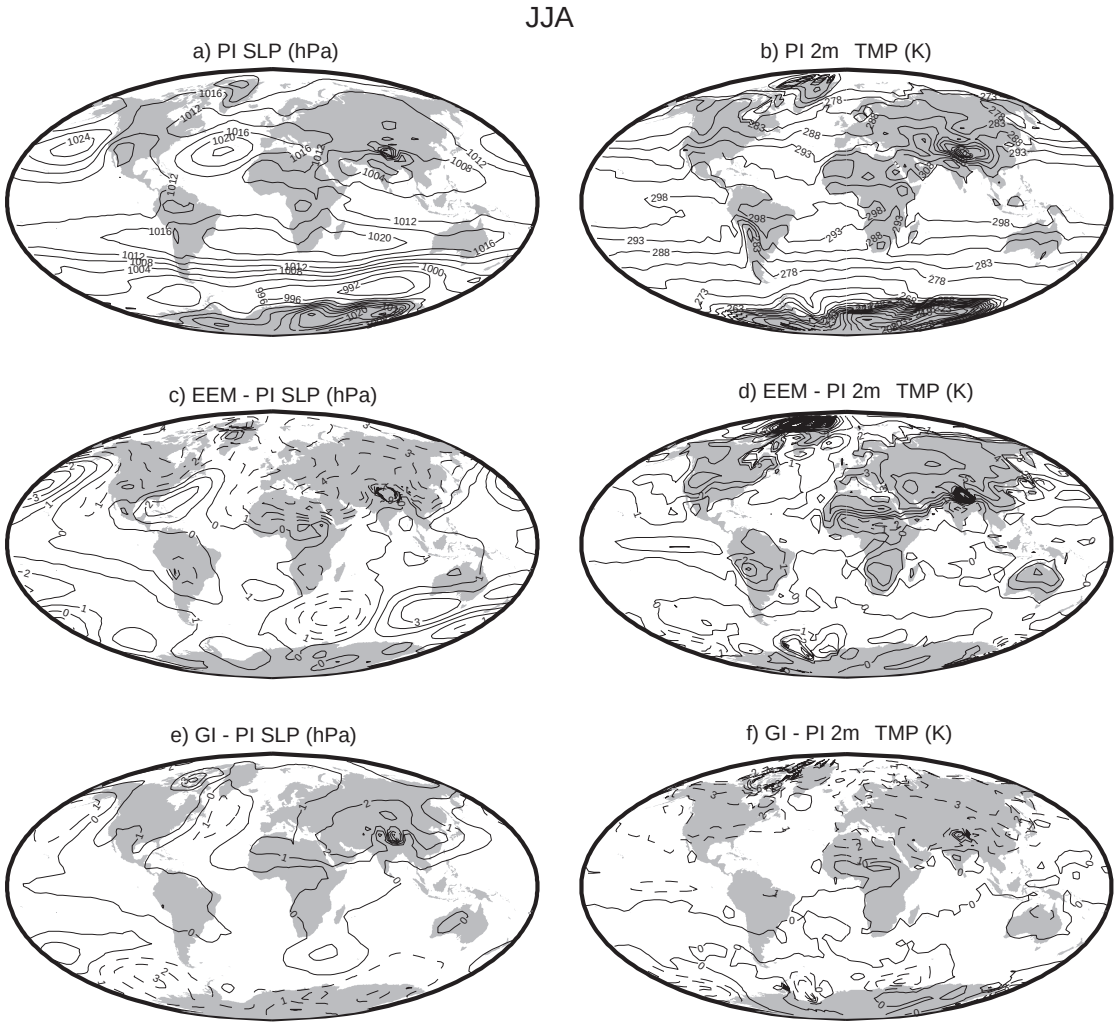

Figure 3.2: Mean sea level pressure (a) and 2m-temperature (b) for JJA in the preindustrial simulation (PI). Mean JJA SLP (c) and 2m-temperature difference (d) between the Eemian and the preindustrial simulation (EEM-PI), and the mean SLP (e) and 2m-temperature difference (f) between the glacial inception and the preindustrial simulation (GI-PI).

in the EEM simulation compared to the PI simulation, except for the monsoon regions in Africa and India. Higher insolation leads to a strengthening of the monsoon, i.e. an enhanced moisture transport from sea to land. This is consistent with stronger 10m-winds in the EEM simulation for these regions (Fig. A.3). Lower insolation during boreal winter months in the early Eemian result in overall lower temperatures in the EEM simulation compared to the PI simulation, except for northeastern Europe. The higher temperatures in this region can be explained by stronger westerlies, causing advection of mild maritime air masses from the North Atlantic toward Europe.

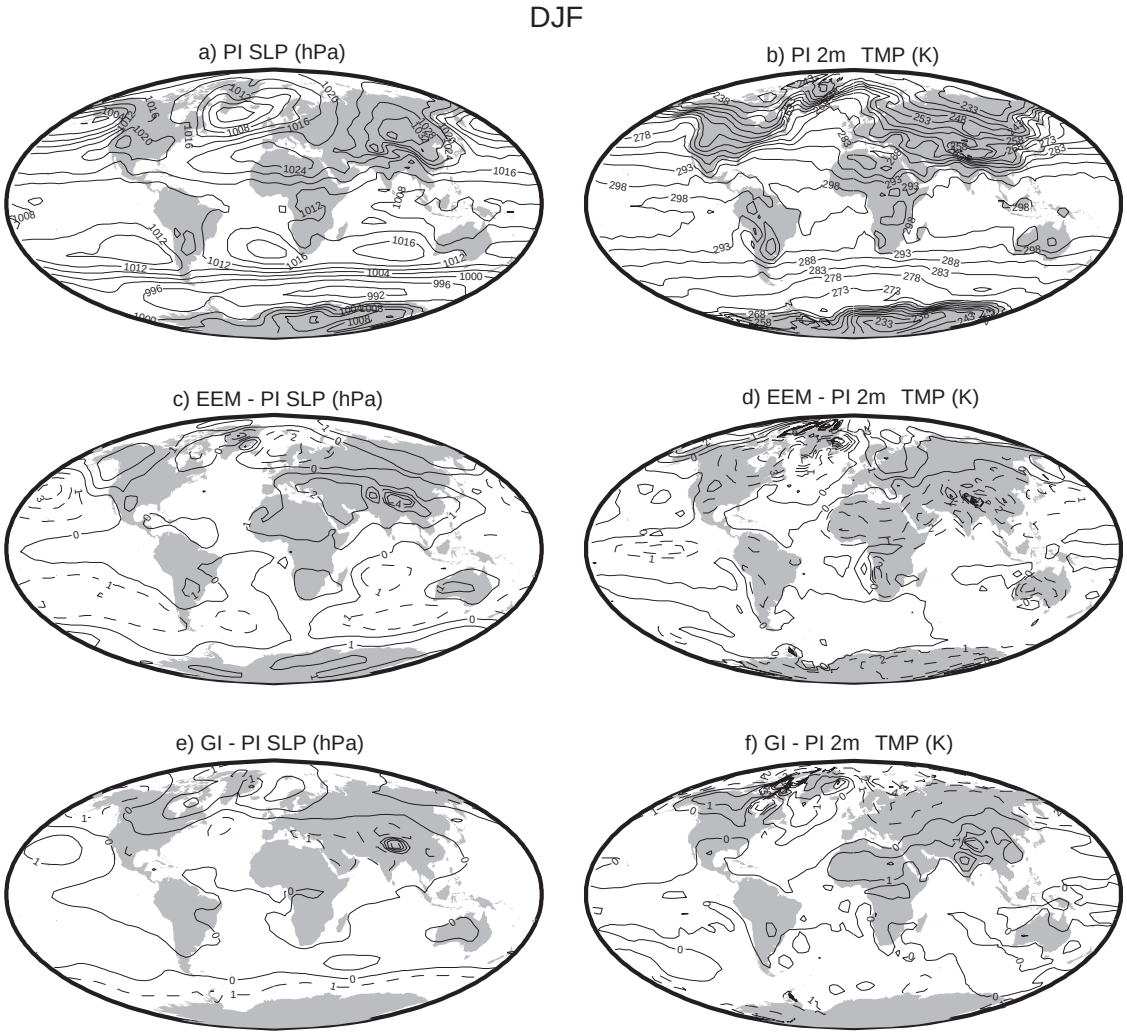

Figure 3.3: As Fig. 3.2, but for DJF. Image from Widmann et al. 2007a

Temperatures in the GI simulation are globally lower during boreal summer, consistent with the lower insolation at 115 kyr BP. Boreal winter temperatures are slightly higher compared to the PI simulation, consistent with the higher insolation. Again, temperatures in northeastern Europe show an opposite sign and are lower in the GI than in the PI simulation. This temperature change could also be explained by modified westerlies in the GI simulation. These changes of the westerlies in the EEM and the GI simulations compared to the PI simulation show that not only temperature is affected by a changed insolation but also the atmospheric circulation.

The response of the atmospheric circulation to changes of the insolation has also been found by many other authors (e.g., Cubasch et al. 1997; Gladstone et al. 2005; Kaspar et al.

2005; Hall et al. 2005). The difference of the mean SLP field over the North Atlantic shows negative deviations over the Norwegian Sea between the EEM and the PI simulation (Fig. 3.3c). This SLP pattern could be interpreted as a positive Northern Annular Mode (NAM) - like phase over the North Atlantic/ European sector, also found by Felis et al. (2004). SLP differences between the GI and PI simulation are inverted to the EEM-PI differences (Fig. 3.3e) and resemble a negative NAM-like state. A physically plausible explanation for the NAM-like response of the atmospheric circulation is given by Robinson (2000) and by Kushnir et al. (2002). They state that changes of the meridional temperature gradient lead to a generation of lower-tropospheric baroclinic eddies and to a convergence of the upper-tropospheric eddy momentum flux, which result in a NAM-like change in the North Atlantic atmospheric circulation. The relevance for orbitally controlled changes of this mechanism over the last 165 kyr is shown by Hall et al. (2005).

3.5 Extratropical atmospheric circulation variability

As the main focus of this study is on scale relationships between circulation and temperature variability, the dominant mode of circulation variability in the extratropical Northern Hemisphere, the Northern Annular Mode, is investigated. The NAM is defined as the first empirical orthogonal function (EOF) of extratropical SLP (90°-20°N), which is shown for boreal winter and summer on annual timescales in Fig. 3.4. The principal component of the first EOF (EOF1) is also called the Northern Annular Mode Index (NAMI). The EOF values, the so-called EOF loadings, are scaled to be the pressure changes associated with a positive change of one standard deviation in the NAMI.

The overall pattern is similar in all three simulations. In general, a pronounced dipole over the North Atlantic corresponding to the North Atlantic Oscillation and a weaker dipole over the North Pacific are evident in winter. The EOF loadings are slightly larger in the EEM simulation during winter in the Atlantic sector, and smaller during winter in the Pacific compared to the other two simulations. There are only small differences in summer between the EEM and PI simulations. In the GI simulation the Pacific centre is stronger during winter than in the EEM and PI simulation and similar over the Atlantic sector. In summer the NAM is slightly stronger in the Arctic centre in the GI simulation than in the other two simulations. The fraction of variance explained by EOF1 is very similar in all simulations and seasons. The second and third EOFs do not differ much between the simulations (not shown).

Not only the mean SLP field and the dominant mode of the circulation variability are considered, but also the characteristics of the SLP field at high and low NAMI states. This is done using composite maps, which show the mean SLP field over a sample of seasons where the NAMI is higher or lower than two times the NAMI standard deviation. The results for winter on annual timescales are shown in Fig. 3.5 and differences of EEM-PI and GI-PI of

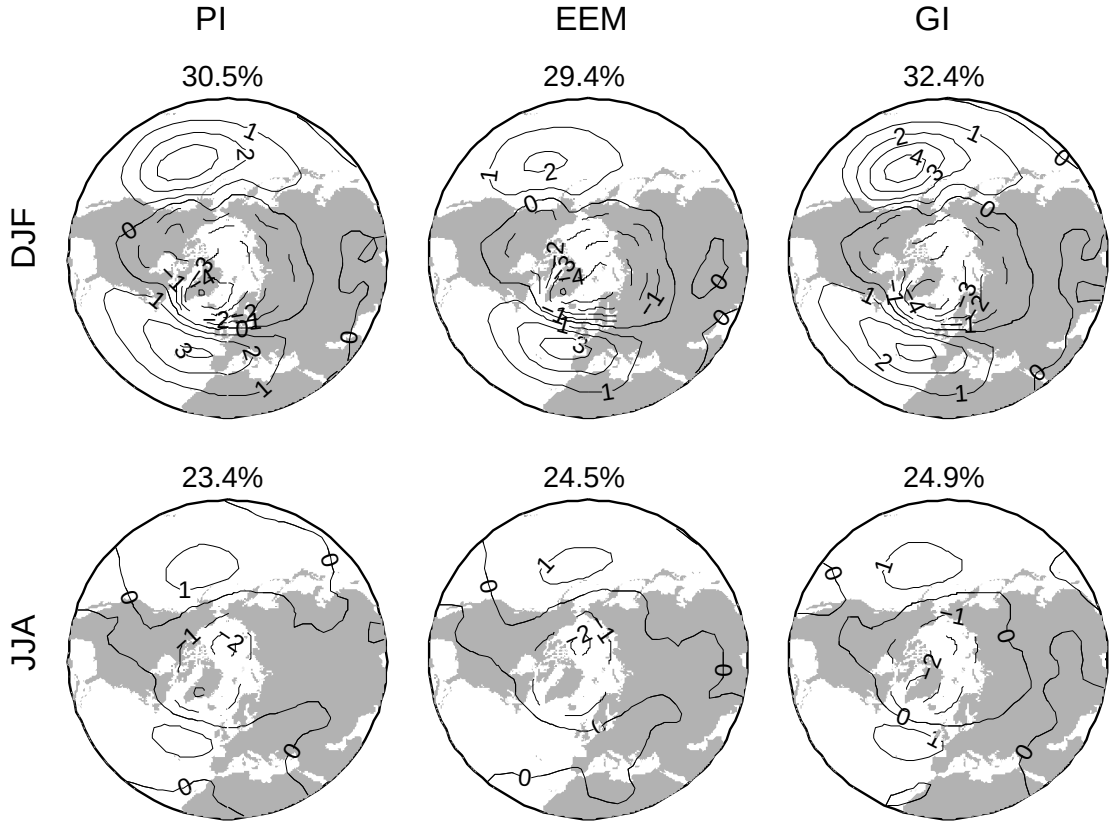

Figure 3.4: First simulated extratropical EOF for seasonal SLP on annual timescales: DJF (top), JJA (bottom); PI simulation (right), EEM (center), GI (left). Corresponding explained variance on top of each panel. Similar to Fig. 34.2 in Widmann et al. 2007a.

the corresponding composite maps are shown in Fig. 3.6. Consistent with the stronger mean westerlies during winter over Eurasia, the westward atmospheric flow at positive and negative NAM phases extends further into Eurasia in the EEM compared to the other two simulations. Whereas the atmospheric flow over western Europe at positive NAM states is westerly in all simulations, winds are weak at negative NAM states in the PI and GI simulation, but still somewhat stronger in the EEM simulation. Between western Siberia and the Lake Baikal region a strong SLP gradient at positive NAM situations is evident in the EEM, but not in the other two simulations. For a negative NAM there is no westerly flow over this area in all simulations. Composite maps for spring show similar differences as for winter (not shown), whereas for summer and autumn no substantial differences between the simulations are evident (not shown).

Although the similarity of the NAM patterns (first SLP EOF) implies that the absolute SLP difference between positive and negative NAMI situations is similar in all simulations,

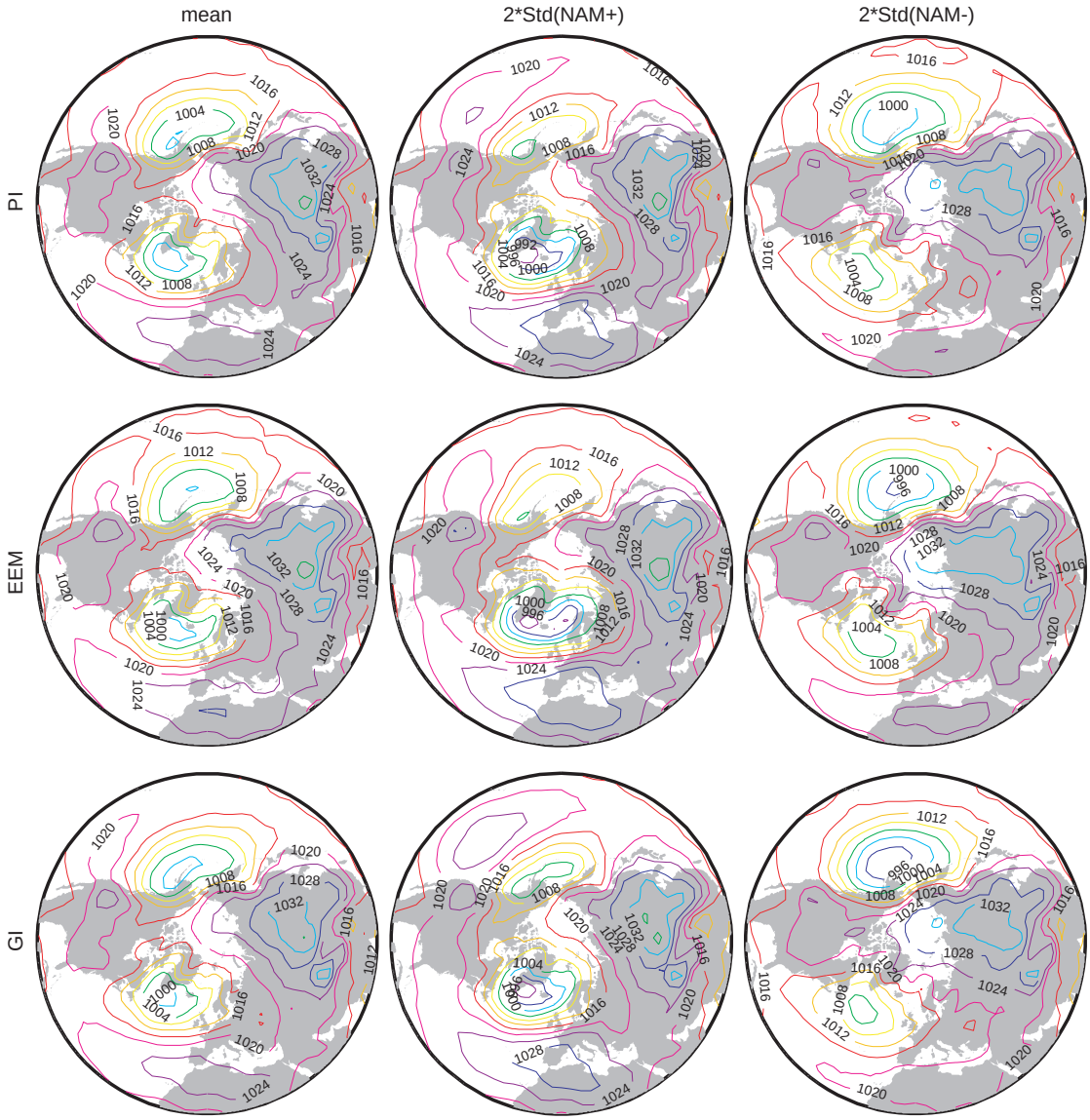

Figure 3.5: Mean SLP field (left) and composite maps of winter SLP for strong positive (middle) and negative (right) NAM situations on annual timescales. PI simulation (top), EEM (middle), GI (bottom). Similar to Fig. 34.3 in Widmann et al. 2007a.

results in winter suggest that the difference in the atmospheric flow characteristics between positive and negative NAMI phases over Europe (western Siberia) is smaller (larger) in the EEM simulation than in the PI and GI simulation. This discrepancy between the similar NAM and the differences in the composite maps can be understood in the following way: Even if the absolute difference (between positive and negative NAMI states) in the wind speed (related to the SLP gradient) is the same, the flow character could range either from

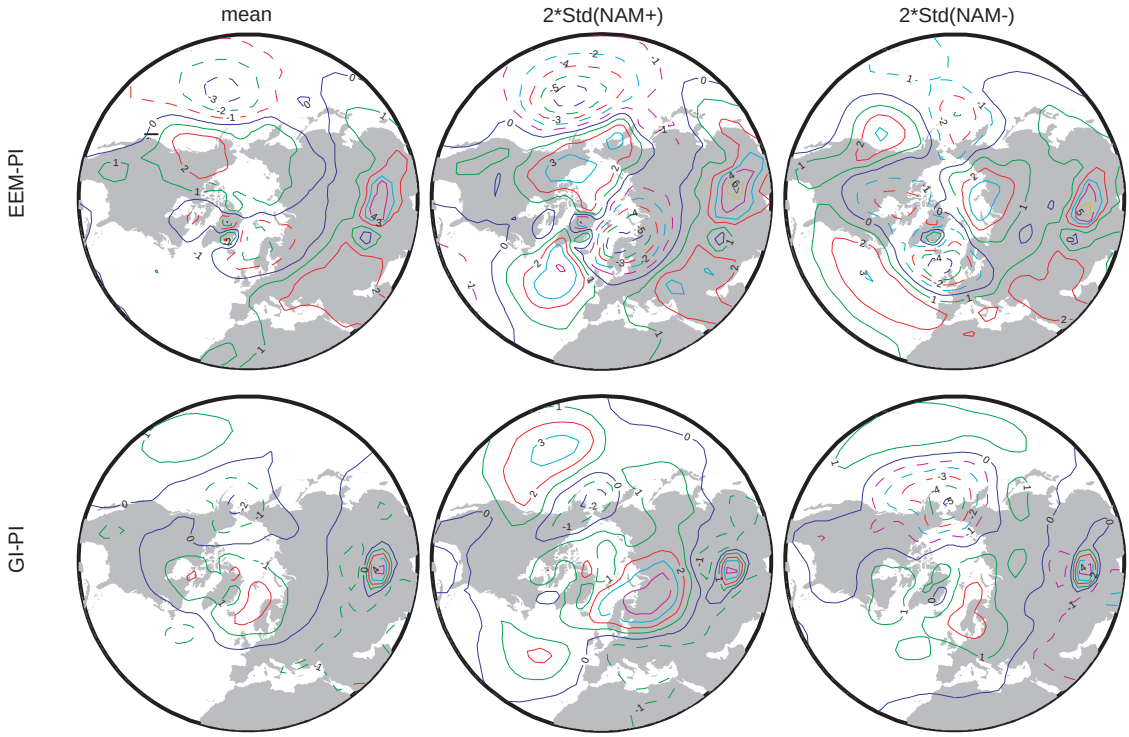

Figure 3.6: Differences of the mean SLP field (left) and differences of composite maps of winter SLP for strong positive (middle) and negative (right) NAM situations. EEM-PI simulation (top), GI-PI (bottom).

very weak to moderate (in PI and GI) or from moderate to strong (in EEM). The first could be expected to make a larger difference for the regional climate than the latter. This potentially nonlinear relationship between the atmospheric flow and regional climate may lead to a changed relationship between the NAMI and the regional climate, even if the NAM pattern does not change. In particular, this effect could lead to a weaker (stronger) relationship between European (western Siberian) temperatures and the NAMI in the early Eemian compared to the other two periods.

3.6 Relationship between atmospheric circulation and northern hemisphere temperature

3.6.1 Northern Annular Mode - temperature signal

To test the hypothesis that the influence of the NAM on temperature variability is sensitive to orbital forcing in some regions, the relationship between the NAMI and temperature during the three periods on annual to multidecadal timescales is investigated. Regression and

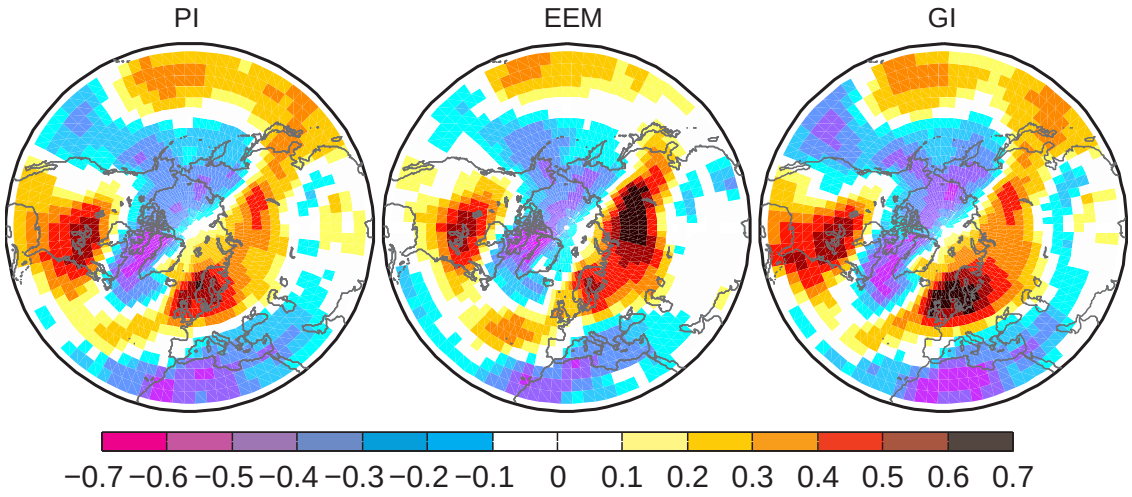

Figure 3.7: January NAM-temperature signal as correlation coefficients on annual timescales for three simulations: PI, preindustrial simulation (left); EEM, early Eemian simulation at 125 kyr BP (middle); GI, glacial inception simulation at 115 kyr BP(right). All correlations are significant at the 5% level.

correlation coefficients between the NAMI and the 2m-temperature in the three simulations are analyzed.

The correlation coefficients for January on annual timescales are shown in Fig. 3.7. In all three simulations the overall spatial structure resembles the observed NAM-temperature signal (Hurrell 1995; Thompson and Wallace 2000) reasonably well (not shown). All three simulations show large areas where the NAM influences regional temperature variability with correlation coefficients of up to 0.6. Positive correlations exists over the Eurasian continent and North America which identify the relationship between high storm activity over the North Atlantic and corresponding mild winters in Europe at positive NAMI. Negative correlations are evident over the Mediterranean, the western Arctic and the eastern Pacific. This leads, for instance, to warm winters in the Labrador region due to less inflow of arctic air masses in situations with a negative NAMI.

The overall pattern of the NAM-temperature signal is similar in all three simulations, but differences in the magnitude of the signal and the location of the maxima are evident. To identify the changes between the simulations, differences of the correlation coefficients are shown in Fig. 3.8. Differences between the EEM and the PI simulations show negative deviations of correlation coefficients from western Europe to the Norwegian Sea, over the southern part of North America and south of Japan. Positive deviations are evident over the Labrador Sea, the west coast of North America and parts of North Africa. As the absolute NAM-temperature signal has the opposite sign as these deviations, the NAM-temperature

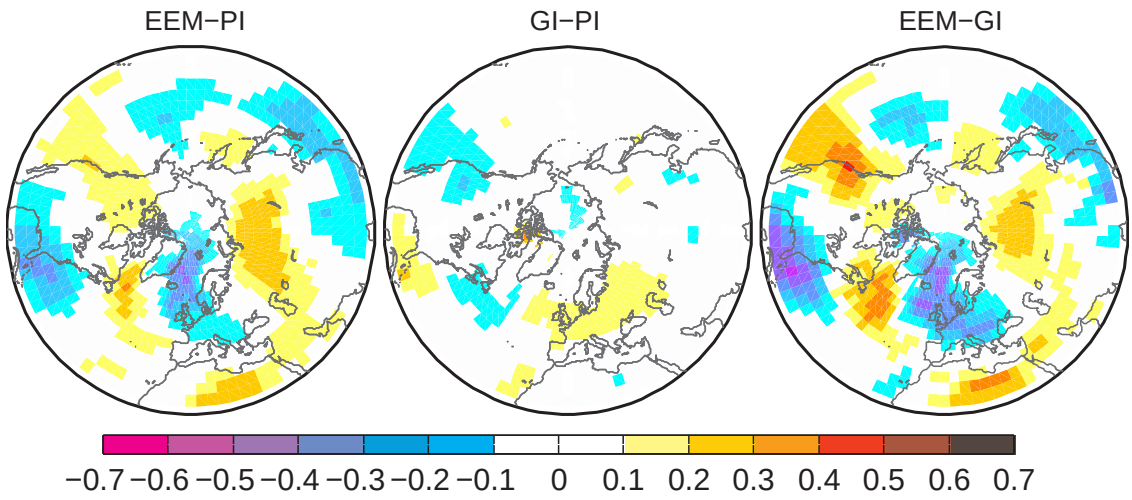

Figure 3.8: As Fig. 3.7, but differences of the NAM-temperature signal between the simulations, EEM-PI (left), GI-PI (middle) and EEM-GI (right). All correlations are significant at the 5% level.

signal is weaker over these regions in the EEM than in the PI simulation. Only the positive deviations over central Siberia show that the correlation coefficients between the NAMI and the temperature are higher in the EEM than in the PI simulation. Hence, the NAM explains less northern hemisphere temperature variability in the early Eemian than in the preindustrial simulation, except for central Siberia.

The NAM-temperature signal in the GI simulation is more similar to the PI than the EEM to the PI simulation. However, there are still some differences between the simulations. Positive (western Europe to the Ural and Gulf of Mexico to the Saragossa Sea) and negative (American west coast) deviations indicate that the NAM-temperature signal is slightly stronger in the GI compared to the PI simulation.

Consistent with the large insolation differences, deviations of the NAM-temperature signal between the EEM and the GI simulation are larger in magnitude and in their spatial extent compared to the other two differences (EEM-PI; GI-PI). The deviations of the correlation coefficients indicate that the NAM-temperature signal is generally smaller in the EEM compared to the GI simulation, except for central Siberia.

The DJF NAM-temperature signal between the EEM and the PI simulations on multidecadal timescales (Fig. A.6) shows similar deviations compared to differences on the annual timescale.

3.6.2 Large-scale circulation and central European temperature

The analysis of the NAM-temperature signal shows that in central Europe the NAM explains less temperature variability in the EEM than in the PI simulation. However central European temperature (CET) is still influenced by circulation variability, but different to the NAM. To identify which circulation pattern is most linearly linked to CET, regression and correlation coefficients between the CET and the SLP-field over the North Atlantic/European domain are calculated (Fig. A.7). CET is defined as the mean of the 2m-temperature at eight grid cells in western and central Europe.

In both simulations the regression coefficient pattern is synoptically plausible. The SLP field over the northern North Atlantic is negatively correlated with the CET, which indicates that lower pressure over Iceland leads to a positive CET anomaly due to enhanced zonal flow and vice versa. The Mediterranean and the southern parts of the North Atlantic are positively correlated with the CET, which shows that higher pressure leads to a more southwesterly flow toward Europe, which result in a positive CET anomaly. The difference map between the EEM and the PI simulation shows that in the EEM simulation the influence of the SLP variability on the CET variability is concentrated over the northern North Atlantic. The difference between the two simulations shows a pattern similar to an inverted NAM pattern, which is consistent with the reduced NAM-temperature signal over Europe in the EEM simulation. Hence, if one wants to estimate circulation variability, in terms of SLP variability, from temperature sensitive proxy data, one has to be aware of the changed upscaling pattern.

3.7 Temperature teleconnections

To investigate whether the discussed changes of the NAM-temperature signal have an effect on temperature teleconnections in the Northern Hemisphere, the link between simulated temperatures at different locations is investigated using the same GCM simulations as above. Besides the study of the effect of circulation on temperature teleconnections, an improved understanding of temperature teleconnection also helps to decide whether high temporal resolution temperature estimates from proxy data from different locations can be expected to have similar or opposite variations. As in this study quasi-equilibrium simulations are used, only the part of temperature teleconnections that is due to internally variability could be investigated. The influence of more rapidly changing external forcings compared to orbital variations, like solar or volcanic forcing, on the temperature variability could not be investigated. The part of internally generated variability that is responsible for the link between temperatures in different regions is mainly triggered by circulation variability. I.e., if the simulated circulation variability is realistic, the simulated temperature teleconnections can be expected to partly account for the real-world teleconnections and thus for temperature teleconnections found in empirical data. Furthermore, differences of temperature teleconnections

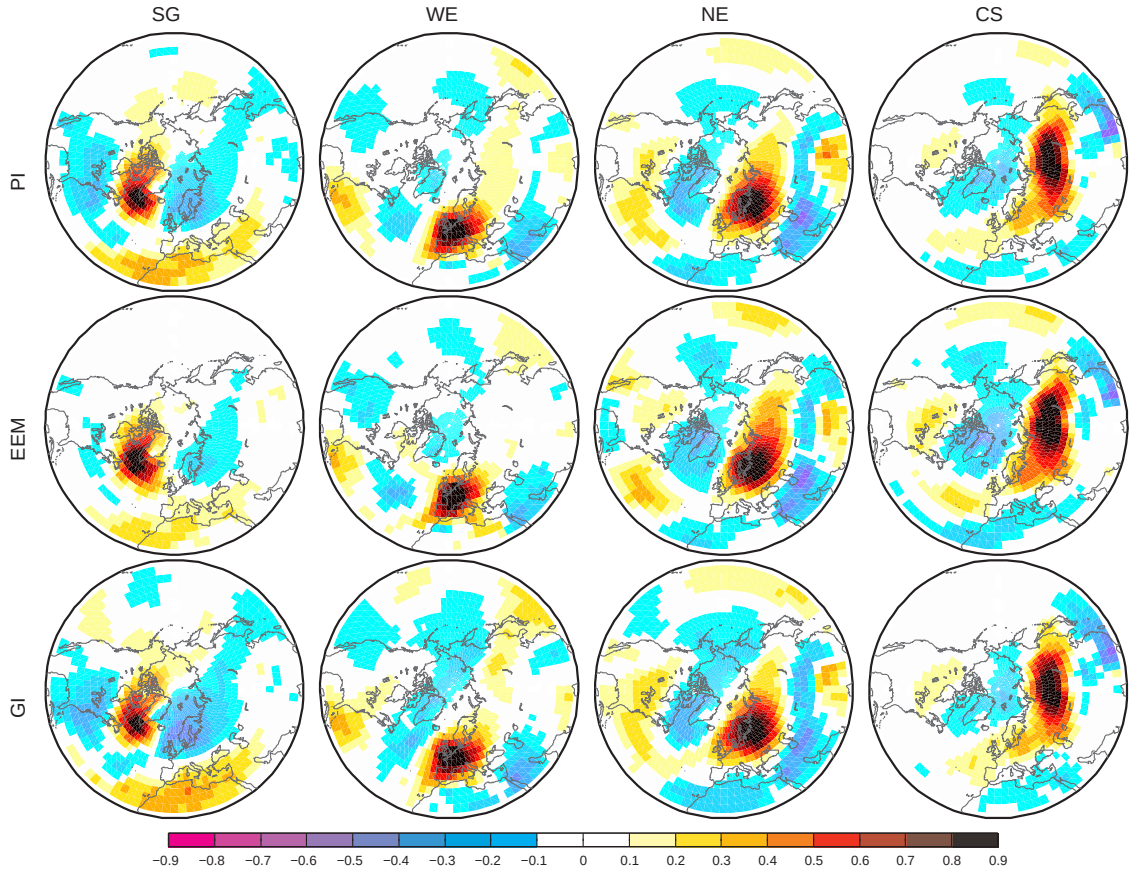

Figure 3.9: Temperature teleconnections as correlation maps between annual January 2m-temperatures for a reference region and for all other grid points. First column, South of Greenland (SG); second column, western Europe (WE); third column, northeastern Europe (NE); fourth column, central Siberia (CS); first row, PI; second row, EEM; third row, GI. All correlations are significant at the 5% level.

between the three quasi-equilibrium simulations are due to modified internally generated variability and also to the orbitally forced circulation variability. The temperature teleconnections of four regions for January on annual timescales are compared (Fig. 3.9):

- south of Greenland (SG)
- western Europe (WE)
- northeastern Europe (NE)
- central Siberia (CS)

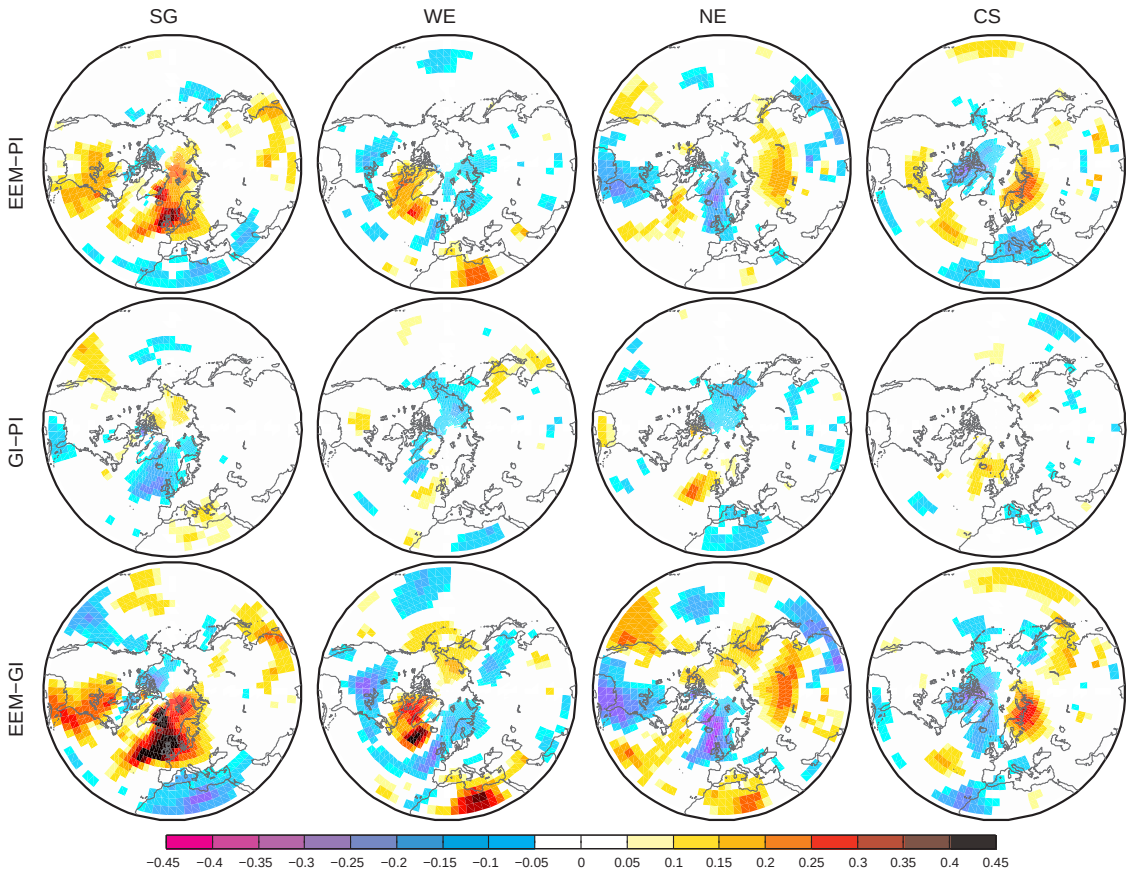

Figure 3.10: Differences of temperature teleconnections as correlation maps between annual January 2m-temperatures for a reference region and for all other grid points. First column, South of Greenland (SG); second column, western Europe (WE); third column, northeastern Europe (NE); fourth column, central Siberia (CS); first row, EEM-PI; second row, GI-PI; third row, EEM-GI. All differences of correlations are significant on the 5% level.

Regions are selected with respect to an expected sensitivity of the NAM-temperature signal and are defined as the spatial mean of the 2m-temperature over six grid cells that cover the investigated areas. Each region shows a highly positively correlated area around its centre in all three simulations, due to the autocorrelation of nearby grid cells. The overall spatial structure of the teleconnection pattern is similar in all simulations. However small differences between the simulations are evident. Temperature teleconnections for SG are weaker for most regions of the Northern Hemisphere in particular over an area from western Europe to the Arctic Sea and for parts in North America in the EEM compared to the other two simulations. WE temperature also shows weaker teleconnections around the Labrador Sea or even changes the sign in the EEM simulation compared to PI. Teleconnections for NE

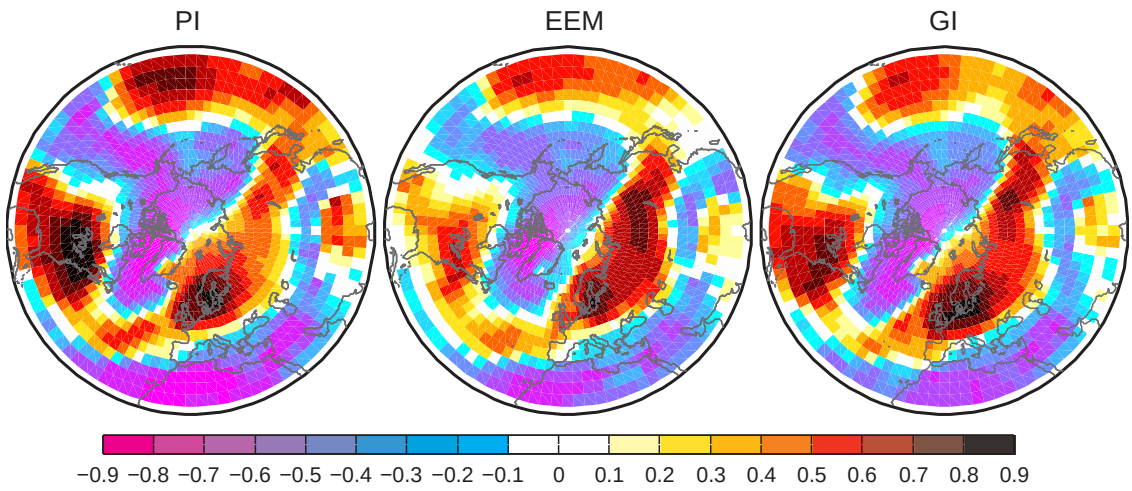

Figure 3.11: Pattern correlation between one-point temperature correlation maps and the NAM-temperature signal for January on annual timescales for PI (left), EEM (middle) and GI (right). All correlations are significant at the 5% level.

temperatures in the EEM simulation are weaker around the Labrador Sea and change sign over the Gulf of Mexico and along the east coast of North America compared to the two other experiments. NE teleconnections are also stronger east of Greenland and for parts in Siberia in EEM simulation. CS teleconnections are generally stronger in the EEM simulation. Temperature teleconnections in the GI and PI simulation are very similar, except for the area SG, where they are stronger over the northeastern North Atlantic in the GI simulation. Again, the differences between the EEM and the GI simulation are larger than differences between these two and the PI simulation.

The temperature teleconnection differences (Fig. 3.10) between the simulations are consistent with the differences of the NAM-temperature signal (Fig. 3.8). For regions where the NAM-temperature signal is weaker in the EEM simulation compared to the other simulations, temperature teleconnections for these regions are also smaller and vice versa. For instance, the weaker NAM-temperature signal over south of Greenland, western Europe and south-eastern North America is consistent with the generally smaller temperature teleconnections for SG and WE temperatures and the stronger NAM-temperature signal over central Siberia is consistent with the generally stronger CS teleconnections. The relationship between the NAM-temperature signal and temperature teleconnections is investigated by pattern correlation (Fig. 3.11). Pattern correlation at one grid cell is defined as the latitude-weighted correlation between the NAM-temperature signal and the temperature teleconnection pattern for this grid cell (also know as one point correlation). Hence, pattern correlation maps consists of a pattern correlation coefficient at each grid cell.

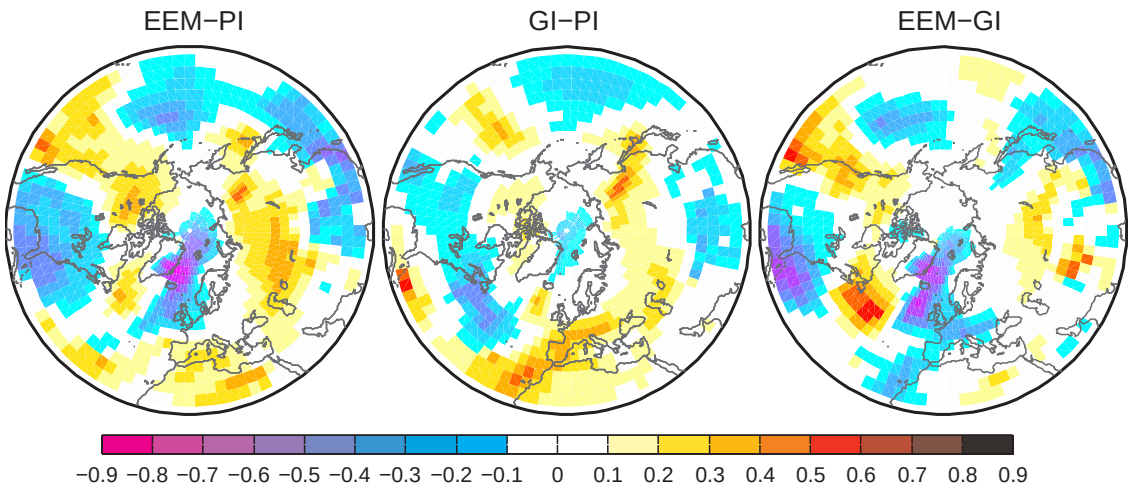

Figure 3.12: Differences of pattern correlation maps between EEM-PI (left), GI-PI (middle) and EEM-GI (right). All differences of correlations are significant on the 5% level.

Pattern correlations show that temperature teleconnections are related to the strength of the NAM-temperature signal. For regions where the NAM-temperature signal is moderate to strong, the teleconnections resemble the NAM-temperature signal. For regions where the NAM-temperature signal is weak the teleconnection has a spatial structure different to the NAM-temperature signal. This is corroborated by the difference of the pattern correlation maps between the simulations (Fig. 3.12). Differences show smaller correlation coefficients over most parts of the Northern Hemisphere in the EEM compared to the PI simulation, which is consistent with a weaker NAM-temperature signal (Fig. 3.8) over these areas and the weaker temperature teleconnections (Fig. 3.10) for south of Greenland and western Europe. But also the stronger pattern correlation coefficients over Siberia are in accordance with the stronger NAM-temperature signal and stronger teleconnections for central Siberia. The unchanged pattern correlations over northeastern Europe confirm the almost unchanged NAM-temperature signal over this area and the only small differences in the NE teleconnections. The NE teleconnection differences in Siberia, the Labrador Sea and North America result from the changed NAM-temperature signal in these regions and not from differences of the NAM-temperature signal over northeastern Europe. Differences between the GI and PI simulation are small and similar to differences of the NAM-temperature signal. Pattern correlation differences EEM-GI show similar pattern as EEM-PI differences but with larger magnitudes, except for central Siberia. This corresponds to the EEM-GI differences of the NAM-temperature signal and of the temperature teleconnections. Hence, all pattern correlation maps indicate that changes of the NAM-temperature signal can affect temperature teleconnections.

Chapter 4

Conclusions and Outlook

4.1 Conclusions

In the presented thesis it is shown, as found by other authors (e.g., Montoya et al. 2000; Felis et al. 2004; Hall et al. 2005; Kaspar et al. 2005), that variations of orbital forcing affect the mean climate. Due to insolation changes, global temperatures are higher (lower) during boreal summer and lower (higher) during boreal winter in the early Eemian (glacial inception) compared to preindustrial temperatures. Only monsoon regions in Asia and Africa during summer and northeastern Europe during winter, show an opposite temperature response. Whereas the different temperatures in the monsoon regions can be explained by stronger (weaker) monsoons due to higher (lower) land/sea temperature contrast in the early Eemian (glacial inception), temperature response in northeastern Europe is related to modified atmospheric circulation. Differences of the mean atmospheric circulation in winter show a NAM-like pattern relatively to the preindustrial period, which can be interpreted as positive NAM during the early Eemian (Felis et al. 2004) and as a slightly negative NAM during the glacial inception relatively to preindustrial period. This NAM-like response of the atmospheric circulation to orbital forcing variations, is responsible for the opposite response of northeastern European winter temperatures than expected from changes of the insolation.

In contrast to other studies, which primarily focus on the mean climate, here the effect of the circulation changes discussed above on the relationship between the large-and the mesoscale climate is also investigated. Compared to the effect on the mean climate, the effect of orbital variation on the circulation variability, in terms of the dominant pattern of SLP variability, is only small, particularly over the North Atlantic/ European sector. The combined effect of the modified mean circulation and an almost unchanged circulation variability do not only affect the mean circulation and the mean temperature, but also lead to a fundamental change of the atmospheric flow characteristics in winter on annual timescales between positive and negative NAMI states. During the preindustrial period a clear switch between strong

westerly flow at positive NAM and very weak westerly flow at negative NAM in winter is evident over Europe, this clear switch vanishes during the early Eemian with westerly flow during both positive and negative NAMI states. In the glacial inception period this switch is slightly more pronounced compared to the preindustrial period. Over Siberia the difference of the atmospheric flow between positive and negative NAM is greater in the early Eemian than in the other two simulated periods.

These differences in the winter atmospheric flow characteristics lead to a modified relationship between the NAM and regional temperatures, which is confirmed by differences of the NAM-temperature signal. For the period of the early Eemian the influence of the NAM on western European January temperatures is weaker and the influence during the glacial inception is similar or even stronger on annual to multi-decadal timescales, compared to the preindustrial period.

Modifications of the relationship between the large-scale circulation and the regional temperature strongly affect the relationship between temperatures at different locations on annual timescales, so called temperature telconnections. Differences between the monthly simulated temperature teleconnections in the different periods show high accordance with changes of the NAM-temperature signal in January. This shows that temperature teleconnections in the Northern Hemisphere are dominated by the Northern Annular Mode, in regions where the influence of the NAM on the regional temperature is moderate to strong. Temperature teleconnections are influenced by mechanisms different to the NAM but still exist where the NAM has no large effect on regional temperatures. This relationship between the NAM-temperature signal and temperature teleconnections is also corroborated by pattern correlation maps between the two.

Besides the gained knowledge of the effect of orbitally induced circulation changes to the relationship between the scales, the results are also relevant to the interpretation of proxy data on annual to mulitdecadal timescales. Proxy data with high enough dating accuracy and temporal resolution to investigate the large-scale circulation on annual to multidecadal timescales are currently not available for the Eemian, but first steps toward the required properties seem promising (e.g., Seelos 2004). When such proxy data become available, the gained knowledge of the changed relationship between the large-and the regional-scale climate should be taken into account, when the large-scale circulation is inferred from them.

The knowledge of the sensitivity of temperature teleconnections to orbital forcing variations can help to understand and merge proxy data with high temporal resolution (annual to decadal) from different regions. Furthermore this knowledge could be used to indicate regions where temperature teleconnections are stable (e.g., Siberia in the early Eemian) or not (e.g., western Europe in the early Eemian) and therefore are adequate to merge proxy data from other regions or not. Note, that the results of this thesis for the interpretation of proxy data is only relevant for proxy data that contain climate information for the winter season, but often

proxy data contain climate information different to the winter season (e.g., for the growing season) this should also been taken into account when one uses the results of this thesis.

To summarize, orbitally forced changed mean circulation leads to differences of the relationship between atmospheric circulation and regional temperatures during the winter season on annual to multidecadal timescales. Resulting differences of the NAM-temperature signal modify temperature teleconnection in the Northern Hemisphere, too. This modification of the scale relationship should be taken into account when aspects of the large-scale climate are inferred from proxy data for the investigated periods. Furthermore for periods with insolation changes comparable to those of the investigated periods, e.g., the mid-Holocene (6 kyr BP), as well as for externally forced circulation changes similar to those of orbitally induced circulation changes, the same effect on the scale relationship can be expected.

4.2 Outlook

This work contributes to the growing knowledge of the climate system, particularly to the knowledge of the sensitivity of relationships between climate at different scales to external forcing variations. However not all topics are completely answered and new aspects have arisen which seems to may be worthy on future study. In the following a short outlook of possible future work is presented.

Kaspar et al. (2004), who used simulations with the same model and same boundary conditions but slightly different initial conditions, stated that winter temperature anomalies during the early Eemian are, at least partly, related to the lower sea-ice extent in the Barents Sea. Inflow of air masses from the region of the Barents Sea could contribute to relatively warm European winter temperatures. But blocking situations over the European continent, which are responsible for easterly winds and resulting advection of air masses from the Barents Sea, are only poorly resolved in simulations of the atmospheric part (ECHAM4) of ECHO-G under a spectral resolution of T30 (Müller 2003). Thus simulations with ECHAM4 with higher spatial resolution or other GCMs (e.g., ECHAM5) or a regional climate model could investigate the role of the lower sea-ice extent and resulting warmer sea surface temperature to European winter temperature during the early Eemian.

The regional focus of the presented study has concentrated on the North Atlantic/ European sector, but differences over the Pacific domain are often greater. Hence, studies which investigate the effect of a changed circulation over the Pacific on the relationship between the scales could be undertaken for the investigated periods. As the influence of the ENSO is greater on the Pacific regions than the North Atlantic/ European sector, the effect of a possible change of ENSO to the relationship between the large-and regional-scale would also be interesting.

A comparison between model simulations and proxy data for the region from western

Siberia to northern China could help to investigate the importance of changed westerlies and the interaction with the East-Asian monsoon on this region in the Eemian.

Similar analysis to that in this thesis and the aforementioned could be done with already existing transient simulations with the same model for the mid-Holocene (Wagner et al. 2007). One could expect similar sensitivity of the large- to meso-scale relationship to orbital forcing variations, due to comparable insolation differences compared to the preindustrial period. The quality of proxy data is much better during the mid-Holocene compared to the last interglacial. Therefore, the large-scale circulation could be inferred from proxy data with respect to the modified large- to meso-scale relationship.

Appendix A

Simulated relationship between regional temperatures and large-scale circulation: 125 kyr BP (Eemian) and the preindustrial period

Nikolaus Groll[1], Martin Widmann[1], Julie Jones[1], Frank Kaspar[2] and Stephan Lorenz[2]
1 Institute for Coastal Research, GKSS Research Centre
PO Box, D21502 Geesthacht, Germany
2 Model and Data Group, Max Planck Institute for Meteorology
PO Box, D22022 Hamburg, Germany
Published in:
Journal of Climate 2005, **18**(19), 4032-4045, doi:10.1175/JCLI3327.1

Abstract

To investigate relationships between large-scale circulation and regional-scale temperatures during the last (Eemian) interglacial, a simulation with a general circulation model (GCM) under orbital forcing conditions of 125 kyr BP is compared with a simulation forced with Late Holocene preindustrial conditions. Consistent with previous GCM simulations for the Eemian, higher northern summer 2m temperatures are found, which are directly related to the different insolation. Differences in the mean circulation are evident such as, for instance, stronger

northern winter westerlies toward Europe, which are associated with warmer temperatures in central and northeastern Europe in the Eemian simulation, while the circulation variability, analyzed by means of a principal component analysis of the sea level pressure (SLP) field, is very similar in both periods.

As a consequence of the differences in the mean circulation the simulated Arctic Oscillation (AO) temperature signal in the northern winter, on interannual to multi-decadal time scales, is weaker during the Eemian than today over large parts of the Northern Hemisphere. Correlations between the AO index and the central European temperature (CET) decrease by about 0.2. The winter and spring SLP anomalies over the North Atlantic/ European domain that are most strongly linearly linked to the CET cover a smaller area and are shifted westwards into the North Atlantic during the Eemian. However, the strength of the connection between CET and these SLP anomalies is similar in both simulations.

The simulated differences in the AO-temperature signal and in the SLP anomaly, which is linearly linked to the CET, suggest that during the Eemian the link between the large-scale circulation and temperature-sensitive proxy data from Europe may differ from present day conditions and that this difference should be taken into account when inferring large-scale climate from temperature-sensitive proxy data.

A.1 Introduction

The quantification of natural climate variability and the understanding of its causes are a prerequisite for assessing the influence of human activities on climate, as well as for making meaningful long-term climate predictions. Investigating variability on long time scales requires estimates for the climate before the instrumental period. These can be obtained from climate proxy data and from numerical simulations. Intensively studied periods include the Holocene, the Last Glacial Maximum (e.g., Joussaume and Taylor 2000), and the last interglacial (e.g., Kubatzki et al. 2000; Kukla et al. 2002; van Kolfschoten et al. 2003).

In this paper we analyze aspects of the climate during the last interglacial, the Eemian, which is thought to have been as warm as today's climate and which lasted approximately from 126 to 110 kyr BP (Shackleton et al. 2003). We are motivated by a large amount of terrestrial proxy data that have been investigated for the Eemian compared to earlier interglacials. These proxy data have been used to reconstruct local or regional climatic and environmental conditions (e.g., Cheddadi et al. 1998; Kühl and Litt 2003), with some uncertainties due to analytical problems and nonclimatic influences on the proxy data. When considered together, these regional reconstructions lead to an approximate description of large-scale climate, although merging the information from individual records into a large-scale picture is complicated by dating uncertainties, which cause large uncertainties for estimating both the duration of (Shackleton et al. 2003) and the climate variability within (Tzedakis et al. 2003) the Eemain.

Regional atmospheric temperatures on centennial and longer time scales can be influenced by many factors, including insolation changes due to variations in the earth's orbit or in solar irradiance, changed radiative balance due to altered composition of the atmosphere or the land surface, and forced or random changes in ocean circulation and in turn in sea surface temperatures (SSTs). The regional temperatures can not only be directly linked to the forcing factors through changes in the regional radiative balance, but also through changes in the mean atmospheric circulation in response to the forcings. Feedbacks between the atmosphere, the ocean, the cryosphere, and the biosphere can further modify the temperature response to varying atmospheric forcings.

On interannual to multi-decadal time scales there is considerable variability of the atmospheric circulation, which additionally influences regional temperatures. A large fraction of this variability is random and internally generated within the atmosphere or within the coupled atmosphere-ocean system, but atmospheric circulation variability can also be caused by fast varying forcing factors such as changes in solar irradiance, atmospheric concentrations of volcanic aerosols, or SST fluctuations due to internal ocean dynamics. In contrast to longer-term circulation changes, which are usually described as a changed mean state, the shorter-term changes are commonly understood as anomalies from a longer term, for instance centennial, mean circulation. These anomalies are often expressed in a compact way in terms of amplitudes of dominant variability modes such as the Arctic Oscillation (AO) or North Atlantic Oscillation (NAO). The influence of interannual to multidecadal circulation variability on regional temperatures has been intensively studied for the instrumental period (e.g., Hurrell 1995; Wallace et al. 1995). First model-based studies for earlier periods in the late Holocene have recently been undertaken (e.g., Zorita et al. 2004). As far as we know our study addresses this issue for the first time for the last interglacial.

Describing the link between circulation and temperature is needed for understanding the circulation signal in temperature-sensitive proxy data. For the Late Holocene, proxy data have been directly linked to circulation variability by means of regression-based upscaling models. These models have been applied to reconstruct circulation anomalies from temperature- and precipitation-sensitive proxy data (e.g., Cook et al. 2002; D'Arrigo et al. 2003; Jones and Widmann 2003). The same approach has also been used to reconstruct large-scale temperature fields from proxy data and long instrumental records (e.g., Mann et al. 1999; Briffa et al. 2001; Esper et al. 2002; Luterbacher et al. 2004). In all of these cases the statistical models were fitted during the overlap period of the proxy records and the instrumental meteorological measurements, and stability of the statistical relationship throughout the reconstruction period has been assumed. This approach is not directly applicable to earlier periods, such as the Eemian, for several reasons. First, the dating uncertainties do not allow for using proxy records from multiple sites as multivariate predictors. Second, most Eemian proxies with high temporal resolution, in particular terrestrial records, do not cover both the Eemian and the

preindustrial period and thus one cannot fit and apply statistical models directly. Finally, the Eemian climate may have differed considerably from conditions during the instrumental period, and therefore one cannot expect the upscaling relationships to be similar to those derived under modern conditions.

The first problem cannot be overcome unless at least the relative dating between the records becomes more accurate, for instance, by using marker events. Thus, for the Eemian one is so far restricted to applying upscaling relationships to individual proxy records. The second problem may be resolved soon. Until recently the maximum temporal resolution of published Eemian terrestrial continuous proxy data was around 100 years (e.g., Tzedakis et al. 2003), but now records with higher temporal resolution are becoming available (e.g., Seelos 2004; Seelos and Sirocko 2004). Yet, even if the first and second issues were resolved, one would still be confronted with the third problem. This cannot be easily addressed based on proxy data only because there are no proxy data that are directly sensitive to circulation; therefore, one cannot investigate the empirical relationship between large-scale circulation and regional temperature.

In this paper we tackle the third issue by using a simulated climate as a surrogate for the real Eemian climate and by analyzing the relationship between regional temperatures and the large-scale circulation. We use a quasi-equilibrium simulation with the ECHAM4/HOPE-G (ECHO-G; Legutke and Voss 1999) coupled atmosphere-ocean general circulation model (AOGCM) with orbital forcing for 125 kyr BP (Kaspar et al. 2004). This simulation should represent a period when the deglaciation after the previous glacial was finished and a relatively stable climate was reached. For comparison we apply the same analysis to a quasi-equilibrium simulation for preindustrial conditions around the year 1800 A.D. with the same model (Lorenz and Lohmann 2004).

GCM-based upscaling models, the so-called pseudoproxy approach, have been used already for the Holocene for aiding the interpretation of proxy-based climate reconstructions (e.g., Zorita and González-Rouco 2002; Rutherford et al. 2003; von Storch et al. 2004), but not yet for the Eemian. Some simulations for the Eemian have been undertaken with energy balance models (e.g., Crowley and Kim 1994), and models of intermediate complexity (e.g., Kubatzki et al. 2000; Crucifix and Loutre 2002), which do not represent the atmosphere in enough detail for pseudoproxy studies. Earlier simulations with atmosphere only GCMs (e.g., Royer et al. 1984; Prell and Kutzbach 1987; Kutzbach et al. 1991; de Noblet et al. 1996; Khodri et al. 2003; Vettoretti and Peltier 2004) and coupled AOGCMs (e.g., Montoya et al. 2000) focussed on the mean climate of the atmosphere and the ocean. A transient simulation of the Eemian climate has been undertaken by Felis et al. (2004) using the same model as in our study, but with an acceleration technique for the orbital forcing (Lorenz and Lohmann 2004). The simulation used in our study provides 1000 years of simulated equilibrium climate for the early Eemian period (125 kyr BP) and is thus more suited for our study than the simulation

of Felis et al. (2004), which provides only few years with orbital forcing at 125 kyr BP.

A brief description of the model and its setup is given in Section A.2. In Section A.3 mean circulation and temperature are discussed as well as the circulation variability. In Section A.4 the relationship between large-scale circulation and and regional temperatures is analyzed and finally a summary and conclusions are presented in Section A.5.

A.2 Model description and experimental setups

A.2.1 The climate model

The climate model used in the present study is the ECHO-G coupled AOGCM (Legutke and Voss 1999), which consists of the atmospheric model ECHAM4 (Roeckner et al. 1996) and the ocean model HOPE (Wolff et al. 1997) with a thermodynamic-dynamic sea-ice model included (HOPE-G). In the analyzed simulations the ECHAM4 model has a spectral resolution of T30 (approximately $3.75° \times 3.75°$) with 19 vertical levels. The ocean model HOPE-G has a horizontal resolution of T42 (about $2.8° \times 2.8°$) with a meridional grid refinement in the tropical regions for the purpose of modeling ENSO variability and a vertical resolution of 20 levels. To avoid a climate drift a flux correction for heat and freshwater was applied; globally averaged over the ocean both fluxes are zero. The ECHO-G coupled AOGCM has been used in a number of recent climate variability studies (Baquero-Bernal et al. 2002; Marsland et al. 2003; Zorita et al. 2003; Rodgers et al. 2004; von Storch et al. 2004; Zorita et al. 2004).

A.2.2 Experimental setups

Two quasi-equilibrium simulations with fixed external forcing are analyzed: one for present day insolation with preindustrial (around AD 1800) greenhouse gas (GHG) concentrations (hereafter PI) (Lorenz and Lohmann 2004) and one with Eemian forcing conditions of 125 kyr BP (hereafter EEM) (Kaspar et al. 2004). In the latter, insolation is calculated according to Berger (1978). GHG concentrations are taken from the Vostok ice core (CO_2 and CH_4: Petit et al. 1999; N_2O: Sowers 2001). The changes in external forcing and boundary conditions are shown in Table A.1.

Both model simulations are started with the same initial state from a 1000 yr quasi-equilibrium run with present day greenhouse gases of the same model. After a model spin up of 1300 years (1000 years) in PI (EEM), a 1000 year long simulation period in both runs is analyzed. Both simulations show a global temperature trend of -0.039 K century^{-1} in PI and -0.015 K century^{-1} in EEM. In this study we primarily focus on the Northern Hemisphere where the temperature decrease is lower than the global trend. To compensate for this decrease we detrended the model output at all grid cells prior to analysis. Vegetation is fixed to its modern state in both runs. Note that therefore the feedback of a changed vegetation on

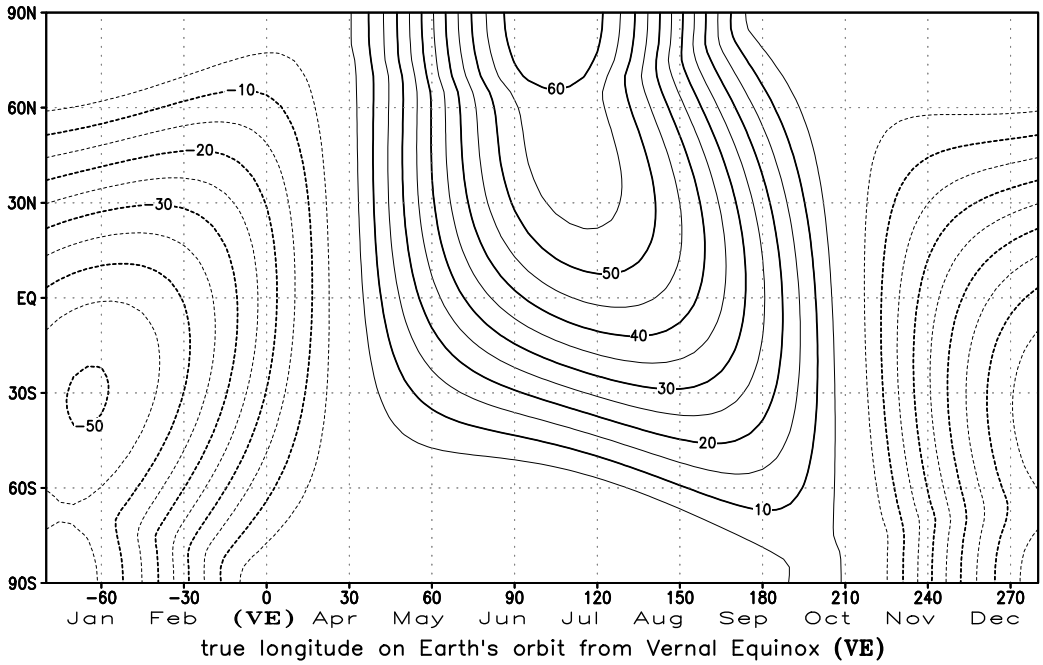

Figure A.1: Zonally averaged insolation anomalies 125 000 years before present (125 kyr BP) as a function of true longitude on the Earth's orbit from vernal equinox (Wm^{-2}), according to Berger (1978).

the climate system (e.g. Doherty et al. 2000; Crucifix et al. 2002) is not included in our simulations. However, short test simulations with the same orbital forcing with a changed vegetation showed only minor effects on the large-scale climate in our model.

The EEM GHG concentrations are slightly lower than in PI, but the differences are small and it can be expected that they have only a minor influence on the differences between the two model runs and that the differences between the model runs are mainly caused by changes in the orbital parameters. Eccentricity is higher in the Eemian, but the effect on the global annual average of incoming solar radiation at the top of the atmosphere is only about 0.1%. Obliquity is slightly greater at 125 kyr BP and with a fixed vernal equinox at 21 March, the perihelion occurs in July at 125 kyr BP instead of in January as in the preindustrial period. The combined effect of changes in obliquity and in the timing of the perihelion leads to a higher (lower) global average insolation in northern (southern) Eemian summer of about 12% (11%) (Fig. A.1) and to a larger (smaller) seasonality in incoming radiation in the Northern (Southern) Hemisphere.

Insolation is prescribed in the model with respect to the true longitude (angle on the orbit relative to the vernal equinox) on the changed earth orbit. Due to Kepler's law the time the Earth takes on the orbit per true longitude is different in the two simulated periods. As a consequence, a given date corresponds to a different true longitude on the orbit. This leads

Table A.1: Experimental setup for PI: simulation with preindustrial GHG concentrations and current parameters of the earth's orbit; EEM: simulation with GHG concentrations and earth's orbital parameters for 125 kyr BP; vernal equinox (VE).

experiment	CO_2 (ppm)	CH_4 (ppb)	N_2O (ppb)	Eccentricity (%)	Obliquity axis tilt (°)	Perihelion (° from the VE)	Duration of simulation (yr)	Duration of model spinup (yr)
PI (1800 A.D.)	280	700	265	1.67	23.44	282.7	1000	1300
EEM (125 kyr BP)	270	630	260	4.00	23.79	127.3	1000	1000

to different dates of the solstices and fall equinox (vernal equinox is fixed) and to a reduction or extension of seasons (defined as sections on the orbit), for instance to a shorter northern summer and a longer northern winter, as shown in detail in Joussaume and Braconnot (1997).

In this study only monthly mean fields are analyzed, which are calculated by a standard postprocessing routine, based on a 360 day calendar year with 30 days month^{-1}. Thus, we compare the climate averaged over slightly different sections of the earth's orbit. The effect of this on our results has been estimated by calculating all results for the Eemian simulation with respect to shorter northern summers (June and July) and longer northern winters (November to February) and comparison with the results for the preindustrial simulation with the standard definition of seasons. The differences caused by the different seasonal definitions are significantly smaller than those between the different simulations. Thus, here only results based on the standard season definition are discussed.

A.3 Large-scale climate

As a basis for understanding the changes in the relationship between large-scale circulation and regional temperature the differences in the mean climate and the circulation variability in the Eemian (125 kyr BP) and preindustrial simulations are discussed in this section.

A.3.1 Long-term seasonal means

A study by Min et al. (2004) with the same model as used in our study but with present day GHG concentrations shows that ECHO-G is capable of simulating the present day mean climate well. The overall structure of long-term seasonal means of sea level pressure (SLP), 2m-temperature, 10m-wind field and the zonal wind at 200 hPa in EEM and PI are plausible. A detailed comparison of the simulated preindustrial and present day climate with observations is beyond the scope of this paper. We only discuss differences between PI and EEM, and thus potential model biases can be expected to be compensated for to a large extent. A short comparison of the simulated and the climate estimated from proxy data is given at the end of this section.

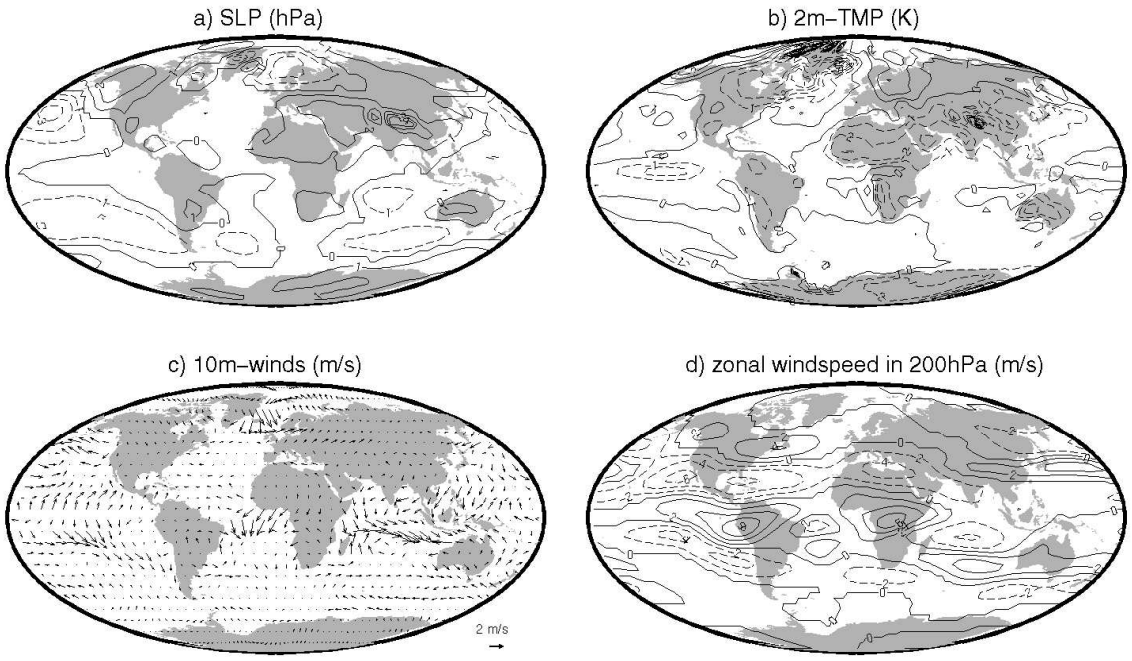

Figure A.2: Mean simulated difference (EEM minus PI) for DJF: (a) sea level pressure (hPa),(b) 2m temperature (K), (c) 10m wind (ms^{-1}) and (d) zonal windspeed at 200hPa (ms^{-1}). Solid (dashed) lines are positive (negative) anomalies.

A comparison of the boreal winter [December - Febuary (DJF)] SLP field in the two simulations (Fig. A.2a) shows lower SLP in EEM than in PI over the ocean basins and higher SLP over most parts of the land surface with the exception of northern and eastern Europe. Due to the lower insolation during DJF in the early Eemian compared to the preindustrial period, temperature is nearly everywhere lower in EEM compared to PI (Fig. A.2b). An exception to this is the temperature in northern and eastern Europe, which is higher in EEM than in PI, with a maximum difference of 3 K over the Barents Sea. The difference in the 10m-wind field (Fig. A.2c) shows weaker westerlies in the North Pacific as well as in the Southern Oceans, also trade winds in the Pacific Ocean are weaker. Stronger westerlies in northern Europe in EEM are evident, consistent with the lower pressure in that area amplifying the pressure gradient. These wind changes can partly explain the higher temperatures in northern Europe (Fig. A.2b). Another contribution for the positive temperature anomalies comes from a lower sea ice extent (Kaspar et al. 2004) in this region (not shown). Changes in the ocean circulation (e.g., North Atlantic Deepwater formation), which could also contribute to the temperature anomaly in the Barents sea, are small. A northward (southward) shift of the Atlantic (Pacific) jet (Fig. A.2d) and a strengthening of the equatorial jet over South America and Africa can be seen, indicating that circulation changes do not only occur near the surface.

In northern summer [June-August (JJA)] the SLP (Fig. A.3a) in the Eemian simulation is

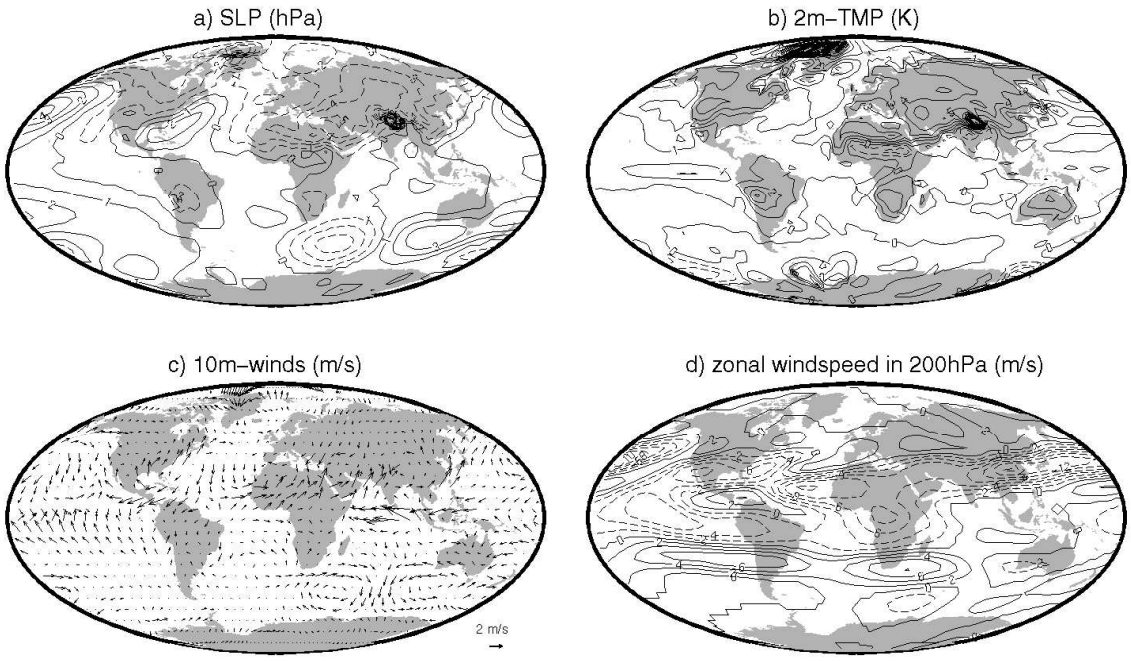

Figure A.3: As Fig. A.2 but for JJA.

lower over the continents except over Australasia and Antarctica and higher over the North Pacific and over large parts of the Southern Oceans. Also an eastward shift of the Atlantic high and the southern Indian Ocean low pressure in EEM compared to PI can be found. An overall temperature increase (Fig. A.3b) due to higher insolation in the early Eemian in the northern summer months can be seen, in particular over the Northern Hemisphere continents, up to 4 K in Siberia and Central Asia. Only in the monsoon regions of India and Africa is there a slight decrease, probably due to enhanced moisture transport from sea to land. This is consistent with stronger southwest monsoon winds (Fig. A.3c) toward India and western Africa in EEM. A strengthening of the Southern Hemisphere and equatorial jets (Fig. A.3d) is evident. Windspeeds at the 200 hPa level over the Northern Hemisphere are reduced in EEM.

The simulated temperature differences between EEM and PI are consistent with temperature fields reconstructed from proxy-data (e.g., Frenzel et al. 1992; Kaspar et al. 2004). The simulated stronger African monsoon in EEM is consistent with a proxy-based study by Rohling et al. (2002). This agreement between simulated and reconstructed fields show that the model is capable of reproducing a realistic mean climate at 125 kyr BP.

A study by Montoya et al. (2000) of the same period of the last interglacial with an earlier version (ECHAM1) of the atmospheric model ECHAM4 and the LSG ocean model instead of HOPE-G shows agreement in the overall structure of simulated temperature, wind, and sea level pressure fields in summer. Only on the subcontinental scale are some differences evident, due to the lower spatial resolution of the model used by Montoya et al. (2000). In the winter

season there are some differences. In particular, in the Northern Hemisphere the temperature anomalies in the North Atlantic/ European domain are shifted westwards and inverted. SLP anomalies over the North Pacific/ North American domain are also inverted. However, a comparison between the two studies is problematic because in Montoya et al. (2000) simulated differences between the early Eemian and the present day climate are discussed, whereas in our study the last interglacial is compared with a control run with preindustrial GHG concentrations.

A.3.2 Variability of the Northern Hemispheric circulation

A standard approach to obtain the dominant patterns of variability in a dataset is to derive empirical orthogonal functions (EOFs). The first extratropical SLP EOF (20°- 90°N) is physically interpretable, and is known as the AO or Northern Hemisphere Annular Mode (Thompson and Wallace 2000). The time-dependent amplitude of the AO, which is given by the first principal component (PC), is known as the Arctic Oscillation Index (AOI). In the top (bottom) panels of Fig. A.4 the first SLP EOFs for EEM (PI) for the four standard seasons are shown. Both experiments show very similar patterns, particularly in the winter season, namely a pronounced dipole over the North Atlantic corresponding to the NAO and a weaker dipole over the North Pacific. The EOF loadings, which here are scaled to be the pressure changes associated with a positive one standard deviation change in the AOI, are slightly larger in EEM in winter and spring in the Atlantic sector and smaller in winter in the Pacific. In the other seasons there are only small difference between EEM and PI. The fraction of variance explained by EOF1 (Fig. A.4) is very similar in both runs in all seasons. The second and third EOFs (not shown) do not differ much between the two runs.

The complexity of the circulation is reflected in the eigenvalue spectrum of the covariance matrix, or equivalently in the fraction of variance explained by the EOFs. A simple circulation is associated with a faster drop in explained variances or eigenvalues than a complex circulation. A suitable measure for the complexity is the number of independent degrees of freedom (DOFs), which can be calculated from the eigenvalue spectrum (Bretherton et al. 1999). In the EEM and PI simulations the explained variances and the DOFs based on monthly SLP are very similar in all seasons (e.g. in winter DOF = 8.0 in EEM and DOF = 7.3 in PI). EOF analysis of the 500hPa geopotential height shows similar results (not shown). The stability of the EOFs in the 1000yr long equilibrium simulations are tested by splitting the simulations into ten 100yr long time slices (not shown). The difference between the EOFs for the subperiods are small compared to the difference between EEM and PI.

The EOF pattern and its corresponding indices are calculated separately for each season and simulation and thus describe anomalies to different means. In order to study the combined effect of changes in the SLP mean and EOF1 we calculated SLP composite maps for AOI situations with plus or minus two standard deviations (Fig. A.5). The distribution of the AOI

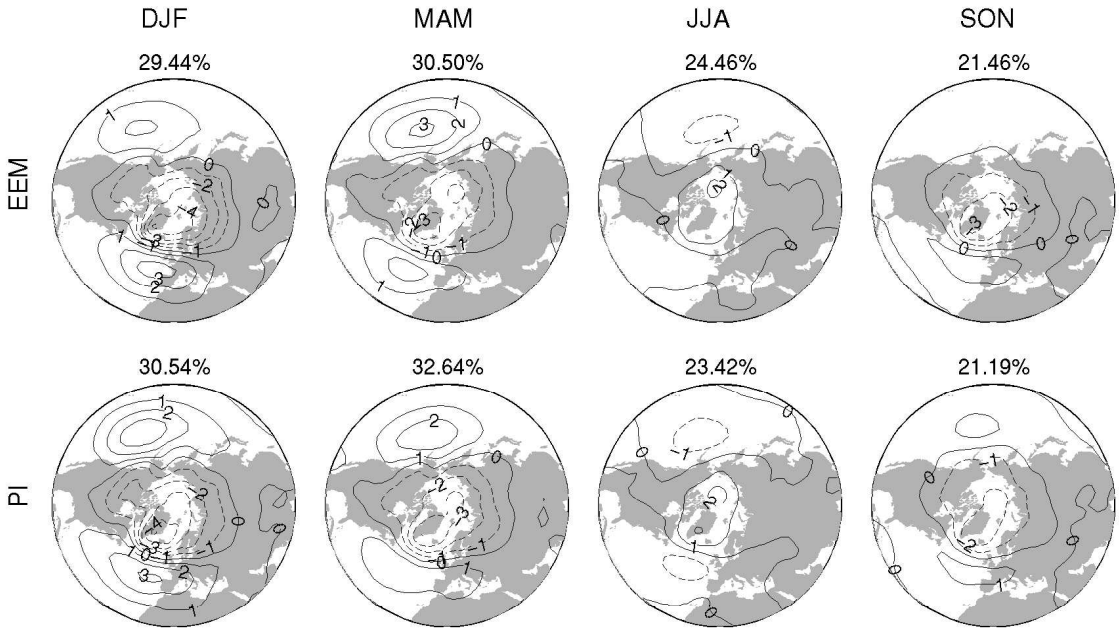

Figure A.4: First EOF for seasonal SLP: 1000yr (top) EEM and (bottom) PI. Percentages of explained variance are shown at the top of each panel.

is nearly Gaussian in both runs, so that for every composite plot a set of about 25 seasons out of 1000 in the entire simulation is used.

1. North Atlantic/ Europe
   In the positive DJF AO phase there is no large difference between the two simulations (Fig. A.5, center column), but in the negative phase (Fig. A.5, middle column) the zonal flow over Europe is stronger in EEM, which could lead to a stronger oceanic influence in eastern parts of Europe. The positive spring AO state (not shown) is associated with weaker zonal flow over the Atlantic and toward Europe in EEM than in PI. For negative spring AO phases there is no large difference in the southern and central parts of Europe, but a higher SLP gradient between Greenland and the Norwegian Sea in EEM could establish a more temperate climate in northern Europe during negative phases. In summer and fall (not shown) there is no difference between the two runs in the SLP fields associated with positive and negative AO phases.

2. North Pacific/ North America
   In winter there is no difference in positive or negative AO phases between the two model runs in this region. In spring weaker zonal flow towards the Pacific coast occurs in both AO phases in EEM. In summer and fall a greater SLP gradient over North America is evident in both AO phases.

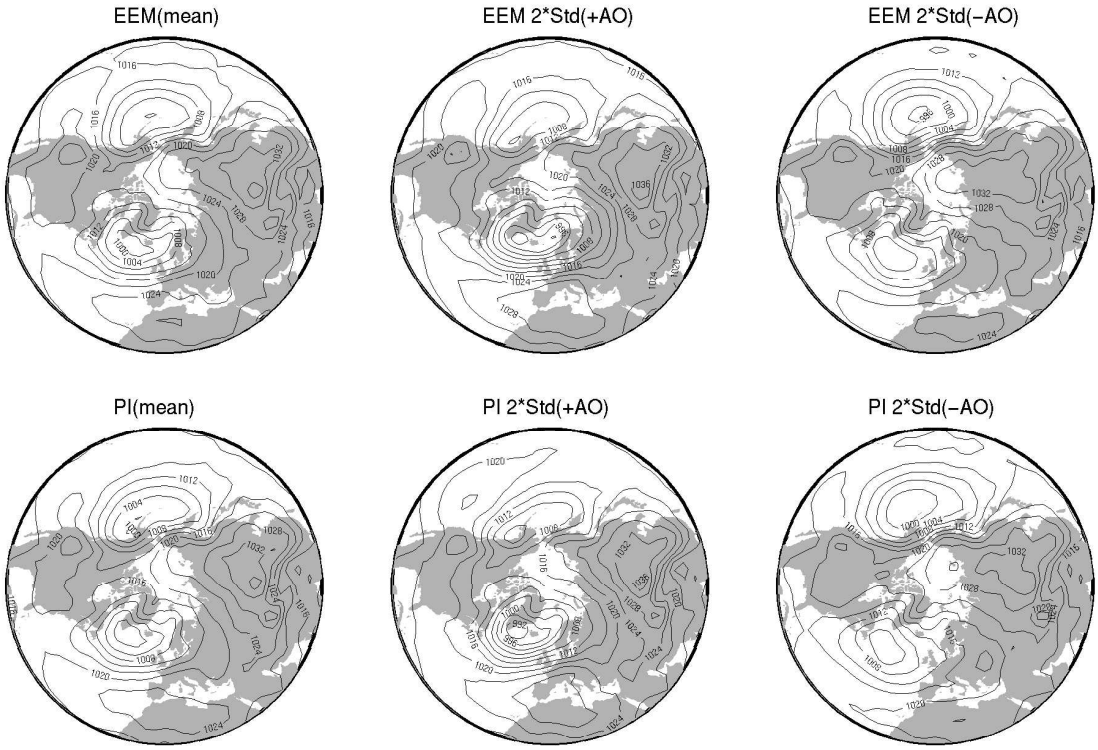

Figure A.5: Composites of DJF SLP for strong (two standard deviations) AO situations: (top) EEM and (bottom) PI simulation. (left) Mean state, (middle) positive, and (right) negative AO.

In summary, the composite maps indicate a stronger DJF SLP gradient over Europe in EEM in negative AO phases compared to PI, whereas in positive AO phases the SLP gradient over Europe is very similar in both simulations. This suggests that the difference in the characteristics of the zonal flow over Europe between positive and negative AO phases is smaller in the early Eemian than in the preindustrial period and that this could lead to a weaker relationship between European temperature and the AO in the Eemian.

A.4 Relationships between large-scale circulation and regional temperature

In this section we investigate how circulation variability is linked to regional temperatures and thus, in turn, to temperature-sensitive proxy data. All correlations and differences discussed in this section are at least significant at the 1% level due to the long model simulation, but only correlations and differences that are large enough to be relevant for this study will be discussed.

A.4.1 AO temperature signal

To assess whether temperature-sensitive proxy data from the Northern Hemisphere may contain an AO signal on multidecadal time scales during the Eemian, we now investigate the temperature signal of the AO by calculating correlation and regression coefficients between the standardized AOI and the 2m-temperature of the two simulations. We use a 31-year Hamming filter (Oppenheim and Schafer 1989) for analyzing the AO signal as this time scale is long enough to be resolved by continuous proxy data, but short enough for regional temperature to be strongly linked to circulation variability. As the AO-temperature signal is often considered on interannual time scales, we also calculated the AO-temperature signal with annual data from the simulations (not shown). The overall structure of the annual and multidecadal AO-temperature signal is similar and the differences between the EEM and PI simulation on annual timescale are comparable to those on multidecadal timescales.

The regression (colored) and correlation (contour lines) coefficients for the winter season (DJF) are shown in Figure A.6. The preindustrial simulation (middle panel) reproduces the observed AO-temperature signal (e.g., Hurrell 1995; Thompson and Wallace 2000) reasonably well (not shown). Positive regression coefficients over northern and eastern Europe and Siberia of up to 0.5 K per one standard deviation of the AOI, and a maximum correlation of 0.6 are evident, which reflects that a positive AOI is associated with stronger westerlies and as a consequence with positive temperature anomalies over Europe. Most parts of North America are also positively correlated (max 0.6) with regression coefficients of up to 0.4 K, which also suggests that a positive AOI is associated with positive SST (2m temperature) anomalies over the Sargasso Sea (southeast of the United States). Around the Bering Sea and west of Greenland the AOI is negatively correlated with up to -0.6 with the temperature anomaly (regression coefficient approximately -0.6 K). The negative temperature anomalies are associated with more storms and cold air advection from the Arctic regions in positive AOI situations.

In the EEM simulation the spatial distribution of the DJF AO-temperature signal is very similar (Fig. A.6 left panel), but with generally lower values for the regression and correlation coefficients. To get a more detailed view of the changes in the AO-temperature signal in terms of strength and displacement of centers, the difference (EEM minus PI) was calculated (Fig. A.6 right panel). Negative deviations of regression coefficients of 0.1 K over Europe and parts of North America, together with a weaker correlation (up to -0.2) over western and central Europe as well as in western Canada are evident. Positive differences can be found west of Greenland (0.5 K) that signify a weakened simulated Eemian AO signal in this region because in EEM the signal is less negative (Fig. A.6 left panel). Also in Alaska and in the Sea of Okhotsk positive deviations represent a weaker AO-temperature signal. Only in parts of Siberia is the strength of the AO signal stronger, by up to 0.3 K, and the correlation is higher by about 0.2.

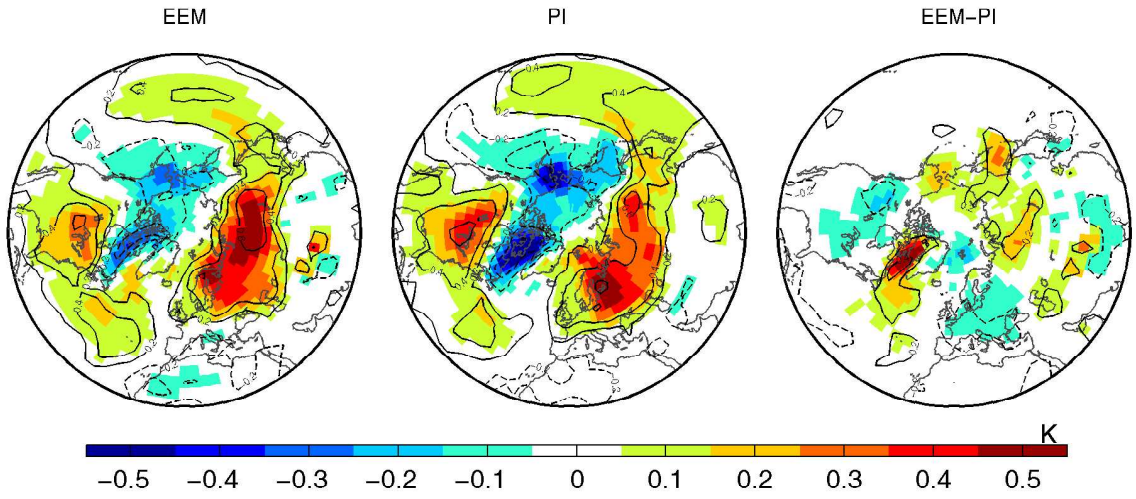

Figure A.6: Winter (DJF) AO-temperature signal for EEM (left), PI (middle) and difference between the simulations (right): regression coefficients in color, only values larger than 0.05 K are shown. Correlation coefficients as contours: positive (negative) correlations are shown as solid (dashed) lines, contour interval 0.2.

As most of the available terrestrial proxy data for the last interglacial are located in Europe, we now focus on the changes of the AO signal in Europe. The greatest differences can be found in central Europe, where regression coefficients drop by about 40% and the correlation drops proportionally from 0.4 in PI to 0.2 in EEM (Fig. A.6). In western Europe there is a weak AO-temperature signal in PI, which completely vanishes in EEM. Thus, in large parts of Europe the AO explains less of the multidecadal winter temperature variability in EEM than in PI. This simulated difference of the AO-temperature signal between the two simulations is consistent with the results discussed in Section A.3.2, where differences in the SLP gradient over Europe between positive and negative AO phases were found to be smaller in EEM than in PI.

A possible explanation for the different mean circulation and the weaker AO temperature signal in most parts of the Northern Hemisphere discussed in Section A.3.2 could be that boreal winter equator to pole difference in insolation and available energy is smaller at 125 kyr BP. Changes in the meridional insolation gradient could lead to changes in the poleward extent of the Hadley cell, or to a reduction of the meridional energy transport by the eddy circulation or to a combination of both. The smaller exchange of heat and air masses between the mid and highlatitudes could lead to a more zonal flow in the midlatitudes. However this simple explanation does not explain the stronger AO signal over Siberia. More analysis is required to find an explanation for this disparity.

In summer (not shown) the AO-temperature signal almost disappears in both simulations,

which reflects the fact that during summer the hemispheric circulation does not play an important role for temperature variability. In the transition seasons (not shown) the AO temperature signal is weaker than in winter.

A.4.2 Large-scale circulation and central European temperature

The analysis of the AO temperature signal showed that the linear relationship between the AO and 2m-temperature in some parts of Europe is weaker in the EEM than in the PI simulation. However, this does not exclude that other SLP anomalies may exist whose amplitudes are strongly linked to European temperatures. One way of defining a SLP pattern that is linearly linked to central European temperature (CET) is through the regression coefficients of local SLP on CET. This definition is optimal in two ways: First, if one wants to estimate SLP anomalies from CET by means of linear regression, the estimate will be the product of the CET and this regression map. Note that an upscaling model for reconstructing circulation from European proxy data could be obtained by first estimating the CET from the proxy data and then multiplying it with the regression map. The second meaning of the regression map was pointed out by Widmann (2005), who showed that the regression coefficient are also proportional to the weights that would be given to the local SLP values for obtaining an estimate of the CET from the SLP field based on singular value decomposition. In the same paper it was also shown that this estimate can be expected to be very close to the result of a multiple linear regression (MLR) applied to the leading SLP PCs (PC-MLR) and that it may be somewhat less affected by overfitting problems. For brevity and because of the convenient dual interpretation of regression maps we restrict the discussion to the regression maps rather than also discussing the PC-MLR weights.

We regressed the SLP field over the North Atlantic and over Europe onto the CET defined as the area mean of the 2m-temperature at eight highly correlated gridcells over western and central Europe (50.1°-46.4°N; 3.75°-15°E). Again a 31-year Hamming filter was used. As climate proxy data frequently represent monthly mean values (for instance the warmest or coldest month, e.g., Aalbersberg and Litt 1998; Klotz et al. 2003), we analyzed regression maps based on monthly rather than on seasonal means.

For both simulations Figure A.7 shows the regression coefficients for filtered monthly means in $hPa\ K^{-1}$ in color and the correlations as contour lines. In January the maximum PI values are south of Italy, indicating that over this area a pressure increase of about 1.25 hPa can be estimated from a CET increase of 1 K with a correlation of about 0.4. The minima with values of around $-2\ hPa\,K^{-1}$ and correlations of about -0.4 reaches from the North Atlantic over Scandinavia into northern Russia. This pattern is synoptically plausible as with the sign shown it is associated with increased southwesterly flow toward central Europe and thus with the advection of mild air masses. With the opposite sign it is associated with a northeasterly flow anomaly and an increased influence of cold, continental air masses. The

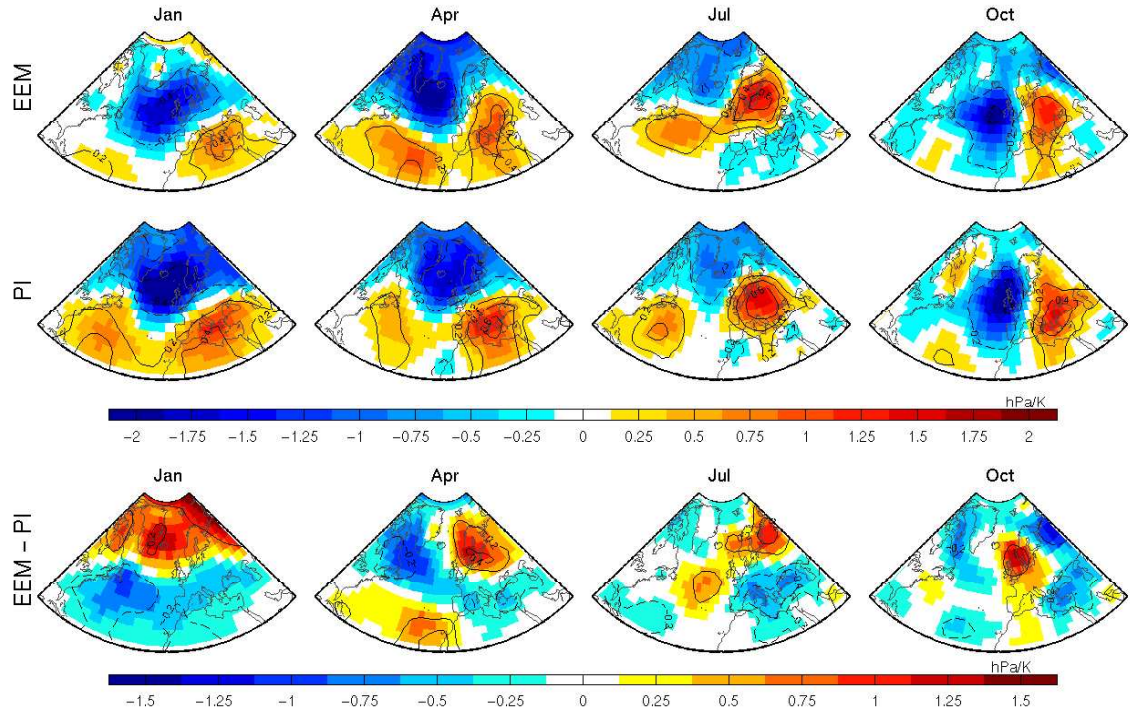

Figure A.7: Regression maps of monthly SLP on CET, filtered with a 31 year Hamming filter for (top) EEM, (middle) PI, and (bottom) difference between the simulations: regression coefficients ($hPaK^{-1}$) in color; only regressions stronger than 0.125 $hPaK^{-1}$ shown. Correlation coefficients as contours: positive (negative) correlation are shown as solid (dashed) lines, contour interval 0.2.

regression pattern in EEM in January also shows positive coefficients over the southern part of the domain and negative values over the North Atlantic, but there are some differences to PI. The region with positive coefficients is concentrated over the Mediterranean Sea and the values are reduced to about 0.75 $hPa\,K^{-1}$. The area of negative coefficients is also smaller and the center is shifted slightly southwest to the North Atlantic. The difference between the two regression patterns is shown in the bottom panel of Fig. A.7. In the southern (northern) half of the domain the regression coefficients are more negative (positive) in the EEM compared to PI. This change suggests that in the EEM simulation the pressure anomalies over the northern North Atlantic have more influence on the CET than pressure anomalies over the southern North Atlantic and the Mediterranean Sea.

In April the spatial structure of the regression coefficients is the same as in January, but the two simulations differ slightly. The high positive values (1.25 $hPa\,K^{-1}$) in the PI around the Mediterranean are slightly reduced (1 $hPaK^{-1}$), and the positive area is extended east of the Baltic Sea. The positive values over the Atlantic are higher (from 0.5 to 1 $hPa\,K^{-1}$) in EEM. The area with negative regression coefficients over Iceland is shifted into the center of

the North Atlantic in EEM. In July the regression pattern is dominated by positive coefficients (1.5 $hPa\,K^{-1}$) over the European continent, which suggests that pressure anomalies over land induce summer CET anomalies (e.g., summer high pressure). This indicates that the continental summer climate and regional effects dominate the link between SLP and CET. The difference between the two runs is small, the center is slightly shifted to the north in EEM. In October the regression coefficients have a dipole form, with positive values over the continent and negative values over the Atlantic. In EEM the pattern is slightly weaker and is shifted westward. October marks the transition between summer with dominating pressure over land and winter with pressure influence from the North Atlantic.

To obtain a measure for the strength of the linear coupling between the SLP field and the CET, the time-dependent amplitude of the regression pattern, the so-called time expansion coefficient (TEC), was calculated and correlated with the CET. The TEC was derived by an orthogonal projection of area-weighted SLP data onto the regression map, or in other words, as the scalar product of the two fields. The correlations range between 0.4 to 0.7 in both model runs with higher values in winter and summer months and lower correlations in the transition months. The squared correlation has a twofold meaning. It is the fraction of variance of the TEC of the regression map that can be explained by linear regression from the CET. This interpretation is appropriate when the upscaling problem is considered. The correlation is also the fraction of temperature variance that can be explained by linear regression from the TEC. It can be expected to be similar to the fraction of temperature variance that can be explained by a PC-MLR (Widmann 2005).

Thus, in both simulations the amplitude of the SLP-CET regression pattern can be equally well estimated form the CET, but the differences in the regression maps show that in the EEM simulation a smaller and different area of the SLP field in winter and spring can be explained by a linear upscaling relationship from the CET. Note that the very similar correlations in both simulations are not in conflict with the lower correlation in EEM between the AOI and the CET found earlier. The January and April regression patterns strongly project positively on the AO-NAO pattern but are not identical to it. The difference EEM-PI of the regression maps in January resembles very closely the inverted AO-NAO pattern, which is consistent with the reduced AOI-CET correlation discussed in Section A.4.

A.5 Summary and Conclusions

Two quasi-equilibrium simulations with an AOGCM, forced with different incoming solar radiation and greenhouse gas concentrations, typical for the last interglacial (EEM) and the preindustrial period (PI), respectively, were compared. Simulated mean fields of circulation and temperature show substantial differences between the two runs. In winter 2m-temperatures in northern and eastern Europe are higher in the EEM simulation, partly re-

lated to stronger westerly flow toward these areas. In summer an overall increase in Northern Hemisphere 2m-temperatures can be found due to increased insolation. EOF analysis shows only slight differences in SLP variability in the North Atlantic and North Pacific. Composite SLP maps of situations with a strong positive or negative AOI, which capture the combined effect of the differences in the mean and the AO pattern, show considerable differences between the two periods during negative AO-phases, with larger SLP gradients and increased zonal flow over Europe in EEM compared to PI.

The stability of the AO-temperature signal was investigated by means of regression and correlation maps between the 31 year filtered seasonal AOI and the filtered 2m-temperature field. The signal is strongest in winter in both simulations, but in EEM it is significantly weaker over Europe, west of Greenland and north of Japan, but stable or higher over Siberia than in PI. In particular in central Europe the winter AO-temperature regression coefficients are reduced in EEM by up to 40% and the correlation drops by about 0.2. These changes in the relationship between AOI and CET are consistent with the lower variation in the EEM simulation of the strength of the winter zonal flow over Europe between positive and negative AOI states. Thus, the simulations suggest that during early Eemian winters less of the multi-decadal temperature variability over Europe can be explained by the AO, and it can be expected that less information on the multi-decadal AOI mean can be derived from temperature-sensitive proxy data from Europe. Over Siberia the simulated AO temperature signal is strong in both simulations.

To find the circulation pattern that has the strongest linear link to the temperature over Europe we regressed the 31 year filtered monthly SLP over the Atlantic and Europe on the filtered central european temperature (CET). The resulting regression maps show that winter and spring CET variability is linearly related to the SLP contrast between the high and the midlatitudes in both simulations. In July the CET variability is dominated by SLP variations over the European continent, and in fall by the contrast of the pressure anomalies over Europe and the Atlantic. In winter the difference between the two simulations is a weaker link during the early Eemian between the CET and SLP over the the southern North Atlantic, the Mediterranean and eastern Europe. In spring similar differences occur over the Mediterranean and eastern Europe, but the southern North Atlantic is more strongly linked during the early Eemian. In July and October only small differences are found.

The correlations between the time expansion coefficients of the regression maps and the CETs show that, despite the differences in the regression maps, the link between the amplitudes of the regression maps and the CETs is equally strong in both periods with correlations up to about 0.7 in winter. This is not in conflict with the reduced AOI-CET correlation during Eemian winters, as the January preindustrial regression map strongly projects positively on the AO-NAO pattern and the difference EEM-PI of the regression maps in January resembles the inverted AO-NAO pattern. In other words, the wintertime SLP pattern with the

strongest linear connection to the CET is in the preindustrial period more similar to the AO-NAO pattern than during the early Eemian.

Our model-based results confirm other numerical simulations that suggest that insolation changes due to changes in the earth's orbit do not only directly change temperatures, but also significantly alter the mean circulation over some areas, including Europe (e.g., Montoya et al. 2000; Felis et al. 2004). In addition our study shows that multidecadal circulation variability is very similar during the early Eemian and the preindustrial period but that, presumably as a consequence of the different mean circulation, the relationship between circulation variability and regional temperatures differs substantially. These changes should be taken into account if circulation variability is estimated from temperature-sensitive proxy data for the Eemian.

Acknowledgments We thank Norbert Kühl for his comments and the four anonymous reviewers for their valuable comments which helped us to improve the manuscript. Stephanie Legutke is acknowledged for her support with the ECHO-G model and Beate Gardeike for help with figure preparation. This work was funded within the EEM (Climate change at the very end of a warm stage) and the GHOST project (Global Holocene Spatial and Temporal variability) by the Federal Ministry of Education and Research under the DEKLIM program (Deutsches Klimaforschungsprogramm).

References

Aalbersberg, G., and T. Litt, 1998: Multiproxy climate reconstructions for the Eemian and Early Weichselian. *Journal of Quaternary Science*, **13**, 367–390.

Baquero-Bernal, A., M. Latif, and S. Legutke, 2002: On dipole-like variability of sea surface temperature in the tropical Indian Ocean. *J. Climate*, **15**, 1358–1368.

Berger, A.L., 1978: Long-term variations of daily insolation and Quaternary climatic changes. *J. Atmos. Sci.*, **35**, 2362–2367.

Bretherton, C., M. Widmann, V.P. Dymnikov, J.M. Wallace, and I. Bladé, 1999: The effective number of spatial degrees of freedom of a time-varying field. *J. Climate*, **12**, 1990–2009.

Briffa, K.R., T.J. Osborn, F.H. Schweingruber, I.C. Harris, P.D. Jones, S.G. Shiyatov, and E.A. Vaganov, 2001: Low frequency temperature variations from a northern tree-ring density network. *J. Geophys. Res.*, **106**, 2929–2941.

Cheddadi, R., K. Mamakowa, J. Guiot, J.L. de Beaulieu, M. Reille, V. Andrieu, W. Granoszewski, and O. Peyron, 1998: Was the climate of the Eemain stable? A quantitative climate reconstruction from seven European pollen records. *Palaeogeogr., Palaeoclimatol., Palaeoecol.*, **143**, 73–85.

Cook, E.R., R.D. D'Arrigo, and M.E. Mann, 2002: A very-well verified, multiproxy reconstruction of the winter North Atlantic Oscillation Index since A.D. 1400. *J. Climate*, **15**, 1754–1764.

Crowley, T., and K.Y. Kim, 1994: Milankovitch forcing of last interglacial sea level. *Science*, **265**, 1566–1568.

Crucifix, M., and M.F. Loutre, 2002: Transient simulations over the last interglacial period (126-115 kyr BP): feedback and forcing analysis. *Climate Dyn.*, **19**, 417–433.

Crucifix, M., M.F. Loutre, P. Tulkens, T. Fichefet, and A. Berger, 2002: Climate evolution during the Holocene: a study with a Earth system model of intermediate complexity. *Climate Dyn.*, **19**, 43–60.

D'Arrigo, R.D., E.R. Cook, M.E. Mann, and J.C. Jacoby, 2003: Tree-ring reconstructions of

temperature and sea-level pressure variability associated with the warm-season Arctic Oscillation since AD1650. *Geophys. Res. Lett*, **30**, 1549, doi: 10.1029/2003GL017250.

de Noblet, N., P. Braconnot, S. Joussaume, and V. Masson, 1996: Sensitivity of simulated Asian and African summer monsoons to orbitally induced variations in insolation 126, 115 and 6kBP. *Climate Dyn.*, **12**, 589–603.

Doherty, R., J. Kutzbach, J. Foley, and D. Pollard, 2000: Fully coupled climate/dynamical vegetation model simulations over the Northern Africa during the mid-Holocene. *Climate Dyn.*, **16**, 561–573.

Esper, J., E.R. Cook, and F.H. Schweingruber, 2002: Low-frequency signals in long tree-ring chronologies for reconstructing past temperature variability. *Science*, **295**, 2250–2254.

Felis, T., G. Lohmann, H. Kuhnert, S.J. Lorenz, D. Scholz, J. Pätzold, S.A. Al-Rousan, and S.M. Al-Moghrabi, 2004: Increased seasonality in Middle East temperatures during the last interglacial period. *Nature*, **429**, 164–168.

Frenzel, B., M. Pécsi, and A.A. Velichko, 1992: *Atlas of paleoclimates and paleoenvironments of the northern hemisphere, Late Pleistoncene - Holocene. (data also aviable on http://www.pangea.de/Projects/PKDB/PaleoAtlas.html).* Geographical Research Institute, Hungarian Academy of Science, Budapest, Gustav Fischer Verlag, Budapest-Stuttgart: 153pp.

Hurrell, J.W., 1995: Decadal trends in the North Atlantic Oscillation: Regional temperature and precipitation. *Science*, **269**, 676–679.

Jones, J.M., and M. Widmann, 2003: Instrument- and tree-ring-based estimates for the Antarctic Oscillation. *J. Climate*, **16**, 3511–3524.

Joussaume, S., and P. Braconnot, 1997: Sensitivity of paleoclimate simulation results to season definitions. *J. Geophys. Res.*, **102**, 1943–1956.

Joussaume, S., and K.E. Taylor, 2000: The Paleoclimate Modeling Intercomparison Project. In: *Paleoclimate Modeling Intercomparison Project (PMIP): proceedings of the third PMIP workshop, La Huardièr, Canada, 4-8 October 1999*, P. Braconnot (Ed.), WCRP-111, WMO/TD-No.1007, Geneva, Switzerland, pp. 9–24. World Meteorological Organisation (WMO): World Climate Research Programme.

Kaspar, F., N. Kühl, and U. Cubasch, 2004: Simulation of the Eemian interglacial with a coupled ocean-atmosphere model. In: *EGU 1st General Assembly, Nice, France, 26-30 April 2004. Geophys. Research Abstracts.*, Volume 6, EGU04-A-04034.

Khodri, M., G. Ramstein, and N. de NobletDucoudré, 2003: Sensitivity of the northern extratropics hydrological cycle to the changing insolation forcing at 126 and 115 ky BP. *Climate Dyn.*, **21**, 273–287.

Klotz, S., J. Guiot, and V. Mosbrugger, 2003: Continental European Eemian and early Würmian climate evolution: comparing signals using different quantitative reconstruction approaches based on pollen. *Global Planet. Change*, **36**, 277–294.

Kubatzki, C., M. Montoya, S. Rahmstorf, A. Ganopolski, and M. Claussen, 2000: Comparison of the last interglacial climate simulated by a coupled global model of intermediate complexity and an AOGCM. *Climate Dyn.*, **16**, 799–814.

Kühl, N., and T. Litt, 2003: Quantitative time series reconstruction of Eemian temperature at three European sites using pollen data. *Vegetation History and Archaeobotany*, **12**, 205–214.

Kukla, G.J., M.L. Bender, J.L. de Beaulieu, G. Bond, W.S. Broecker, P. Cleveringa, J.E. Gavin, T.D. Herbert, J. Imbrie, J. Jouzel, L.D. Keigwin, K.L. Knudsen, J.F. McManus, J. Merkt, D.R. Muhs, H. Müller, R.Z. Poore, S.C. Porter, G. Seret, N.J. Shackleton, C. Turner, P.C. Tzedakis, and I.J. Winograd, 2002: Last Interglacial Climates. *Quat. Res.*, **58**, 2–13.

Kutzbach, J.E., R.G. Gallimore, and P. Guetter, 1991: Sensitivity experiments on the effect of orbitally-caused insolation changes on the interglacial climate of northern latitudes. *Quat.Int.*, **10-12**, 223–229.

Legutke, S., and R. Voss, 1999: The Hamburg atmosphere-ocean coupled circulation model ECHO-G. Technical Report 18, German Climate Computing Center (DKRZ), Hamburg.

Lorenz, S.J., and G. Lohmann, 2004: Acceleration technique for Milankovitch type forcing in a coupled atmosphere-ocean circulation model: method and application for the Holocene. *Climate Dyn.*, **23**, 727–743, doi:10.1007/s00382–004–0469–y.

Luterbacher, J., D. Dietrich, E. Xoplaki, M. Grosjean, and H. Wanner, 2004: European seasonal and annual temperature variability, trends, and extremes since 1500. *Science*, **303**, 1499–1503.

Mann, M.E., R.S. Bradley, and M.K. Hughes, 1999: Northern hemisphere temperatures during the past millennium: Inferences, uncertainties, and limitations. *Geophys. Res. Lett*, **26**, 759–762.

Marsland, S.J., M. Latif, and S. Legutke, 2003: Variability of the Antarctic Circumpolar Wave in a coupled ocean-atmosphere model. *Ocean Dynamics*, **53**, 323–331.

Min, S.K., S. Legutke, A. Hense, and W.T. Kwon, 2004: Climatology and Internal Variability in a 1000-Year Control Simulation with the Coupled Climate Model ECHO-G. Technical Report No.2, Gruppe Modelle & Daten, Max Plank Institute for Meteorology, Hamburg, Germany, 67pp.

Montoya, M., H. von Storch, and T.J. Crowley, 2000: Climate Simulation for 125 kyr BP with a Coupled Ocean-Atmosphere General Circulation Model. *J. Climate*, **13**, 1057–1071.

Oppenheim, A., and R.W. Schafer, 1989: *Discrete-Time Signal Processing*, pp. 447–448. Englewood Cliffs, NJ: Prentice-Hall.

Petit, J.R., V. Jouzel, D. Raynaud, N.L. Barkov, J.M. Barnola, I. Basile, M. Bender, J. Chappellaz, J. Davis, G. Delaygue, M. Delmotte, V.M. Kotlyakov, M. Legrand, V.M. Lipenkov, C. Lorius, L. Pépin, C. Ritz, E. Salzmann, and M. Stievenard, 1999: Climate and atmospheric history of the past 420,000 years from the Vostok ice core - antarctica. *Nature*, **399**, 429–436.

Prell, W.L., and J.E. Kutzbach, 1987: Monsoon variability over the past 150,000 years. *J. Geophys. Res.*, **92**, 8411–8425.

Rodgers, K., P. Friederichs, and M. Latif, 2004: Tropical Pacific decadal variability and its relation to decadal modulation of ENSO. *J. Climate*, **17**, 3761–3774.

Roeckner, E., K. Arpe, L. Bengtsson, M. Christoph, M. Claussen, L. Dümenil, M. Esch, M. Giorgetta, U. Schlese, and U. Schulzweida, 1996: The atmosphere general circulation model ECHAM-4: model description and simulation of present-day climate. Technical Report 218, Max Planck Institute for Meteorology.

Rohling, E.J., T.R. Cane, S. Cooke, M. Sprovieri, I. Bouloubassi, K.C. Emeis, R. Schiebel, D. Kroon, F.J. Jorissen, A. Lorre, and A.E.S. Kemp, 2002: African monsoon variability during the previous interglacial maximum. *Earth Planet. Sci. Lett.*, **202**, 61–75.

Royer, J.F., F. Deque, and P. Pestiaux, 1984: A sensitivity experiment to astronomical forcing with a spectral GCM: Simulation of the annual cycle at 125000 and 115000BP. Volume C126 of *Milankovitch and Climate*, pp. 733–736. NATO ASI Series, Reidel.

Rutherford, S., M.E. Mann, T.L. Delworth, and R.J. Stouffer, 2003: Climate Field Reconstruction under stationary and non stationary Forcing. *J. Climate*, **16**, 462–479.

Seelos, K., 2004: *Entwicklung einer numerischen Partikelanalyse auf Basis digitaler Dünnschliffaufnahmen und Anwendung der Methode auf die ELSA-HL2-Kernsequenz 66-41 m.* Ph. D. thesis, University of Mainz, Germany, 173pp.

Seelos, K., and F. Sirocko, 2004: RADIUS - Rapid Particle Analysis of Digital Images by Ultra-High Resolution Scanning of Thin Sections. *Sedimentology*, **53**, 669–681,doi:10.1111/j.1365–3091.2005.00715.x.

Shackleton, N.J., M.F. Sánchez Goñi, D. Pailler, and Y. Lancelot, 2003: Marine Isotope Substage 5e and the Eemain Interglacial. *Global Planet. Change*, **36**, 151–155.

Sowers, T., 2001: N_2O record spanning the penultimate deglaciation from the Vostok ice core. *J. Geophys. Res.*, **106**, 31,903–31,914.

Thompson, D.W.J., and J.M. Wallace, 2000: Annular Modes in Extratropical Circulation. Part I: Month-to-Month Variability. *J. Climate*, **13**, 1000–1016.

Tzedakis, P., M.R. Frogley, and T.H.E. Heaton, 2003: Last Interglacial conditions in southern Europe: evidence from Ioannina, northwest Greece. *Global Planet. Change*, **36**, 157–170.

van Kolfschoten, T., P.L. Gibbard, and K.L. Knudsen, (Ed) 2003: The Eemian Interglacial: a Global Perspective. *Global Planet. Change*, **36**, 147–217.

Vettoretti, G., and W.R. Peltier, 2004: Sensitivity of glacial inception to orbital and greenhouse gas climate forcing. *Quat. Sci. Rev.*, **23**, 499–519, doi:10.1016/j.quascirev.2003.08.008.

von Storch, H., E. Zorita, J. Jones, Y. Dimitriev, F. Gonzlez-Rouco, and S. Tett, 2004: Reconstructing past climate from noisy data. *Science*, **306**, 679–682.

Wallace, J.M., Y. Yuang, and J. Renwick, 1995: Dynamic contribution to hemispheric mean temperature trends. *Science*, **270**, 780–783.

Widmann, M., 2005: One-dimensional CCA and SVD and their relationship to regression maps. *J. Climate*, **18**, 2785–2792.

Wolff, J.O., E. Maier-Reimer, and S. Legutke, 1997: The Hamburg Ocean Primitive Equation Model HOPE. Technical Report 13, German Climate Computing Center (DKRZ).

Zorita, E., and F. González-Rouco, 2002: Are temperature-sensitive proxies adequate for North Atlantic Oscillation reconstructions? *Geophys. Res. Lett*, **29**, 48–1–48–4.

Zorita, E., F. González-Rouco, and S. Legutke, 2003: Testing Mann et al. (1998) Approach to Paleoclimate Reconstructions in the Context of a 1000-Yr Control simulation with the ECHO-G Coupled Climate Model. *J. Climate*, **16**, 1378–1390.

Zorita, E., H. von Storch, F.J. Gonzales-Rouco, U. Cubasch, J. Luterbacher, S. Legutke, I. Fischer-Bruns, and U. Schlese, 2004: Climate Evolution in the Last Five Centuries Simulated by an Atmosphere- Ocean Model: Global Temperatures, the North Atlantic Oscillation and the Late Maunder Minimum. *Meteorol. Z.*, **13**, 271–289.

Appendix B

Sensitivity of temperature teleconnections to orbital changes in AO-GCM simulations

Nikolaus Groll and Martin Widmann
Institute for Coastal Research, GKSS Research Centre
PO Box, D21502 Geesthacht, Germany
Published in:
Geophysical Research Letters, **33**, L12705, doi:10.1029/2005GL025578

Abstract

Teleconnections of interannual January air temperature variations over four regions are investigated based on quasi-equilibrium simulations with the general circulation model ECHO-G for three periods: the last interglacial (125 kyr BP - early Eemian); the last glacial inception (115 kyr BP) and the preindustrial period. The simulated teleconnections represent the teleconnection component due to internal climate variability and are in many regions closely linked to the temperature signal of the Arctic Oscillation. The hemispheric-scale structure of temperature teleconnections is robust with respect to orbital forcing, but differences between the simulations are found on spatial scales up to several 1000 km. In the Eemian simulation teleconnections between temperatures in central Siberia (south of Greenland) and temperatures in many extratropical northern hemispheric regions are stronger (weaker) compared to the other two simulations, while teleconnections for northeastern and western Europe show more complex differences.

B.1 Introduction

Variations in incoming solar radiation due to changes in solar output and in the earth's orbit can affect atmospheric temperature and circulation. Regional temperatures can be directly influenced by variations in the incoming solar radiation in a given area, but also by circulation changes. A response of atmospheric circulation to insolation forcing has been found in many simulations with general circulation models (GCMs) (e.g., Cubasch et al. 1997; Kaspar et al. 2005; Hall et al. 2005). During the early Eemian a positive Arctic Oscillation index (AOI) relative to the preindustrial period has been noted by Felis et al. (2004). This change of the AOI is consistent with the mean simulated SLP difference between the Eemian and the preindustrial period presented by Groll et al. (2005). The latter study showed that the differences in the mean and variability of circulation lead to changed relationships between multi-decadal variations in the AOI and regional temperature.

A physical explanation for the AO response to changes in the meridional temperature gradient was given by Robinson (2000) and by Kushnir et al. (2002), who point out that the associated changes in the generation of lower-tropospheric baroclinic eddies and in the upper-tropospheric convergence of the eddy momentum flux lead to an AO-like change of the Northern Hemispheric circulation. Hall et al. (2005) demonstrated the relevance of this mechanism for orbitally controlled circulation changes over the last 165000 years.

Here we focus on the sensitivity of interannual temperature teleconnections to changes in the orbital forcing and analyze coupled atmosphere-ocean GCM simulations for the preindustrial period, the last interglacial and the last glacial inception. In order to understand this sensitivity, we investigate the link between temperature teleconnections and circulation. Note that we use the term teleconnections for the hemispheric pattern of correlation coefficients between temperatures in a given area and those at all other locations, excluding the positive correlations in the vicinity of the center region.

An improved understanding of teleconnections helps to decide whether temperature-sensitive proxy records from different regions can be expected to have similar or opposite variations. Networks of temperature-sensitive proxy records with high enough temporal resolution and absolute dating accuracy to investigate teleconnections are not available for the periods investigated in this paper. Therefore we use model simulations as a surrogate for the real climate to investigate teleconnections of high-frequency temperature variability.

Our study uses quasi-equilibrium simulations and thus temperature variations within a simulation are entirely due to internal variability (mainly atmospheric circulation variability). In the real world changing forcing factors such as solar variability or volcanic aerosols also affect temperatures on interannual to decadal time scales. To the extent that the simulated circulation variability is realistic, the simulated temperature teleconnections account for the component in the real-world teleconnections that is due to internally generated variability, and also for the component that is due to forced circulation variability with the same structure

Table B.1: Greenhouse Gas Concentration (GHG conc.) and Earth Orbital Parameters Used in the Three Experiments (Exp). PI: simulation with preindustrial GHG conc. and today's orbital parameters; EEM and GI: simulation with GHG conc. and orbital parameters of 125 kyr BP and 115 kyr BP respectively..

Exp	CO_2, ppm	CH_4, ppb	N_2O, ppb	Eccent., %	Obliquity, axis tilt°	Perihelion, °
PI	280	700	310	1.67	23.44	282.7
EEM	270	630	260	4.00	23.79	127.3
GI	265	520	270	4.14	22.41	290.9

as the internally generated variability. This study should therefore be viewed as a first step towards a systematic understanding of the teleconnections of regional temperatures and of their sensitivity to the structure of the large-scale circulation, which in turn is related to orbital forcing.

We focus on January, because in winter high-frequency temperature variations are mostly dominated by large-scale circulation variability and thus a noticeable link between circulation changes and temperature teleconnections can be expected. Similar results for other boreal winter months and for decadal variability have been obtained, but are not shown.

B.2 Model description and experimental setups

This study is based on simulations with the coupled atmosphere-ocean GCM ECHO-G. It consists of the atmospheric model ECHAM-4 (Roeckner et al. 1996) and the ocean model HOPE (Wolff et al. 1997), in a version that includes a thermodynamic-dynamic sea-ice model (HOPE-G). The atmospheric model uses a spectral resolution of T30 (approx. $3.75° \times 3.75°$) with 19 vertical levels. The ocean model has a horizontal resolution of about $2.8° \times 2.8°$ with a grid refinement in the tropical regions and 20 vertical levels. To avoid a climate drift in long simulations a constant-in-time flux adjustment is applied.

Three existing quasi-equilibrium simulations are analyzed: one for present day insolation with preindustrial (AD 1800) greenhouse gas concentrations (hereafter PI) (Lorenz and Lohmann 2004); one for the Eemian - the last interglacial - at 125 kyr BP (hereafter EEM) (Kaspar et al. 2005) and one for the last glacial inception (hereafter GI) at 115 kyr BP (Cubasch et al. 2006). Insolation for a given set of orbital parameters is calculated according to (Berger 1978), greenhouse gas concentrations (GHG conc.) are taken from the Vostok ice core (Petit et al. 1999; Sowers 2001), and vegetation is fixed to its modern state in all simulations. After a model spin up of 1300 (1000) years for PI (EEM and GI), a 1000 yr long simulation period is analyzed. Orbital parameters and GHG conc. of the three simulations are shown in Table B.1. In January the insolation gradient between the North Pole and the

Equator is lower by about $40\,Wm^{-2}$ in EEM and $20\,Wm^{-2}$ higher in GI compared to PI. GHG conc. differences between the three simulations are small and it can be expected that the differences in the simulated climate are mainly due to the changed orbital parameters.

B.3 Teleconnections of regional temperatures

We analyze teleconnections of the interannual variability of January temperatures in the three GCM simulations for four regions: the region south of Greenland (SG); western Europe (WE); northeastern Europe (NE) and central Siberia (CS). In these regions temperature variability is dominated by atmospheric circulation variability, particularly during winter. Regional temperature series are defined as the spatial mean of six grid cells from the 2m-temperature field. We use 1000 years from each simulation to calculate the correlation between detrended simulated monthly temperature means from the specified regions and detrended monthly temperatures at all other grid cells in the extratropical Northern Hemisphere. All discussed differences between the three simulations are significant at the 5% level and are robust when different 500 year long subperiods are considered.

As expected each region shows in all simulations an area with high positive correlation coefficients around its center (Fig. B.1). Although the large-scale spatial structure of the teleconnections is similar in all simulations, there are small, but clearly noticeable differences between EEM and PI for some regions (Fig. B.1, bottom panels). SG temperatures show weaker teleconnections over large parts of the North/ East Atlantic and Arctic Ocean and along the east coast of North America in EEM compared to PI. Teleconnections of WE temperatures are weaker or change sign over the Labrador Sea and south of Greenland in EEM compared to PI. Teleconnection changes for NE temperatures are evident in the Gulf of Mexico, east of Greenland and parts of Siberia. CS temperature teleconnections are stronger west of Greenland and over northwest Russia and the Mediterranean in EEM than in PI. The teleconnection differences between GI and PI are small and therefore not shown.

B.4 Relation to changes in the AO-temperature signal

Teleconnections between interannual winter temperatures can be expected to be mainly caused by large-scale circulation variability. We thus investigate how the changes in the temperature teleconnections are related to changes in the AO-temperature signal. Groll et al. (2005) showed that the AO-temperature signal is sensitive to changes in the orbital forcing on multi-decadal time scales. They suggested that these differences in the AO-temperature signal result from a more zonal mean flow in the early Eemian compared to the preindustrial period, which leads to a shift of the maximum of the AO-temperature signal from Europe to Siberia. We express the AO-temperature signal as the correlation coefficients between the AOI and the 2m

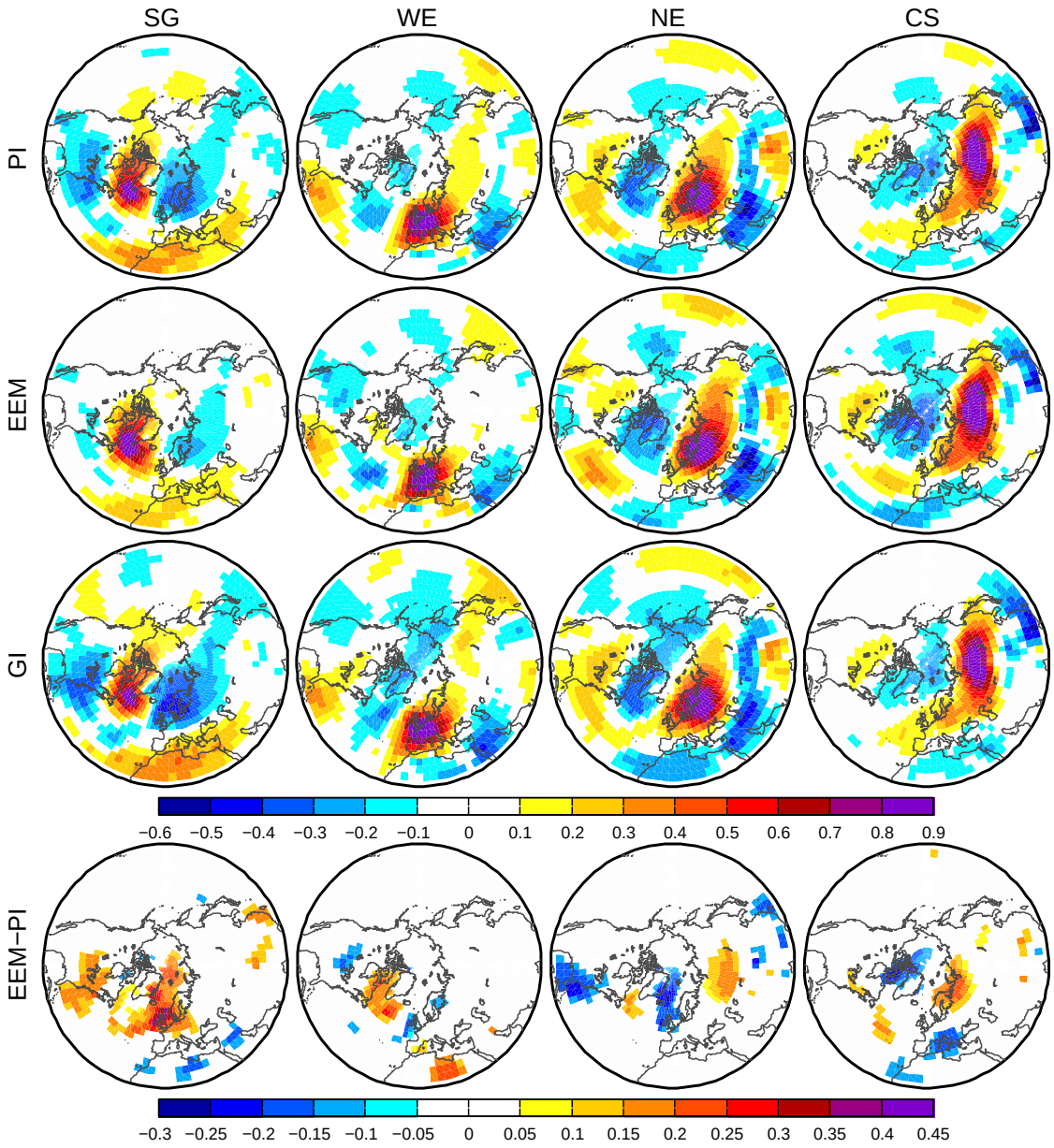

Figure B.1: Teleconnections in (top) PI, (second row) EEM, (third row) GI, and (bottom) differences EEM-PI for annually resolved 2m January temperatures. Shown are correlation coefficients between detrended extratropical Northern Hemisphere grid cell temperatures and four regional temperatures derived as the spatial mean of six grid cells that represents: south of Greenland (SG); western Europe (WE); northeastern Europe (NE); central Siberia (CS). All correlations and differences shown are significant at the 5% level.

January temperatures and, in contrast to Groll et al. (2005), consider annual resolution. The AOI is defined as the first principal component of extratropical (20°-90°N) sea level pressure.

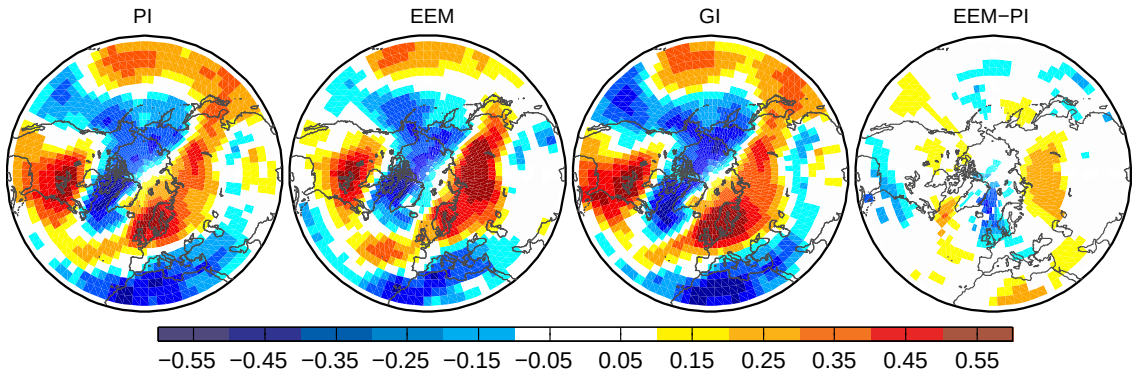

Figure B.2: January AO-temperature signal as correlation coefficients between the AOI and 2m temperature for PI, EEM, GI and difference EEM-PI. All correlations and differences shown are significant at the 5% level.

All three simulations yield a similar spatial distribution of correlation coefficients (Fig. B.2). However, there are small differences in the position of the nodes and centers of the AO-temperature signal. For instance correlations are weaker over Northwest Europe and the Labrador Sea and higher over Siberia in EEM compared to the other simulations. These differences correspond to the weaker teleconnections for SG and WE in EEM shown in Fig. B.1, which indicates that these temperature teleconnections are related to the AO-temperature signal and thus a weaker link between the AOI and regional temperatures leads to weaker temperature teleconnections. The higher AO-temperature correlations over Siberia and the stronger CS teleconnection with northwestern Russia and the Mediterranean (Fig. B.1) also confirm this relationship.

The hypothesis that temperature teleconnections are closely related to the AO-temperature signal is corroborated by pattern correlation maps, in which the value at each grid cell is given by the latitude-weighted pattern correlation between the AO-temperature signal and the temperature teleconnection map for this grid cell. These pattern correlations maps (Fig. B.3) resemble the AO-temperature signal (Fig. B.2). Hence temperature teleconnections are similar to the AO-temperature signal for all regions where the AO-temperature signal is moderate to strong.

Differences of the pattern correlation maps from the different simulations show large areas with smaller correlations in EEM compared to PI, but also higher correlations over Siberia, which is consistent with the weaker AO-temperature signal over SG and WE, a stronger signal over CS, and a similar signal over NE. Differences between GI and PI are only small and therefore not shown.

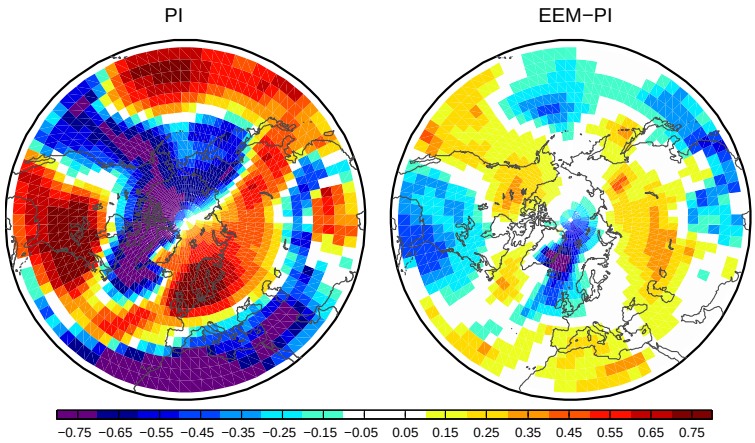

Figure B.3: Pattern correlation between one-point temperature correlation maps and the AO-temperature signal for (left) PI and (right) difference EEM-PI. All correlations and differences shown are significant at the 5% level.

B.5 Conclusions

Our results, which are based on quasi-equilibrium GCM simulations, suggest that the component of real-world temperature teleconnections that is due to internally generated variability is moderately sensitive to orbital forcing. The hemispheric-scale structures of teleconnections are similar, but clearly noticeable differences exist over regions up to several 1000 km. Pattern correlations between the AO-temperature signal and temperature teleconnections indicate that the AO is in many regions the main reason for temperature teleconnections.

Differences in teleconnections are found between the early Eemian and the preindustrial simulation, but not between the glacial inception and the preindustrial simulation. These differences in temperature teleconnection may be relevant for understanding links between temperature-sensitive proxy data with high temporal resolution from different regions.

Acknowledgments

We thank Julie M. Jones, Kerstin Prömmel and two anonymous reviewers for their valuable comments which helped to improve the manuscript. We also thank Frank Kaspar and Stephan J. Lorenz for providing their model simulations. Beate Gardeike is acknowledged for help with figure preparation. This work was funded within the EEM project (Climate change at the very end of a warm stage) by the Federal Ministry of Education and Research under the DEKLIM program (Deutsches Klimaforschungsprogramm).

References

Berger, A.L., 1978: Long-term variations of daily insolation and Quaternary climatic changes. *J. Atmos. Sci.*, **35**, 2362–2367.

Cubasch, U., G.C. Hegerl, R. Voss, J. Waszkewitz, and T.C. Crowley, 1997: Simulation with an O-AGCM of the influence of variations of the solar constant on the global climate. *Climate Dyn.*, **13**, 757–767.

Cubasch, U., E. Zorita, F. Kaspar, K. Prömmel, H. von Storch, and F. Gonzales-Rouco, 2006: Simulation of the role of solar forcing on climate. *Advances in Space Research*, **37**, 1629–1634, doi:10.1016/j.asr.2005.04.07.

Felis, T., G. Lohmann, H. Kuhnert, S.J. Lorenz, D. Scholz, J. Pätzold, S.A. Al-Rousan, and S.M. Al-Moghrabi, 2004: Increased seasonality in Middle East temperatures during the last interglacial period. *Nature*, **429**, 164–168.

Groll, N., M. Widmann, J.M. Jones, F. Kaspar, and S.J. Lorenz, 2005: Simulated Relationships between Regional Temperatures and Large-Scale Circulation: 125 kyr BP (Eemain) and the Preindustrial Period. *J. Climate*, **18**, 4035–4048.

Hall, A., A. Clement, D.W.J. Thompson, A. Broccoli, and C. Jackson, 2005: The Importance of Atmospheric Dynamics in the Northern Hemisphere Wintertime Climate Response to Changes in the Earth's Orbit. *J. Climate*, **18**, 1315–1325.

Kaspar, F., N. Kühl, U. Cubasch, and T. Litt, 2005: A model-data-comparison of European temperatures in the Eemian interglacial. *Geophys. Res. Lett*, **32**, L11703, doi:10.1029/2005GL02245.

Kushnir, Y., W.A. Robinson, I. Blade, N.M.J. Hall, S. Peng, and R. Sutton, 2002: Atmospheric GCM response to extratropical SST anomalies: Synthesis and evaluation. *J. Climate*, **15**, 2233–2256.

Lorenz, S.J., and G. Lohmann, 2004: Acceleration technique for Milankovitch type forcing in a coupled atmosphere-ocean circulation model: method and application for the Holocene. *Climate Dyn.*, **23**, 727–743, doi:10.1007/s00382–004–0469–y.

Petit, J.R., V. Jouzel, D. Raynaud, N.L. Barkov, J.M. Barnola, I. Basile, M. Bender, J. Chappellaz, J. Davis, G. Delaygue, M. Delmotte, V.M. Kotlyakov, M. Legrand,

V.M. Lipenkov, C. Lorius, L. Pépin, C. Ritz, E. Salzmann, and M. Stievenard, 1999: Climate and atmospheric history of the past 420,000 years from the Vostok ice core - antarctica. *Nature*, **399**, 429–436.

Robinson, W.A., 2000: A baroclinic mechanism for the eddy feedback on the zonal index. *J. Atmos. Sci.*, **57**, 415–422.

Roeckner, E., K. Arpe, L. Bengtsson, M. Christoph, M. Claussen, L. Dümenil, M. Esch, M. Giorgetta, U. Schlese, and U. Schulzweida, 1996: The atmosphere general circulation model ECHAM-4: model description and simulation of present-day climate. Technical Report 218, Max Planck Institute for Meteorology.

Sowers, T., 2001: N_2O record spanning the penultimate deglaciation from the Vostok ice core. *J. Geophys. Res.*, **106**, 31,903–31,914.

Wolff, J.O., E. Maier-Reimer, and S. Legutke, 1997: The Hamburg Ocean Primitive Equation Model HOPE. Technical Report 13, German Climate Computing Center (DKRZ).

List of Abbreviations

Abbreviation	Explanation
AAO	Antarctic Oscillation
AD	anno domini
AGCM	atmosphere general circulation model
AO	Arctic Oscillation
AOGCM	atmosphere ocean general circulation model
BP	before present
CET	central european temperature
CS	central Siberia
DEKLIM	Deutsches Klimaforschungsprogramm
DJF	[December-January-February]
EBM	energy balance model
ECHAM4	European Centre and Hamburg Version 4
ECMWF	European Center for Medium-Range Weather Forecast
EMIC	earth system model of intermediate complexity
ENSO	El Niño/ Southern Oscialltion
EOF	empirical orthogonal function
EEM	early Eemain simulation
EEM project	Climate change at the very end of a warm stage
exp	experiment
GCM	general circulation model
GHG	greenhouse gas
GI	glacial inception simulation
GHOST project	Global Holocene Spatial and Temporal variability
HOPE	Hamburg Ocean Primitive Equations
JJA	[June-July-August]

Abbreviation	**Explanation**
kyr	one thousand years
MAM	[March-April-May]
Myr	one million years
NAM	Northern Annular Mode
NAMI	Northern Annular Mode Index
NAO	North Atlantic Oscillation
NE	northeastern Europe
OGCM	ocean general circulation model
PI	preindustrial simulation
SAM	Souther Annular Mode
SG	south of Greenland
SLP	sea level pressure
SON	[September-October-November]
VE	vernal equinox
WE	western Europe

List of Figures

References

Aalbersberg, G., and T. Litt, 1998: Multiproxy climate reconstructions for the Eemian and Early Weichselian. *Journal of Quaternary Science*, **13**, 367–390.

Adhémar, J.F., 1842: *Révolutions de la mer, déluges périodiques* (First ed.). Carilian-Goeury et V.Dalmont, 184pp, Paris.

Baquero-Bernal, A., M. Latif, and S. Legutke, 2002: On dipole-like variability of sea surface temperature in the tropical Indian Ocean. *J. Climate*, **15**, 1358–1368.

Beer, J., S. Baumgartner, B. Dittrich-Hannen, J. Hauenstein, P. Kubik, C. Lukasczyk, W. Mende, R. Stellmacher, and M. Suter, 1994: Solar variability traced by cosmogenic isotopes. In: *The Sun as a Variable Star: Solar and Stellar Irradiance Variations*, J. Pap, C. Fröhlich, and H. H. S. Solanki (Eds.), pp. 291–300. Cambridge: Cambridge University Press.

Beer, J., W. Mende, and R. Stellenmacher, 2000: The role of the sun in climate forcing. *Quat. Sci. Rev.*, **19**, 403–415.

Bengtsson, L., K.I. Hodges, E. Roeckner, and R. Brokopf, 2006: On the natural variability of the pre-industrial European climate. *Climate Dyn.*, **27**, 743–760, doi:10.1007/s00382–006–0168–y.

Berger, A.L., 1978: Long-term variations of daily insolation and Quaternary climatic changes. *J. Atmos. Sci.*, **35**, 2362–2367.

Bradley, R., and J. Eddy, 1991: Records of past global changes. In: *Global Changes of the Past*, R. Bradley (Ed.), pp. 5–9. Boulder: Universtity Corporation for Atmospheric Research.

Bradley, R.S., 1999: *Paleoclimatology - Reconstructing Climates of the Quaternary* (Second ed.), Volume 64 of *International Geophysics Series*. 613pp, Acadamic Press.

Brazdil, R., C. Pfister, H. Wanner, H.V. Storch, and J. Luterbacher, 2005: Historical climatology in Europe - The state of the art. *Climatic Change*, **70**, 363–430.

Bretherton, C., M. Widmann, V.P. Dymnikov, J.M. Wallace, and I. Bladé, 1999: The effective number of spatial degrees of freedom of a time-varying field. *J. Climate*, **12**,

1990–2009.

Briffa, K.R., T.J. Osborn, F.H. Schweingruber, I.C. Harris, P.D. Jones, S.G. Shiyatov, and E.A. Vaganov, 2001: Low frequency temperature variations from a northern tree-ring density network. *J. Geophys. Res.*, **106**, 2929–2941.

Broecker, W.S., 1982a: Glacial to interglacial changes in ocean chemistry. *Progress In Oceanography*, **11**, 151–197.

Broecker, W.S., 1982b: Ocean chemistry during glacial time. *Geochimica Et Cosmochimica Acta*, **46**, 1689–1705.

Cheddadi, R., K. Mamakowa, J. Guiot, J.L. de Beaulieu, M. Reille, V. Andrieu, W. Granoszewski, and O. Peyron, 1998: Was the climate of the Eemian stable? A quantitative climate reconstruction from seven European pollen records. *Palaeogeogr., Palaeoclimatol., Palaeoecol.*, **143**, 73–85.

Claussen, M., V. Brovkin, A. Ganopolski, C. Kubatzki, and V. Petoukhov, 2003: Climate change in northern Africa: The past is not the future. *Climatic Change*, **57**, 99–118.

Claussen, M., L.A. Mysak, A.J. Weaver, M. Crucifix, T. Fichefet, M.F. Loutre, S.L. Weber, J. Alcamo, V.A. Alexeev, A. Berger, R. Calov, A. Ganopolski, H. Goosse, G. Lohmann, F. Lunkeit, I.I. Mokhov, V. Petoukhov, P. Stone, and Z. Wang, 2002: Earth system models of intermediate complexity: closing the gap in the spectrum of climate system models. *Climate Dyn.*, **18**, 579–586, doi 10.1007/s00382–006–0168–y.

Collins, M., T.J. Osborn, S.F. Tett, K.R. Briffa, and F.H. Schweingruber, 2002: A Comparison of the Variability of a Climate Model with Paleotemperature Estimates from a Network of Tree-Ring Densities. *J. Climate*, **15**, 1497–1515.

Cook, E.R., R.D. D'Arrigo, and M.E. Mann, 2002: A very-well verified, multiproxy reconstruction of the winter North Atlantic Oscillation Index since A.D. 1400. *J. Climate*, **15**, 1754–1764.

Croll, J., 1875: *Climate and time in their geological relations: a theory of secular changes of the earth's climate*. Appleton and Co., 577pp, New York.

Crowley, T., 2000: Causes of Climate Change Over the Past 1000 Years. *Science*, **289**, 270–277.

Crowley, T., and K.Y. Kim, 1994: Milankovitch forcing of last interglacial sea level. *Science*, **265**, 1566–1568.

Crowley, T., and K.Y. Kim, 1995: Comparison of long-term greenhouse projections with the geologic record. *Geophys. Res. Lett*, **22**, 933–936.

Crucifix, M., and M.F. Loutre, 2002: Transient simulations over the last interglacial period (126-115kyr BP): feedback and forcing analysis. *Climate Dyn.*, **19**, 417–433.

Crucifix, M., M.F. Loutre, P. Tulkens, T. Fichefet, and A. Berger, 2002: Climate evolution during the Holocene: a study with a Earth system model of intermediate complexity. *Climate Dyn.*, **19**, 43–60.

Cubasch, U., G.C. Hegerl, R. Voss, J. Waszkewitz, and T.C. Crowley, 1997: Simulation with an O-AGCM of the influence of variations of the solar constant on the global climate. *Climate Dyn.*, **13**, 757–767.

Cubasch, U., E. Zorita, F. Kaspar, K. Prömmel, H. von Storch, and F. Gonzáles-Rouco, 2006: Simulation of the role of solar forcing on climate. *Advances in Space Research*, **37**, 1629–1634, doi:10.1016/j.asr.2005.04.07.

D'Arrigo, R.D., E.R. Cook, M.E. Mann, and J.C. Jacoby, 2003: Tree-ring reconstructions of temperature and sea-level pressure variability associated with the warm-season Arctic Oscillation since AD1650. *Geophys. Res. Lett*, **30**, 1549, doi: 10.1029/2003GL017250.

de Noblet, N., P. Braconnot, S. Joussaume, and V. Masson, 1996: Sensitivity of simulated Asian and African summer monsoons to orbitally induced variations in insolation 126, 115 and 6kBP. *Climate Dyn.*, **12**, 589–603.

Diffenbaugh, N.S., and L. Sloan, 2004: Mid-Holocene orbital forcing of regional-scale climate: a case study of western North America using a high-resolution (rcm). *J. Climate*, **17**, 2927–2937.

Doherty, R., J. Kutzbach, J. Foley, and D. Pollard, 2000: Fully coupled/ dynamical vegetation model simulations over the Northern Africa during the mid-Holocene orbital forcing of regional-scale climate: a case study of western North America using a high-resolution (rcm). *Climate Dyn.*, **16**, 561–573.

Emeis, K., D.M. Anderson, H. Doose, D. Kroon, and D. Schulz-Bull, 1995: Sea-surface temperatures and the history of monsoon upwelling in the northwest arabian sea during the last 500,000 years. *Quat. Res.*, **43**, 355–361.

Esper, J., E.R. Cook, and F.H. Schweingruber, 2002: Low-frequency signals in long tree-ring chronologies for reconstructing past temperature variability. *Science*, **295**, 2250–2254.

Felis, T., G. Lohmann, H. Kuhnert, S.J. Lorenz, D. Scholz, J. Pätzold, S.A. Al-Rousan, and S.M. Al-Moghrabi, 2004: Increased seasonality in Middle East temperatures during the last interglacial period. *Nature*, **429**, 164–168.

Frenzel, B., M. Pécsi, and A.A. Velichko, 1992: *Atlas of paleoclimates and paleoenvironments of the northern hemisphere, Late Pleistoncene - Holocene. (data also aviable on http://www.pangea.de/Projects/PKDB/PaleoAtlas.html).* Geographical Research Institute, Hungarian Academy of Science, Budapest, Gustav Fischer Verlag, Budapest-Stuttgart: 153pp.

Gallimore, R., R. Jacob, and J. Kutzbach, 2005: Coupled atmosphere-ocean-vegetation simulations for modern and mid-Holocene climates: role of extratropical vegetation cover feedbacks. *Climate Dynamics*, **25**, 755–776.

Gladstone, R.M., I. Ross, P.J. Valdes, A. Abe-Ouchi, P. Braconnot, S. Brewer, M. Kageyama, A. Kitoh, A. Legrande, O. Marti, R. Ohgaito, B. Otto-Bliesner, W.R. Peltier, and G. Vettoretti, 2005: Mid-holocene NAO: A PMIP2 model intercomparison. *Geophys. Res. Lett*, **32**, L16707, doi:10.1029/2005GL023596.

González-Rouco, J.F., H. Beltrami, E. Zorita, and H. von Storch, 2006: Simulation and inversion of borehole temperature profiles in surrogate climates: Spatial distribution and surface coupling. *Geophysical Research Lett.*, **33**, L01703, doi:10.1029/2005GL024693.

Groll, N., and M. Widmann, 2006: Sensitivity of temperature teleconnections to orbital changes in AO-GCM simulations. *Geophys. Res. Lett*, **33**, L12705, doi:10.1029/2005GL025578.

Groll, N., M. Widmann, J.M. Jones, F. Kaspar, and S.J. Lorenz, 2005: Simulated Relationships between Regional Temperatures and Large-Scale Circulation: 125 kyr BP (Eemain) and the Preindustrial Period. *J. Climate*, **18**, 4035–4048.

Hall, A., A. Clement, D.W.J. Thompson, A. Broccoli, and C. Jackson, 2005: The Importance of Atmospheric Dynamics in the Northern Hemisphere Wintertime Climate Response to Changes in the Earth's Orbit. *J. Climate*, **18**, 1315–1325.

Hall, N., and P.J. Valdes, 1997: A GCM simulation of the climate 6000 years ago. *J. Climate*, **10**, 3–17.

Harrison, S.P., J.E. Kutzbach, Z. Liu, P.J. Bartlein, B.L. Otto-Bliesner, D. Muhs, I.C. Prentice, and R.S. Thompson, 2003: Mid-holocene climates of the Americas: a dynamical response to changed seasonality. *Climate Dyn.*, **20**, 663–688.

Hasselmann, K., 1976: Stochastic climate models, Part 1: Theory. *Tellus*, **28**, 473–485.

Hegerl, G., T.J. Crowley, W.T. Hyde, and D.J. Frame, 2006: Climate sensitivity constrained by temperature reconstructions over the past seven centuries. *Nature*, **440**, 1029–1032.

Hoyt, D., and K. Schatten, 1993: A disscussion of plausible solar-irradiance variations. *J. Geophys. Res.*, **98(A11)**, 18898–18906.

Hurrell, J.W., 1995: Decadal trends in the North Atlantic Oscillation: Regional temperature and precipitation. *Science*, **269**, 676–679.

Jones, J.M., and M. Widmann, 2003: Instrument- and tree-ring-based estimates for the Antarctic Oscillation. *J. Climate*, **16**, 3511–3524.

Jones, J.M., and M. Widmann, 2004: Atmospheric science - Early peak in Antarctic oscillation index. *Nature*, **432**, 290–291.

Jones, P.D., K.R. Briffa, T.P. Barnett, and S.F.B. Tett, 1998: High-resolution palaeoclimatic records for the last millennium: interpretation, integration and comparison with General Circulation Model control-run temperatures. *Holocene*, **8**, 455–471.

Jones, P.D., and M.E. Mann, 2004: Climate over past millennia. *Rev. Geophysics*, **42**, RG2002, doi: 10.1029/2003RG000143.

Joussaume, S., and P. Braconnot, 1997: Sensitivity of paleoclimate simulation results to season definitions. *J. Geophys. Res.*, **102**, 1943–1956.

Joussaume, S., and K.E. Taylor, 2000: The Paleoclimate Modeling Intercomparison Project. In: *Paleoclimate Modeling Intercomparison Project (PMIP): proceedings of the third PMIP workshop, La Huardièr, Canada, 4-8 October 1999*, P. Braconnot (Ed.), WCRP-111, WMO/TD-No.1007, Geneva, Switzerland, pp. 9–24. World Meteorological Organisation (WMO): World Climate Research Programme.

Kaspar, F., N. Kühl, and U. Cubasch, 2004: Simulation of the Eemian interglacial with a coupled ocean-atmosphere model. In: *EGU 1st General Assembly, Nice, France, 26-30 April 2004. Geophys. Research Abstracts.*, Volume 6, EGU04-A-04034.

Kaspar, F., N. Kühl, U. Cubasch, and T. Litt, 2005: A model-data-comparison of European temperatures in the Eemian interglacial. *Geophys. Res. Lett*, **32**, L11703, doi:10.1029/2005GL02245.

Khodri, M., G. Ramstein, and N. de NobletDucoudré, 2003: Sensitivity of the northern extratropics hydrological cycle to the changing insolation forcing at 126 and 115 ky BP. *Climate Dyn.*, **21**, 273–287.

Kirchner, I., G. Stenchikov, H. Graf, A. Robock, and J. Antua, 1999: Climate model simulation of winter warming and summer cooling following the 1991 Mount Pinatubo volcanic eruption. *J. Geophys. Res.*, **104(D4)**, 19 039–19 005.

Klotz, S., J. Guiot, and V. Mosbrugger, 2003: Continental European Eemian and early Würmian climate evolution: comparing signals using different quantitative reconstruction approaches based on pollen. *Global Planet. Change*, **36**, 277–294.

Kubatzki, C., M. Montoya, S. Rahmstorf, A. Ganopolski, and M. Claussen, 2000: Comparison of the last interglacial climate simulated by a coupled global model of intermediate complexity and an AOGCM. *Climate Dyn.*, **16**, 799–814.

Kühl, N., and T. Litt, 2003: Quantitative time series reconstruction of Eemian temperature at three European sites using pollen data. *Vegetation History and Archaeobotany*, **12**, 205–214.

Kukla, G.J., M.L. Bender, J.L. de Beaulieu, G. Bond, W.S. Broecker, P. Cleveringa, J.E. Gavin, T.D. Herbert, J. Imbrie, J. Jouzel, L.D. Keigwin, K.L. Knudsen, J.F. McManus,

J. Merkt, D.R. Muhs, H. Müller, R.Z. Poore, S.C. Porter, G. Seret, N.J. Shackleton, C. Turner, P.C. Tzedakis, and I.J. Winograd, 2002: Last Interglacial Climates. *Quat. Res.*, **58**, 2–13.

Kushnir, Y., W.A. Robinson, I. Blade, N.M.J. Hall, S. Peng, and R. Sutton, 2002: Atmospheric GCM response to extratropical SST anomalies: Synthesis and evaluation. *J. Climate*, **15**, 2233–2256.

Kutzbach, J., G. Bonan, J. Foley, and S.P. Harrison, 1996: Vegetation and soil feedbacks on the response of the African monsoon to orbital forcing in the early to middle holocene. *Nature*, **384**, 623–626.

Kutzbach, J.E., 1980: Estimates of past climate at paleolake Chad, North-Africa, based on a hydrological and energy-balance model. *Quat. Res.*, **14**, 210–223.

Kutzbach, J.E., R.G. Gallimore, and P. Guetter, 1991: Sensitivity experiments on the effect of orbitally-caused insolation changes on the interglacial climate of northern latitudes. *Quat.Int.*, **10-12**, 223–229.

Kutzbach, J.E., and B.L. Otto-Bliesner, 1982: The sensitivity of the african-asian monsoonal climate to orbital parameter changes for 9000 years BP in a low-resolution general-circulation model. *J. Atmospheric Sciences*, **39**, 1177–1188.

Lean, J., J. Beer, and R. Bradley, 1995: Reconstructions of solar irradiance since 1610-implications for climate changes. *Geophys. Res. Lett*, **22**, 3195–3198.

Lean, J., and D. Rind, 1999: Evaluating sun-climate relationships since the Little Ice Age. *J. Atmos. Sol.-Terr. Phys.*, **16**, 25–36.

Legutke, S., and R. Voss, 1999: The Hamburg atmosphere-ocean coupled circulation model ECHO-G. Technical Report 18, German Climate Computing Center (DKRZ), Hamburg.

Liu, Z., S.P. Harrison, J. Kutzbach, and B.L. Otto-Bliesner, 2004: Global monsoons in the mid-Holocene and oceanic feedback. *Climate Dyn.*, **22**, 157–182.

Lorenz, S.J., and G. Lohmann, 2004: Acceleration technique for Milankovitch type forcing in a coupled atmosphere-ocean circulation model: method and application for the Holocene. *Climate Dyn.*, **23**, 727–743, doi:10.1007/s00382–004–0469–y.

Loutre, M.F., D. Paillard, F. Vimeux, and E. Cortijo, 2004: Does mean annual insolation have the potential to change the climate? *Earth Planetary Science Lett.*, **221**, 1–14.

Luterbacher, J., D. Dietrich, E. Xoplaki, M. Grosjean, and H. Wanner, 2004: European seasonal and annual temperature variability, trends, and extremes since 1500. *Science*, **303**, 1499–1503.

Luterbacher, J., C. Schmutz, D. Gyalistras, E. Xoplaki, and H. Wanner, 1999: Reconstruction of monthly NAO and EU indices back to AD 1675. *Geophys. Res. Lett*, **26**, 2745–2748.

Luterbacher, J., E. Xoplaki, D. Dietrich, R. Rickli, J. Jacobeit, C. Beck, D. Gyalistras, C. Schmutz, and H. Wanner, 2002: Reconstruction of sea level pressure fields over the Eastern North Atlantic and Europe back to 1500. *Climate Dyn.*, **18**, 545–561.

Mann, M.E., R.S. Bradley, and M.K. Hughes, 1999: Northern hemisphere temperatures during the past millennium: Inferences, uncertainties, and limitations. *Geophys. Res. Lett*, **26**, 759–762.

Marsland, S.J., M. Latif, and S. Legutke, 2003: Variability of the Antarctic Circumpolar Wave in a coupled ocean-atmosphere model. *Ocean Dynamics*, **53**, 323–331.

Mende, M., and R. Stellenmacher, 2001: Effect of Earth Orbital and Solar variability on Climate. In: *Climate of the 21st Century: Changes and Risks*, H. Lozán, H. Graßl, and P. Hupfer (Eds.), pp. 27–33.

Mikolajewicz, U., E. Maier-Reimer, T.J. Crowley, and K.Y. Kim, 1993: Effect of drake and panamanian gateways on the circulation of an ocean model. *Paleoceanography*, **8**, 409–426.

Milankovitch, M., 1941: *Canon of insolation and the ice-age problem*. Königliche Serbische Akademie.

Min, S.K., S. Legutke, A. Hense, and W.T. Kwon, 2004: Climatology and Internal Variability in a 1000-Year Control Simulation with the Coupled Climate Model ECHO-G. Technical Report No.2, Gruppe Modelle & Daten, Max Planck Institute for Meteorology, Hamburg, Germany, 67pp.

Mitchell, J., D. Karoly, G. Hegerl, F. Zwiers, M. Allen, and J. Marengo, 2001: Detection of climate change and attribution of causes. In: *IPCC Third Assessment Report - Climate Change 2001: The Scientfic Basis*, J. Houghton, Y. Ding, D. Griggs, M. Noguer, P. van der Linden, X. Dai, K. Maskell, and C. Johnson (Eds.), pp. 695–738. Cambridge University Press.

Moberg, A., D.M. Sonechkin, K. Holmgren, N.M. Datsenko, and W. Karlen, 2005: Highly variable Northern Hemisphere temperatures reconstructed from low- and high-resolution proxy data. *Nature*, **433**, 613–617.

Molnar, P., P. England, and J. Martinod, 1993: Mantle dynamics, uplift of the tibetan plateau, and the indian monsoon. *Rev. Geophysics*, **31**, 357–396.

Montoya, M., H. von Storch, and T.J. Crowley, 2000: Climate Simulation for 125kyr BP with a Coupled Ocean-Atmosphere General Circulation Model. *J. Climate*, **13**, 1057–1071.

Müller, B., 2003: *Eine regionale Klimasimulation für Europa in der Zeit des späten Maunder-Minimums (1675-1705)*. Ph. D. thesis, University of Hamburg, Germany.

Murdock, T.Q., A.J. Weaver, and A.F. Fanning, 1997: Paleoclimatic response of the closing of the Isthmus of Panama in a coupled ocean-atmosphere model. *Geophysical Research Lett.*, **24**, 253–256.

Ogilvie, A., 1992: Documentary evidence for changes in the climate of iceland, A.D. 1500-1800. In: *Climate Since A.D. 1500*, R. Bradley and P. Jones (Eds.), pp. 92–117. London: Routledge.

Oppenheim, A., and R.W. Schafer, 1989: *Discrete-Time Signal Processing*, pp. 447–448. Englewood Cliffs, NJ: Prentice-Hall.

Petit, J.R., V. Jouzel, D. Raynaud, N.L. Barkov, J.M. Barnola, I. Basile, M. Bender, J. Chappellaz, J. Davis, G. Delaygue, M. Delmotte, V.M. Kotlyakov, M. Legrand, V.M. Lipenkov, C. Lorius, L. Pépin, C. Ritz, E. Salzmann, and M. Stievenard, 1999: Climate and atmospheric history of the past 420,000 years from the Vostok ice core - Antarctica. *Nature*, **399**, 429–436.

Prell, W.L., and J.E. Kutzbach, 1987: Monsoon variability over the past 150,000 years. *J. Geophys. Res.*, **92**, 8411–8425.

Reichert, B.K., L. Bengtsson, and J. Oerlemans, 2001: Midlatitude forcing mechanisms for glacier mass balance investigated using general circulation models. *J. Climate*, **14**, 3767–3784.

Robinson, W.A., 2000: A baroclinic mechanism for the eddy feedback on the zonal index. *J. Atmos. Sci.*, **57**, 415–422.

Robock, A., 2000: Volcanic eruptions and climate. *Rev. Geophys*, **38**, 191–219.

Rodgers, K., P. Friederichs, and M. Latif, 2004: Tropical Pacific decadal variability and its relation to decadal modulation of ENSO. *J. Climate*, **17**, 3761–3774.

Roeckner, E., K. Arpe, L. Bengtsson, M. Christoph, M. Claussen, L. Dümenil, M. Esch, M. Giorgetta, U. Schlese, and U. Schulzweida, 1996: The atmosphere general circulation model ECHAM-4: model description and simulation of present-day climate. Technical Report 218, Max-Planck Institute for Meteorology.

Rohling, E.J., T.R. Cane, S. Cooke, M. Sprovieri, I. Bouloubassi, K.C. Emeis, R. Schiebel, D. Kroon, F.J. Jorissen, A. Lorre, and A.E.S. Kemp, 2002: African monsoon variability during the previous interglacial maximum. *Earth Planet. Sci. Lett.*, **202**, 61–75.

Royer, J.F., F. Deque, and P. Pestiaux, 1984: A sensitivity experiment to astronomical forcing with a spectral GCM: Simulation of the annual cycle at 125000 and 115000BP. Volume C126 of *Milankovitch and Climate*, pp. 733–736. NATO ASI Series, Reidel.

Royer, J.F., M. Deque, and P. Pestiaux, 1983: Orbital forcing of the inception of the laurentide ice-sheet. *Nature*, **304**, 43–46.

Rutherford, S., M.E. Mann, T.L. Delworth, and R.J. Stouffer, 2003: Climate Field Reconstruction under stationary and non stationary Forcing. *J. Climate*, **16**, 462–479.

Saltzman, B., 2002: *Dynamical Paleoclimatology - Generalized Theory of Gobal Climate Change* (First ed.), Volume 80 of *International Geophysics Series*. 354pp, Acadamic Press.

Schrugers, G., U. Mikolajewicz, M. Gröger, E. Maier-Reimer, M. Vizcanino, and A. Winguth, 2006: Dynamics of the terrestrial biosphere, climate and atmosphere CO_2 concentration during interglacials: a comparison between eemian and holocene. *Climate of the Past*, **2**, 205–220.

Seelos, K., 2004: *Entwicklung einer numerischen Partikelanalyse auf Basis digitaler Dünnschliffaufnahmen und Anwendung der Methode auf die ELSA-HL2-Kernsequenz 66-41 m*. Ph. D. thesis, University of Mainz, Germany, 173pp.

Seelos, K., and F. Sirocko, 2004: RADIUS - Rapid Particle Analysis of Digital Images by Ultra-High Resolution Scanning of Thin Sections. *Sedimentology*, **53**, 669–681,doi:10.1111/j.1365–3091.2005.00715.x.

Shackleton, N.J., M.F. Sánchez Goñi, D. Pailler, and Y. Lancelot, 2003: Marine Isotope Substage 5e and the Eemain Interglacial. *Global Planet. Change*, **36**, 151–155.

Shindell, D.T., G.A. Schmidt, M.E. Mann, D. Rind, and A. Waple, 2001a: Solar Forcing of Regional Climate Change During the Maunder Minimum. *Science*, **294**, 2149–2152.

Shindell, D.T., G.A. Schmidt, R. Miller, and D. Rind, 2001b: Northern Hemisphere winter climate response to greenhouse gas, ozone, solar and volcanic forcing. *J. Geophys. Res.*, **106(D7)**, 7193–7210.

Siegenthaler, U., T.F. Stocker, E. Monnin, D. Lthi, J. Schwander, B. Stauffer, D. Raynaud, J.M. Barnola, H. Fischer, V. Masson-Delmotte, and J. Jouzel, 2005: Stable Carbon CycleClimate Relationship During the Late Pleistocene. *Science*, **310**, 1313–1317, doi:10.1126/science.1120130.

Sowers, T., 2001: N_2O record spanning the penultimate deglaciation from the Vostok ice core. *J. Geophys. Res.*, **106**, 31,903–31,914.

Stouffer, R.J., J. Yin, J.M. Gregory, K.W. Dixon, M.J. Spelman, W. Hurlin, A.J. Weaver, M. Ebyd, G.M. Flato, H. Hasumi, A. Hu, J.H. Jungclaus, I.V. Kamenkovich, A. Levermann, M. Montoya, S. Murakami, S. Nawrath, A. Oka, W.R. Peltier, D.Y. Robitaille, A. Sokolov, G. Vettoretti, and S.L. Weber, 2006: Investigating the causes of the response of the thermohaline circulation to past and future climate changes. *J. Climate*, **19**, 1365–1387.

Terray, L., S. Valcke, and A. Piacentini, 1998: The oasis coupler user guide. Version 2.2. Technical Report TR/CMGC/98-05, CERFAS.

Thompson, D.W.J., and J.M. Wallace, 2000: Annular Modes in Extratropical Circulation. Part I: Month-to-Month Variability. *J. Climate*, **13**, 1000–1016.

Tzedakis, P., M.R. Frogley, and T.H.E. Heaton, 2003: Last Interglacial conditions in southern Europe: evidence from Ioannina, northwest Greece. *Global Planet. Change*, **36**, 157–170.

van der Schrier, G., and J. Barkmeijer, 2005: Bjerknes' hypothesis on the coldness during AD 1790-1820 revisited. *Climate Dynamics*, **24**, 355–371.

van Kolfschoten, T., P.L. Gibbard, and K.L. Knudsen, (Ed) 2003: The Eemian Interglacial: a Global Perspective. *Global Planet. Change*, **36**, 147–217.

Vettoretti, G., and W.R. Peltier, 2004: Sensitivity of glacial inception to orbital and greenhouse gas climate forcing. *Quat. Sci. Rev.*, **23**, 499–519, doi:10.1016/j.quascirev.2003.08.008.

von Storch, H., U. Cubach, J. Gonzáles-Rouco, J.J. JF, R. Voss, M. Widmann, and E. Zorita, 2000: Combining paleoclimatic evidence and GCMs by means of data assimilation through upscaling and nudging (DATUN). In: *11th Symposium on Global Change Studies*, pp. 1–4. AMS.

von Storch, H., E. Zorita, J. Jones, Y. Dimitriev, F. González-Rouco, and S. Tett, 2004: Reconstructing past climate from noisy data. *Science*, **306**, 679–682.

Wagner, S., M. Widmann, J. Jones, T. Haberzettl, A. Lücke, C. Mayr, C. Ohlendorf, F. Schäbitz, and B. Zolitschka, 2007: Transient simulations, empirical reconstructions and forcing mechanisms for the Mid-Holocene hydrological climate in Southern Patagonia. *Climate Dyn.*, accepted.

Wallace, J.M., Y. Yuang, and J. Renwick, 1995: Dynamic contribution to hemispheric mean temperature trends. *Science*, **270**, 780–783.

Wang, Y.M., J. Lean, and N.S. Jr., 2005: Modeling the Sun's magnetic field and irradiance since 1713. *Journal of Astrophysics*, **625**, 522–538, doi:10.1086/429689.

Wasson, R.J., and M. Claussen, 2002: Earth system models: a test using the mid-Holocene in the Southern hemisphere. *Quat. Sci. Rev.*, **21**, 819–824.

Weber, S.L., 2001: The impact of orbital forcing on the climate of an intermediate-complexity coupled model. *Global Planetary Change*, **30**, 7–12.

Weber, S.L., 2005: A timescale analysis of the Northern Hemisphere temperature response to volcanic and solar forcing. *Climate of the Past*, **1**, 9–17.

Weber, S.L., and J. Oerlemans, 2003: Holocene glacier variability: three case studies using an intermediate-complexity climate model. *Holocene*, **13**, 353–363.

Widmann, M., 2005: One-dimensional CCA and SVD and their relationship to regression maps. *J. Climate*, **18**, 2785–2792.

Widmann, M., N. Groll, and J.M. Jones, 2007a: Simulated teleconnections during the Eemian, the last glacial inception, and the preindustrial period. In: *The climate of past interglacials*, F. Sirocko, T. Litt, and M. Claussen (Eds.), pp. 517–526. Elsevier.

Widmann, M., H. von Storch, R. Schnur, and I. Kirchner, 2007b: Assimilation of large-scale circulation states into the ECHAM 4 atmospheric GCM with Pattern Nudging. *Climate Dyn.*, in preperation.

Wolff, J.O., E. Maier-Reimer, and S. Legutke, 1997: The Hamburg Ocean Primitive Equation Model HOPE. Technical Report 13, German Climate Computing Center (DKRZ).

Zorita, E., and F. González-Rouco, 2002: Are temperature-sensitive proxies adequate for North Atlantic Oscillation reconstructions? *Geophys. Res. Lett*, **29**, 48–1 – 48–4, doi:10.1029/2002GL015404.

Zorita, E., F. González-Rouco, and S. Legutke, 2003: Testing Mann et al. (1998) Approach to Paleoclimate Reconstructions in the Context of a 1000-Yr Control simulation with the ECHO-G Coupled Climate Model. *J. Climate*, **16**, 1378–1390.

Zorita, E., H. von Storch, F.J. Gonzáles-Rouco, U. Cubasch, J. Luterbacher, S. Legutke, I. Fischer-Bruns, and U. Schlese, 2004: Climate Evolution in the Last Five Centuries Simulated by an Atmosphere- Ocean Model: Global Temperatures, the North Atlantic Oscillation and the Late Maunder Minimum. *Meteorol. Z.*, **13**, 271–289.

Acknowledgments

I would like to thank Prof. Dr. Hans von Storch for the appraisal of this work and for giving me the opportunity to prepare this thesis at the Institute of Coastal Research at the GKSS Research Centre, Geesthacht. I also thank Prof. Dr. Martin Claussen for being the second assessor of this thesis.

Special thanks to Dr. Martin Widmann and Dr. Julie M. Jones who were my actual tutors of the thesis and helped me when ever necessary, and for their scientific discussions which helped me considerably. But also I also would like to thank them for any less formal discussion.

Dr. Frank Kaspar and Stephan J. Lorenz are acknowledged for providing their model simulations and for their help with any question concerning the simulations and the valuable discussion on our article.

I also would like to thank Dr. Eduaro Zorita, Dr. Sebastion Wagner, Dr. Elke Meyer, Dr. Chrisptioh Matulla, Kerstin Prömmel, Markus Ungerböck, Sven Kotlarski and all other colleges at GKSS for providing stimulating ideas and discussions which helped me to improve my work and this manuscript.

Dr. Hermann Kuhn and Dr. Jens Meywerk are acknowledged for their computer support, Fr. Beate Gardeike for helping me a lot with figure preparation and Fr. Liesner for her help with the administration.

Birgit Hünicke, Dr. Martin Döring, Elke and Julie for the fun we had on our trips to and from Geesthacht.

Last but not least I would like to thank Anke and my family for their moral support, in particular during the last month even it wasn't always easy with me, and the "Jeromin Sippe" who gave me the feeling of being welcome in their family.